NASA/TM-2012-217348
NESC-RP-09-00529

# International Space Station (ISS) Heat Rejection Subsystem (HRS) Radiator Face Sheet Damage

*Henry A. Rotter/NESC*
*Langley Research Center, Hampton, Virginia*

**Distribution limited to NASA Contractors and U.S. Government Only**

March 2012

## NASA STI Program . . . in Profile

Since its founding, NASA has been dedicated to the advancement of aeronautics and space science. The NASA scientific and technical information (STI) program plays a key part in helping NASA maintain this important role.

The NASA STI program operates under the auspices of the Agency Chief Information Officer. It collects, organizes, provides for archiving, and disseminates NASA's STI. The NASA STI program provides access to the NASA Aeronautics and Space Database and its public interface, the NASA Technical Report Server, thus providing one of the largest collections of aeronautical and space science STI in the world. Results are published in both non-NASA channels and by NASA in the NASA STI Report Series, which includes the following report types:

- TECHNICAL PUBLICATION. Reports of completed research or a major significant phase of research that present the results of NASA programs and include extensive data or theoretical analysis. Includes compilations of significant scientific and technical data and information deemed to be of continuing reference value. NASA counterpart of peer-reviewed formal professional papers, but having less stringent limitations on manuscript length and extent of graphic presentations.

- TECHNICAL MEMORANDUM. Scientific and technical findings that are preliminary or of specialized interest, e.g., quick release reports, working papers, and bibliographies that contain minimal annotation. Does not contain extensive analysis.

- CONTRACTOR REPORT. Scientific and technical findings by NASA-sponsored contractors and grantees.

- CONFERENCE PUBLICATION. Collected papers from scientific and technical conferences, symposia, seminars, or other meetings sponsored or co-sponsored by NASA.

- SPECIAL PUBLICATION. Scientific, technical, or historical information from NASA programs, projects, and missions, often concerned with subjects having substantial public interest.

- TECHNICAL TRANSLATION. English-language translations of foreign scientific and technical material pertinent to NASA's mission.

Specialized services also include creating custom thesauri, building customized databases, and organizing and publishing research results.

For more information about the NASA STI program, see the following:

- Access the NASA STI program home page at *http://www.sti.nasa.gov*

- E-mail your question via the Internet to help@sti.nasa.gov

- Fax your question to the NASA STI Help Desk at 443-757-5803

- Phone the NASA STI Help Desk at 443-757-5802

- Write to:
  NASA STI Help Desk
  NASA Center for AeroSpace Information
  7115 Standard Drive
  Hanover, MD 21076-1320

NASA/TM-2012-217348
NESC-RP-09-00529

# International Space Station (ISS) Heat Rejection Subsystem (HRS) Radiator Face Sheet Damage

*Henry A. Rotter/NESC*
*Langley Research Center, Hampton, Virginia*

**Distribution limited to NASA Contractors and U.S. Government Only**

National Aeronautics and
Space Administration

Langley Research Center
Hampton, Virginia 23681-2199

March 2012

Available from:

NASA Center for AeroSpace Information
7115 Standard Drive
Hanover, MD 21076-1320
443-757-5802

# International Space Station (ISS) Heat Rejection Subsystem (HRS) Radiator Face Sheet Damage

## February 9, 2012

**Distribution Limited to NASA Contractors and U.S. Government Only**

# Approval and Document Revision History

NOTE: This document was approved at the February 9, 2012, NRB. This document was submitted to the NESC Director on February 29, 2012, for configuration control.

| | | |
|---|---|---|
| Approved: | *Original Signature on File* | 3/1/12 |
| | NESC Director | Date |

| Version | Description of Revision | Author | Effective Date |
|---|---|---|---|
| 1.0 | Initial Release | Mr. Henry Rotter, NASA Technical Fellow for Life Support/Active Thermal, Johnson Space Center | 2/9/12 |

# Table of Contents

## Technical Assessment Report

## List of Figures

## List of Tables

# Technical Assessment Report

## 1.0 Notification and Authorization

The starboard side International Space Station (ISS) heat rejection subsystem radiator (HRSR) was launched on October 2002, and deployed and serviced in November 2007. A survey of previous ISS images and videos verified this radiator was in the normal configuration on August 29, 2008. However, on September 1, 2008, a video survey of ISS indicated a face sheet had debonded and peeled up on HRSR S1-3 panel 7 with no apparent source for the damage. This radiator damage consisted of a large section of the face sheet peeled up, sheared face sheet metal, and debonded from the adjoining face sheet. The face sheet showed considerable wrinkling and evidence of one micrometeoroid orbital debris (MMOD) penetration. The face sheet on the panel's back side showed a smaller wrinkled area with suspected debonding. Since being discovered, S1-3 panel 7 has showed no observable signs of increasing damage. Additionally, multiple dockings of Soyuz, Progress, and Space Shuttle Orbiter, and vibration induced during ISS reboost have resulted in no detectable changes.

Mr. Henry Rotter, NASA Technical Fellow for Life Support/Active Thermal, was selected to lead this assessment. An Initial Evaluation was approved by the NASA Engineering and Safety Center (NESC) Review Board (NRB) on March 12, 2009. The assessment objective was to determine the most probable cause for the ISS HRSR S1-3 panel 7 face sheet damage and any generic risks for the other ISS radiator panels.

NESC's initial recommended plan of action, formed with the ISS Program input, included: requests for previously performed MMOD test data from ISS radiator coupon testing; a request for infrared (IR) imagery of radiator panels for the port and starboard sides (planned for a 15A/ STS-119 extravehicular activity (EVA)); a recommendation for an over pressure test; consideration of additional tests to perform on a subset of the nine panels located at the Johnson Space Center (JSC); conducting a face sheet strength test to determine what pressure can initiate face sheet debonding; and an investigation of how to pressurize the internal panel without weakening the panel structure.

Subsequent investigation resulted in changes to this initial plan. The work performed in support of this assessment is summarized in Section 3.2 and documented throughout this report.

# 2.0 Signature Page

Submitted by:

*Team Signature Page on File – 3/8/12*

Mr. Henry A. Rotter Date

Significant Contributors:

Mr. Steven L. Rickman Date

Mr. Marshall D. Neipert Date

Ms. Patricia A. Howell Date

Signatories declare the findings, observations, and NESC recommendations compiled in the report are factually based from data extracted from Program/Project documents, contractor reports, and open literature, and/or generated from independently conducted tests, analysis, and inspections.

# 3.0 Team List

| Name | Discipline | Organization/Location |
|---|---|---|
| **Core Team** | | |
| Hank Rotter | NASA Technical Fellow for Life Support/Active Thermal | JSC |
| Steven Rickman | NASA Technical Fellow for Passive Thermal | LaRC |
| Gary Rankin | Crew and Thermal Systems Division | JSC |
| Richard Morton | Crew and Thermal Systems Division | JSC |
| Bruce Harkness | Active Thermal | Boeing |
| Marshall Neipert | LS-DYNA® | JSC |
| Dave Wright | Radiator Testing | LMMFC |
| John Raetz | ISS ATCS | Boeing |
| Ajay Koshti | Structural Engineering | Jacobs Technology |
| Gary Reynolds | Active Thermal Systems | Jacobs Technology |
| Walter Wilson | Avionic Systems Division | Jacobs Technology |
| Charles Antill | Systems Engineering | LaRC |
| Patricia Howell | NDE | LaRC |
| William Winfree | NDE | LaRC |
| Pamela Throckmorton | MTSO | LaRC |
| **Consultants** | | |
| Curtis Larsen | NASA Technical Fellow for Loads and Dynamics | JSC |
| Robert Piascik | NASA Technical Fellow for Materials | LaRC |
| Bill Prosser | NASA Technical Fellow for NDE | LaRC |
| **LS-DYNA® Analysis Peer Reviewers** | | |
| Scott Ford | LS-DYNA® | Boeing |
| Babu Meka | LS-DYNA® | Boeing |
| Jeremie Albert | LS-DYNA® | Boeing |
| Nika McManus | LS-DYNA® | Boeing |
| Jon Gabrys | LS-DYNA® | Boeing |
| Siamak Ghofranian | LS-DYNA® | Boeing |
| **Administrative Support** | | |
| Christina Williams | Technical Writer | LaRC, ATK |

## 3.1 Acknowledgements

The investigation team acknowledges Mr. Steven Gentz (NESC), Mr. Timothy Brady (NESC), and Dr. Eugene Ungar (JSC) for their peer review of the final report draft.

## 3.2 NESC Involvement

The NESC involvement augmented the original ISS Program support with the following:

a. Review of design, flight, and assembly data to determine whether problems observed during construction;

b. Review of MMOD test coupons and reports;

c. Review of IR imagery from the 15A flight;

d. Form factor analysis for HRSR surfaces to assist with the interpretation of temperature trends observed in the IR imagery;

e. Development of an LS-DYNA® model to understand the physics of the radiator face sheet failure;

f. Sponsorship of radiator component testing in support of fault tree investigations;

g. Participation in team technical interchange meetings (TIMs) in July 2009, and March 2010; and

h. Engaging support from JSC and Langley Research Center (LaRC) for the IR software analyses.

# 4.0 Executive Summary

On September 1, 2008, a planned external image survey of the International Space Station (ISS) found the heat rejection subsystem radiator (HRSR) S1-3 panel 7 thin (0.010 inch) aluminum face sheet was peeled up (Figure 4.0-1). A survey of previous ISS images and videos verified that this radiator was in the normal configuration on August 29, 2008. A survey of ISS accelerometers and events during this time period found no evidence to determine when this event specifically occurred and offered no clues to its origin.

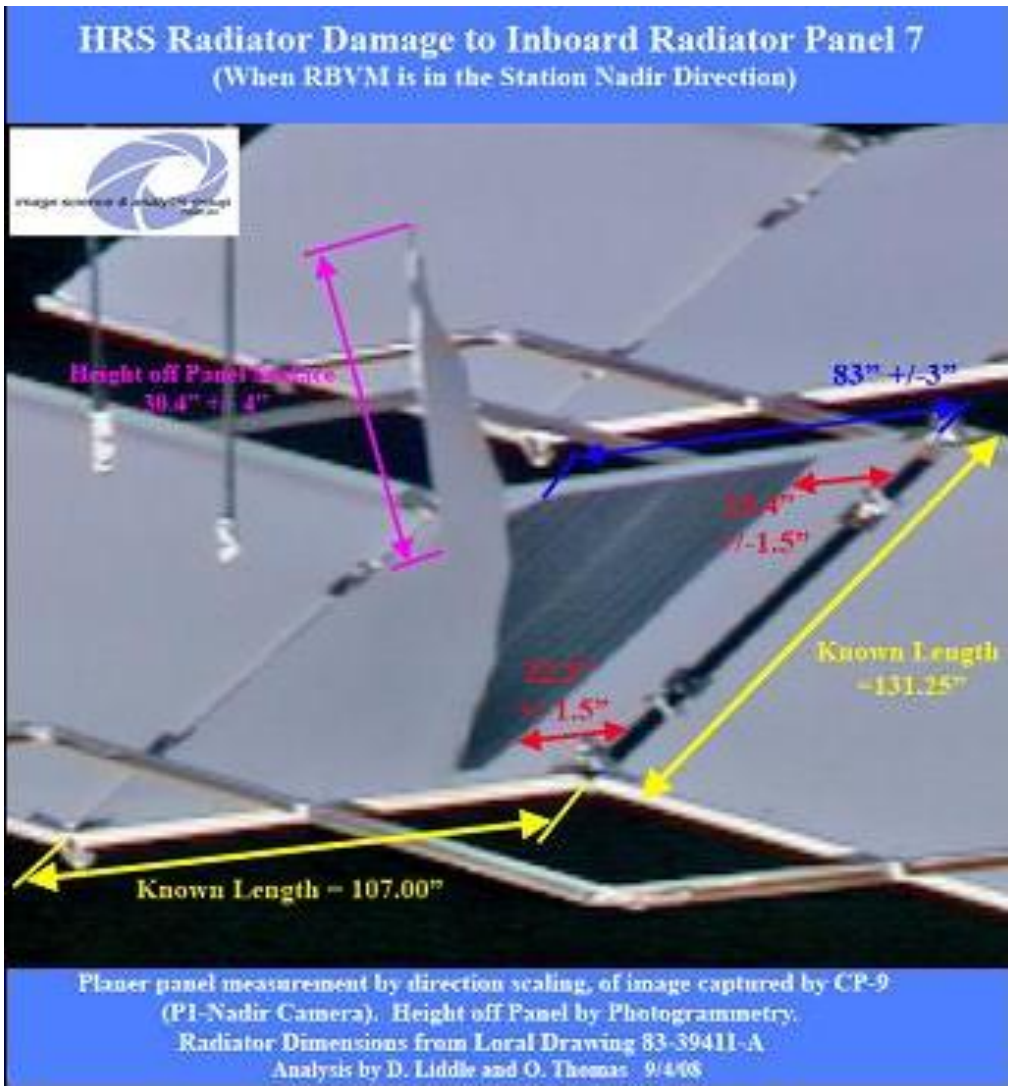


*Figure 4.0-1. HRSR S1-3 Panel 7 Damage*

A detailed image survey showed that approximately half of the panel face sheet had peeled up, but was stable (i.e., not liberating debris) and not increasing in size (Figure 4.0-1). The large section of the peeled up face sheet contained perimeter bolt shearing and tearing, sheared face sheet material, and debonding from one of the adjoining face sheets. The peeled up sheet had significant wrinkles, was debonded from the internal materials, and contained one micrometeoroid orbital debris (MMOD) impact penetration exit (Figure 4.0-2). The back sheet had a small area of wrinkles and some debonding on the outer edge (Figure 4.0-3).

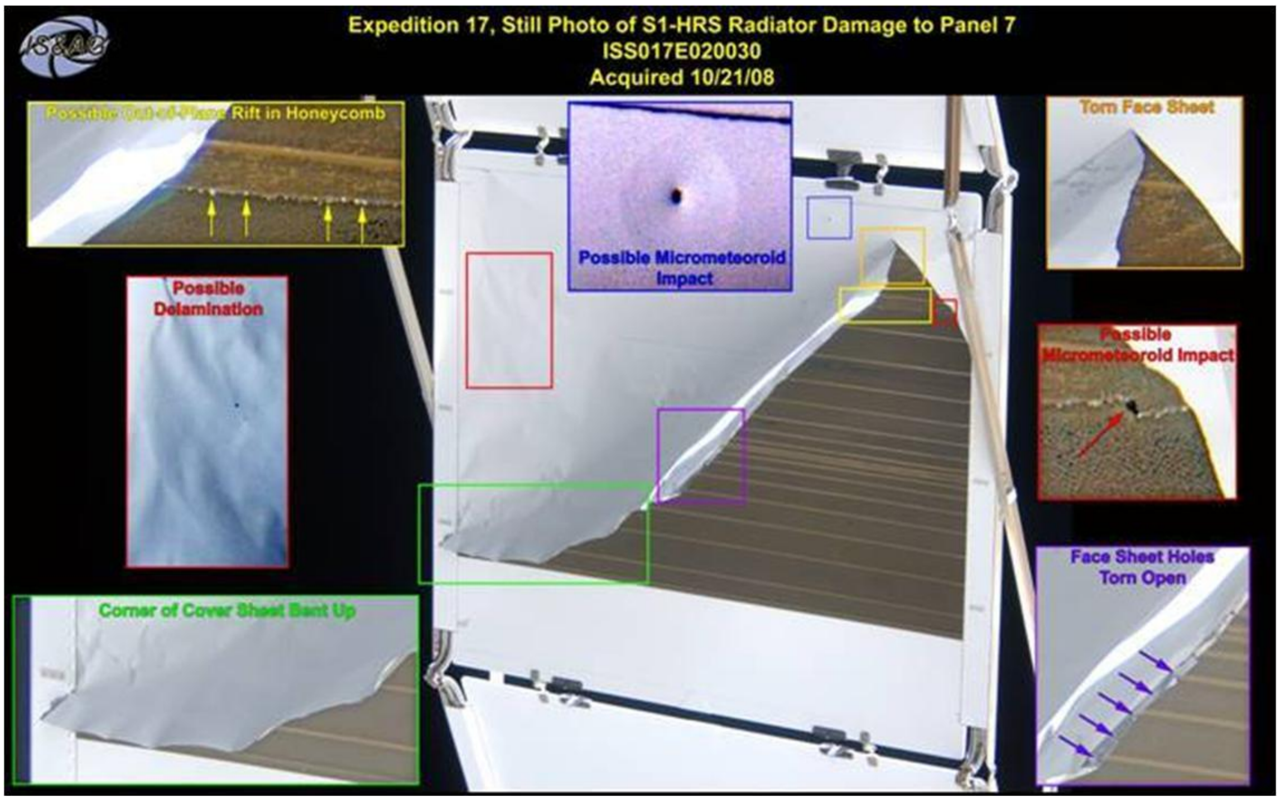


*Figure 4.0-2. Initial Damage Assessment of HRSR S1-3 Panel 7 Survey*

*Figure 4.0-3. S1-3 Panel 7 Back Side Face Sheet*

On February 18, 2009, the ISS Program Manager, Mr. Michael Suffredini, requested the NASA Engineering and Safety Center (NESC) to support the NASA and Boeing External Active Thermal Control System (EATCS) ISS system teams to determine the possible causes of the HRSR face sheet damage.

The NESC supported the team by providing nondestructive evaluation (NDE) expertise to help analyze the ISS infrared (IR) imagery. The analysis found no clues as to why the face sheet peeled up. The joint team identified the remaining panels had no identifiable face sheet anomalies, but identified one panel with a suspected frozen ammonia flow tube.

The NESC sponsored development of a LS-DYNA® model to assess the plausibility of an internal pressure type root cause for the radiator face sheet failure. The radiator face sheet geometry was modeled using basic physics and refined through iterations, which included progressively higher fidelity representations of the radiator face sheet and its attachment to the radiator panel. The analysis showed that low pressure in a large void beneath the face sheet could induce face sheet peeling similar to that observed in the ISS imagery.

The NESC funded the Boeing EATCS ISS system team and the radiator vendor, Lockheed Martin Missiles and Fire Control (LMMFC), to conduct limited testing of eight qualification radiator panels and flight tubing stock. The panels were rechecked for flaws with samples extracted from suspect areas. The checks found no detectable voids or anomalies. A surface flaw was found in the tubing stock, which would have been dispositioned to use "as is."

A small (~10-inch × 10-inch) and a large (15-inch × 20-inch) panel section was sealed at the edges with a pressure feed port installed in the manifold. Each test was to reach 150 pounds per square inch gauge (psig) pressure, but both test articles exhibited internal void volume growth at about 20-40 psig during the helium leak test with audible popping sounds. The face sheet on the small panel was removed and void areas (measuring ~0.5-inch width) observed between the un-vented honeycomb cores in the span between two flow tubes. The gas fed into the panel separated the face sheet near the void pocket and started to form new voids spaced approximately 2-3 inches apart, see Figure 4.0-4. The face sheet separation could allow the gas to jump a tube extrusion and start a new void between adjacent tubes. The face sheet dimples and void patterns were similar to the features seen on the backside of the damaged ISS flight HRSR panel 7. This is a positive indication that the ISS radiator panel 7 had either an ammonia or nitrogen ($N_2$) internal leak.

The NESC, NASA, and Boeing EATCS ISS system teams agreed the face sheet peel up was a dynamic pressure event that was caused by a slow internal tubing leak over several years with the peel up triggered by one of two different ways. One could have been that the face sheet failure occurred when the pressure and void ratio increased to the point that caused a dynamic face sheet peel. The other could have been the face sheet peel was initiated by an MMOD impact (Figure 4.0-2) and subsequent shock wave into the gas void. The deformed ring around the MMOD hole indicates that this impact may have occurred with gas in the void area adjacent to the exit hole, which supports the scenario that the impact wave triggered the face sheet release and displacement.

The NESC-supported tasks contributed to the overall understanding of the HRSR S1-3 panel 7 failure. LS-DYNA® physics-based analysis duplicated many of the features observed in the on-orbit face sheet imagery supporting the notion that the failure was due to a pressure event. Testing demonstrated the formation of islands of delamination and suggested how face sheet delamination may have precipitated the panel failure.

The NESC recommends the ISS Program should continue to monitor operational radiator panels with high-resolution videos and imagery in the effort to detect panel face sheet, and should obtain high-resolution imagery to verify there are no face sheet deformations prior to the first ammonia fill.

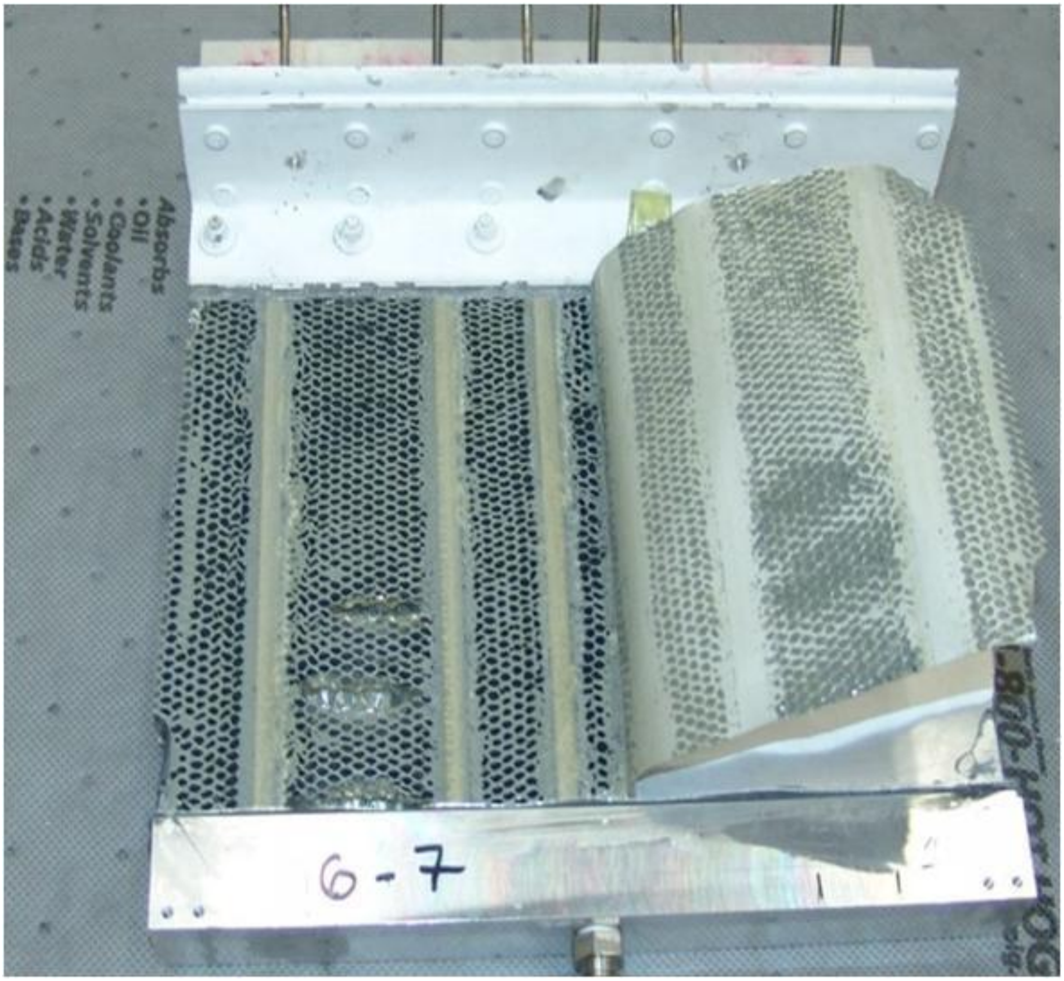


*Figure 4.0-4. Panel Test Segment with Face Sheet Peeled Back*

# 5.0 Problem Description

## 5.1 ISS HRSR Description

The HRSR (Figure 5.1-1, top right and left) is a part of the ISS EATCS. The EATCS is a pumped ammonia liquid system that collects waste heat with coldplates and heat exchangers (HX) from truss electrical power system (EPS) and ISS modules' internal active thermal control systems (i.e., liquid water loops). The waste heat is transported to the HRSR where it is rejected to space. The EATCS does not directly collect heat from the Russian modules.

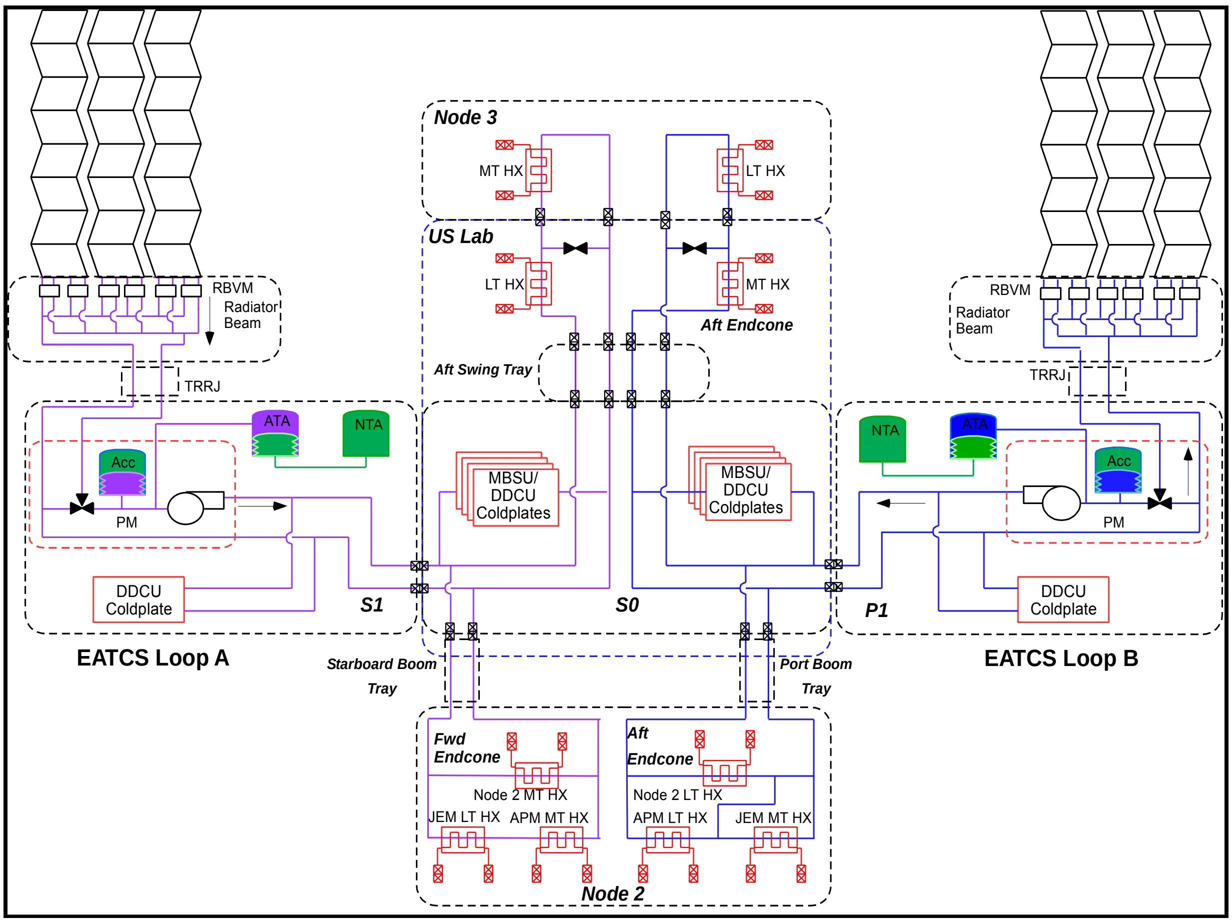


*Figure 5.1-1. EATCS Loop A and B Schematic*

The EATCS provides the collection, distribution, and rejection of excess thermal energy produced by the EPS distribution equipment contained on the S1 and S0 trusses in addition to the excess thermal energy produced in the pressurized modules. The primary EATCS components are located on the S1 (loop A) and P1 (loop B) trusses (Figure 5.1-1). The EATCS is primarily a parallel system where flow is provided to the heat acquisition devices from a main trunk line that extends from S1/P1 through S0 on to the pressurized modules. The heat acquisition devices include the DC-to-DC converter unit (DDCU) coldplates on S1/P1, main bus switching unit and DDCU coldplates on S0, and the interface HX located on the pressurized modules.

Ammonia is pumped through each loop via a pump module (PM) (Figure 5.1-2), and the PM flow control valve (FCV) controls the delivered cooling ammonia temperature by mixing cold radiator fluid with warm radiator bypass fluid that has collected the waste heat from the ISS systems.

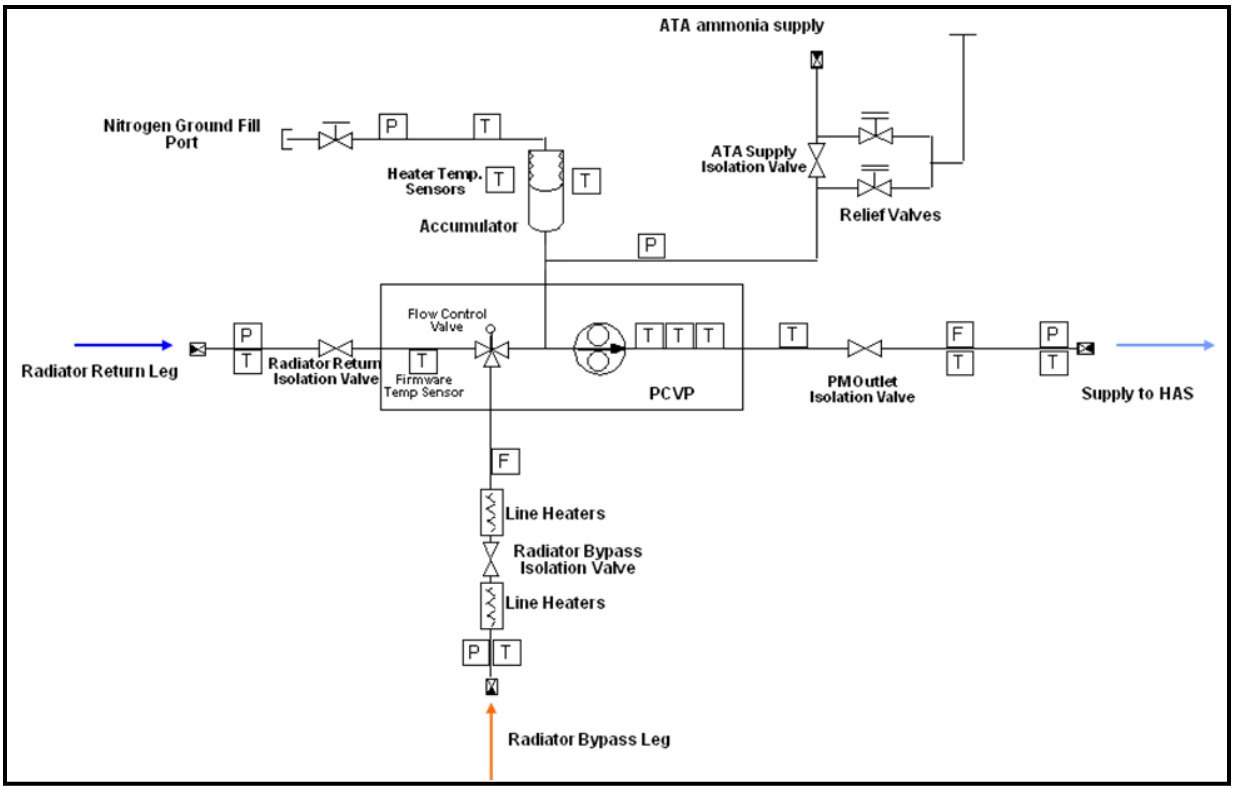


*Figure 5.1-2. PM including FCV*

Ammonia loop fluid thermal expansion make-up is provided by an ammonia tank assembly accumulator that maintains the ammonia loop pressure above its vapor pressure. The FCV routes the warm flow to the thermal radiator rotary joint to the truss radiator beam. At the radiator beam, the ammonia flows through up to six separate flow paths, two per radiator orbital replaceable unit (ORU) for the three radiator ORUs (Figure 5.1-3). Each flow path can be isolated and vented by the radiator beam valve module. The radiator return temperature can be regulated by varying the panel face angle with respect to the Sun and Earth. Each of the three deployable and retractable radiator ORUs has eight panels in a scissor deployment mechanism and each ORU can be deployed separately. Figure 5.1-4 shows the scissor deployment mechanism during the photovoltaic radiator (PVR) deployment and in the fully deployed state. The PVR and the HRSR share a common design approach.

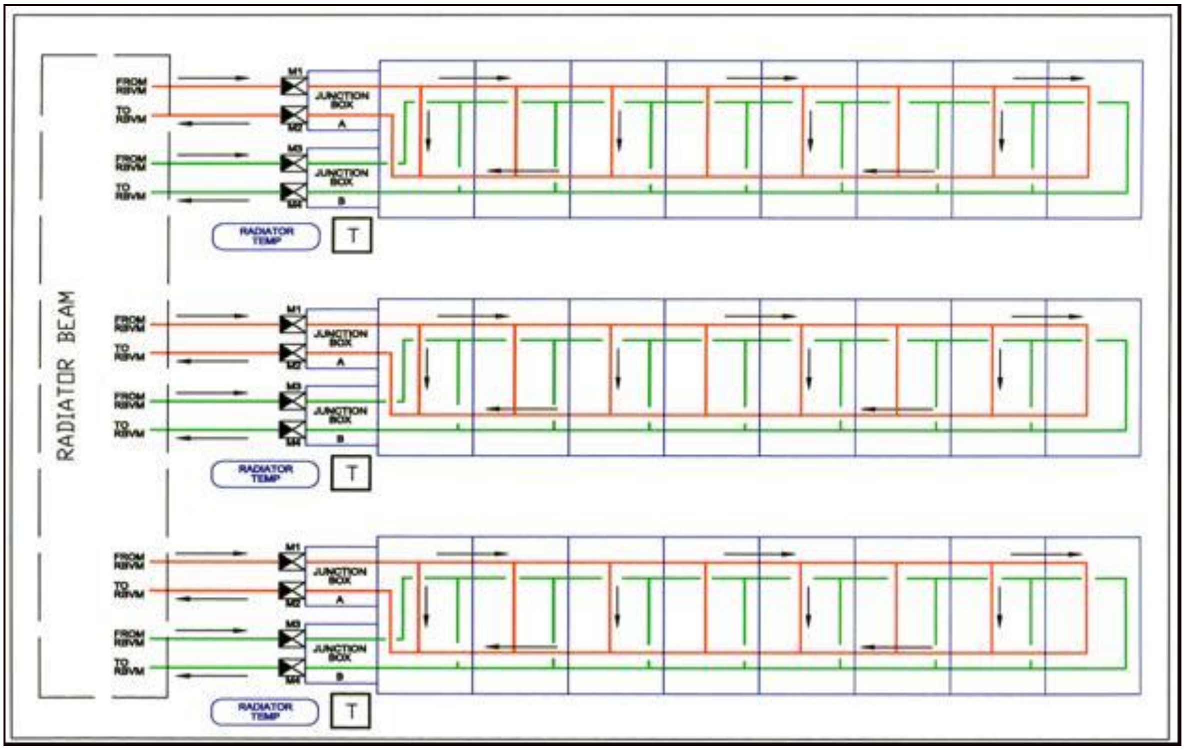


*Figure 5.1-3. EATCS HRSR Array showing the Dual Flow Paths*

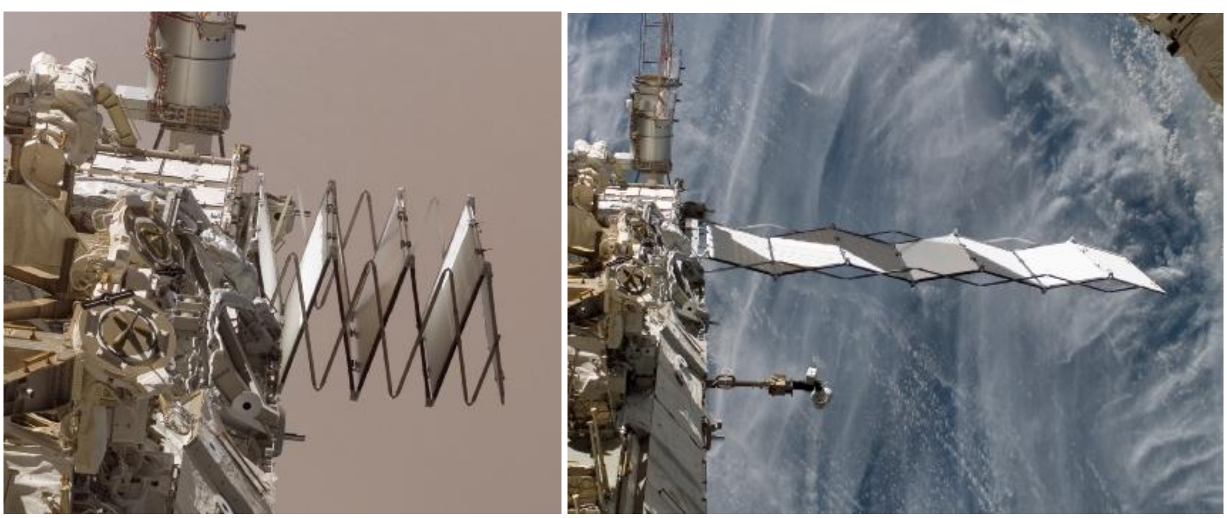

*Figure 5.1-4. PVR Deployment*

The radiator panel design has honeycomb layers epoxy bonded between face sheets. The face sheet optical properties promote good heat rejection and low heat absorption. Each panel is 9 feet by 11 feet wide and rejects heat from both sides. Each face sheet is comprised of three pieces of 0.010-inch-thick aluminum with a middle sheet, 48 inches wide, that overlaps the two outer sheets each by 1 inch. The overlap is bonded to the adjacent face sheets (35 and 23 inches wide) as shown in Figure 5.1-5.

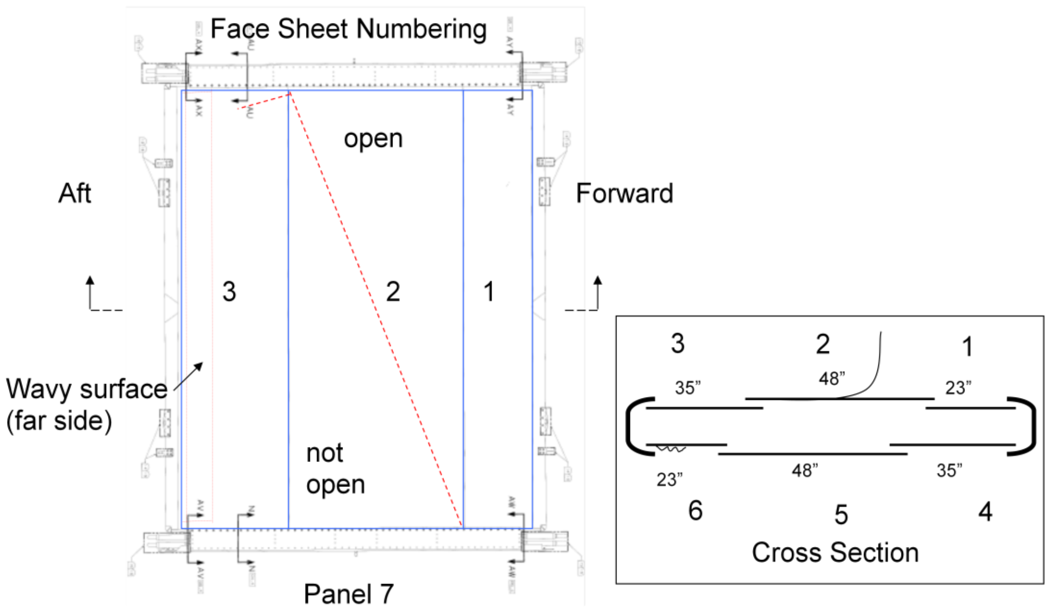


***Figure 5.1-5. HRSR Panel Face Sheets View from Nadir Side***

Figure 5.1-6 shows the radiator panel internal design. Two separate loops flow through the panel. Each loop alternates tube paths and both flow across the panel in the same direction with inlet and outlet headers on each side as shown in the upper right of Figures 5.1-6 and 5.1-7.

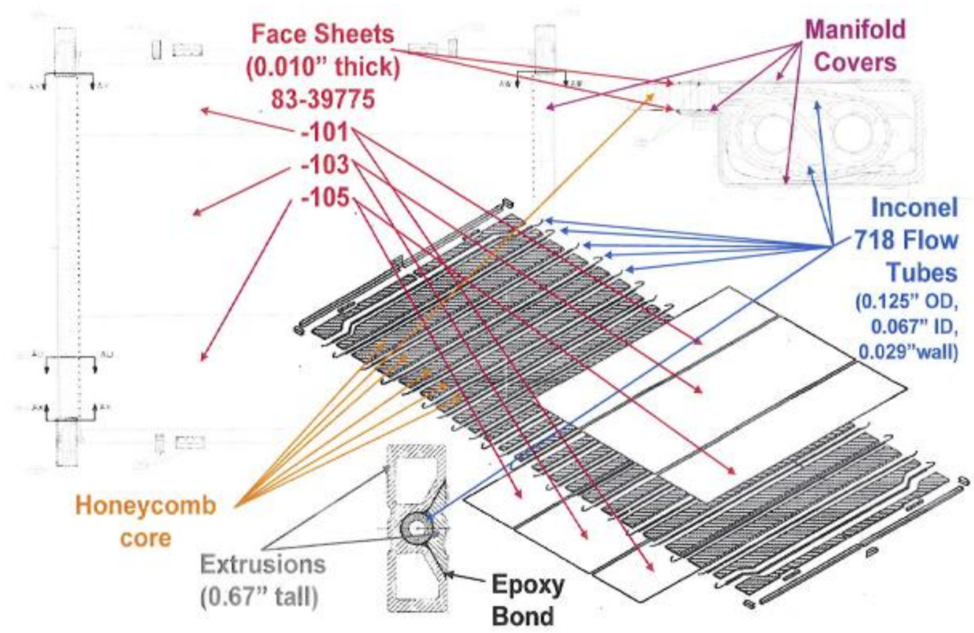


*Figure 5.1-6. Radiator Panel Design Overview*

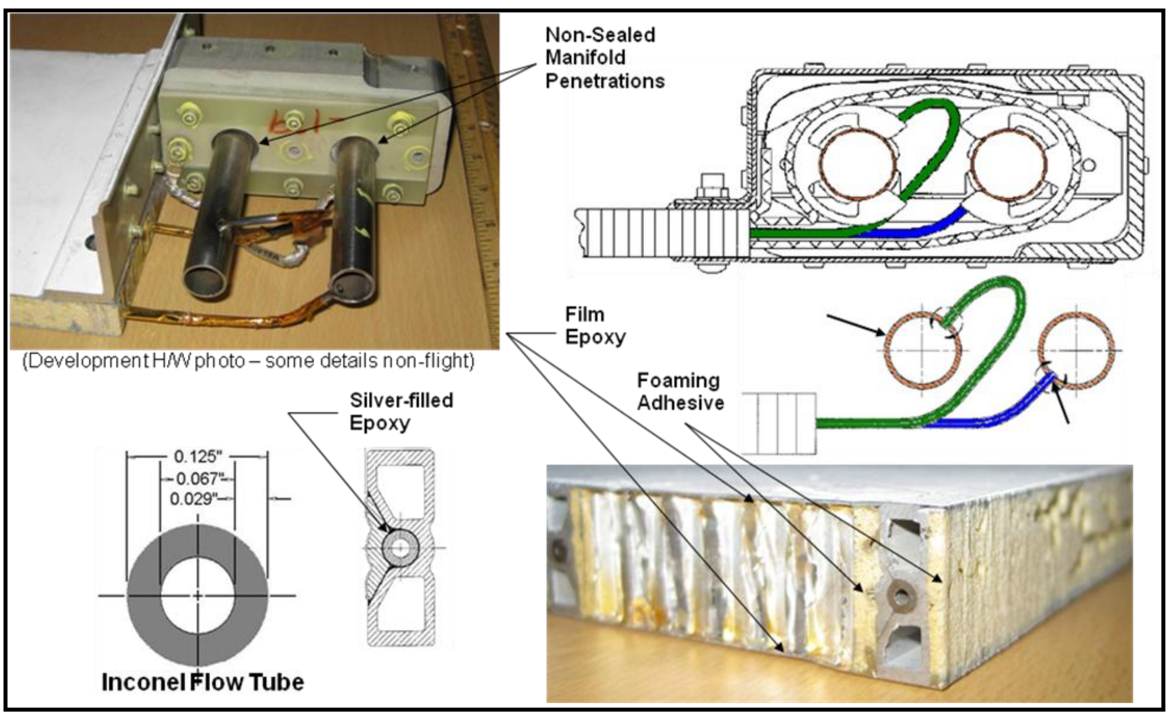


*Figure 5.1-7. Radiator Panel Construction Details*

The tube spacing is closer near the panel center to prevent ammonia freezing due to the higher head load density in the radiator panel. The 0.125-inch Inconel® 718 tubes have a wall thickness of 0.029 inches and are individually proof tested to 39,000 psig for freeze tolerance. Each tube is encased in an aluminum extrusion that is epoxy-bonded to both face sheets. Within each extrusion, the tube is bonded using silver-filled epoxy to maximize heat transfer as shown in Figures 5.1-6 and 5.1-7.

### 5.1.1 Hydraulic Rupture Analysis

The periodic ammonia freezing of the two end panel ORU outer flow paths has the potential to cause an existing flaw in the tubing to grow and create a leak. However, analysis of the panel testing and design indicates that this should not happen under freeze cycling conditions. The panel flow paths were designed to tolerate multiple freeze cycles and withstand the extremely high pressures between two freeze blocks. The outer flow tubes are coldest because their tube pitch is greatest. The larger available radiation area decreases the fluid temperature, which increases its viscosity and decreases the flow rate. Analysis of hydraulic lockup failure in other tubing and piping systems showed that a hydraulic rupture creates a leak path that is related to the flow path diameter and the hole size that is near or larger than the tube diameter. Since there was no detectable ammonia serviced loop leak rate change in the panel after the peel up event, a hydraulic rupture did not occur.

## 5.2 HRSR Design, Flight and Assembly Data

The NESC conducted a review of design, flight, and assembly data to determine whether or not there were any problems observed during construction and assembly.

The radiator panel interior is an unvented honeycomb structure that is sealed by an epoxy bond to the face sheets producing a pressure vessel design. The panel interior volumes could have trapped air during the fabrication vacuum bagging and autoclaving processes. Some voids could have 14.7 pounds per square inch absolute (psia) air trapped in them. However, the number and size of these voids, and the pressure differential would be insufficient to cause a face sheet peel up without other contributing factors based on the Space Shuttle Orbiter radiator and coldplates history and testing.

The ammonia flow path design consists of parent metal tubing through the sealed interior with no welded joints or other junctions internal to the radiator. The supply and return ammonia headers and tube connections are outside of the sealed heat rejection section, so the design risk of a leak in the internal sealed section was considered by the ISS Program to be improbable.

Each outer edge tube has four bends. However, due to the ductile nature of the Inconel® 718 tubing at the on-orbit operating temperatures, multiple freezing cycles should not increase the risk of a tube crack induced by the bends.

A review of the silver-filled epoxy used for tube bonding to the extrusion, and to bond the extrusion pieces together raised a question regarding compatibility with ammonia. At the request of the ISS Program, the White Sands Test Facility conducted a short-term epoxy ammonia exposure test. The test results were suggestive of a chemical reaction of the silver-filled epoxy with ammonia, but did not answer the question of degradation due to long-term exposure. However, the sealing properties of the silver-filled epoxy were not tested after the ammonia exposure since the sealing capability of the extrusion was not a design requirement since the tubing is raw stock parent metal and was considered low risk for leaks. The sealing capability of the extrusion silver-filled epoxy for ammonia and $N_2$ was not tested and it is unknown if the epoxy would have prevented a flow tube leak from pressurizing the radiator panel interior.

The NESC team reviewed the radiator panel assembly and test procedures conducted during the assembly:

- A tap test was conducted during assembly to detect face sheet bond voids of more than 1-square-inch. The tap test technique was validated and was performed by trained LMMFC technicians. The tap testing detection limitations of the qualification and spare flight panels would not detect a 0.5-inch × 2-inch void or smaller over the flow tube extrusions or 0.5-inch × 0.5-inch or smaller void over the honeycomb core.
- The panel internal flow tubing was proof-pressure-tested at 39,000 psig prior to installation in the radiator panel and had a leak rate of less than $1.7 \times 10^{-3}$ standard cubic centimeters per second (sccs) $N_2$.
- The eight-panel array assembly mechanical and welded connections were helium-leaked tested for the 15-year life requirement.
- The panel array was shipped for flight with 75-80 psia $N_2$ pad pressure.

Boeing reported that a review of the assembly and prelaunch testing data for the HRSR S1-3 panel 7 found no discrepancy reports or waivers that could reasonably be attributed to the failure. The panel 7 and array assembly leak rates were not recorded, but were verified by LMMFC quality assurance to meet the 15-year requirement of $1.7 \times 10^{-3}$ sccs $N_2$.

After the S1 radiator arrays were launched and installed on ISS during flight 9A in October 2002, a review of the flight data determined that there was a $N_2$ pad pressure leak of approximately $2 \times 10^{-5}$ sccs from the S1-3 radiator array flow path 1 side. This leak rate was less than half of the allowable leak rate requirement and some percentage of the leak was through the seals in the array quick disconnects. There was no indication of a $N_2$ leak from flow path two prior to ammonia servicing in November 2007, as shown in Figure 5.2-1. The ammonia quick disconnects (QDs) leakage allowable is $9.2 \times 10^{-5}$ sccs $N_2$ and the panel 7 flow path's proof pressure test minimum detectable leak rate was $1.5 \times 10^{-3}$ sccs $N_2$. The on-orbit leak rate was not detectable by the ground as tested so it may have existed prior to launch.

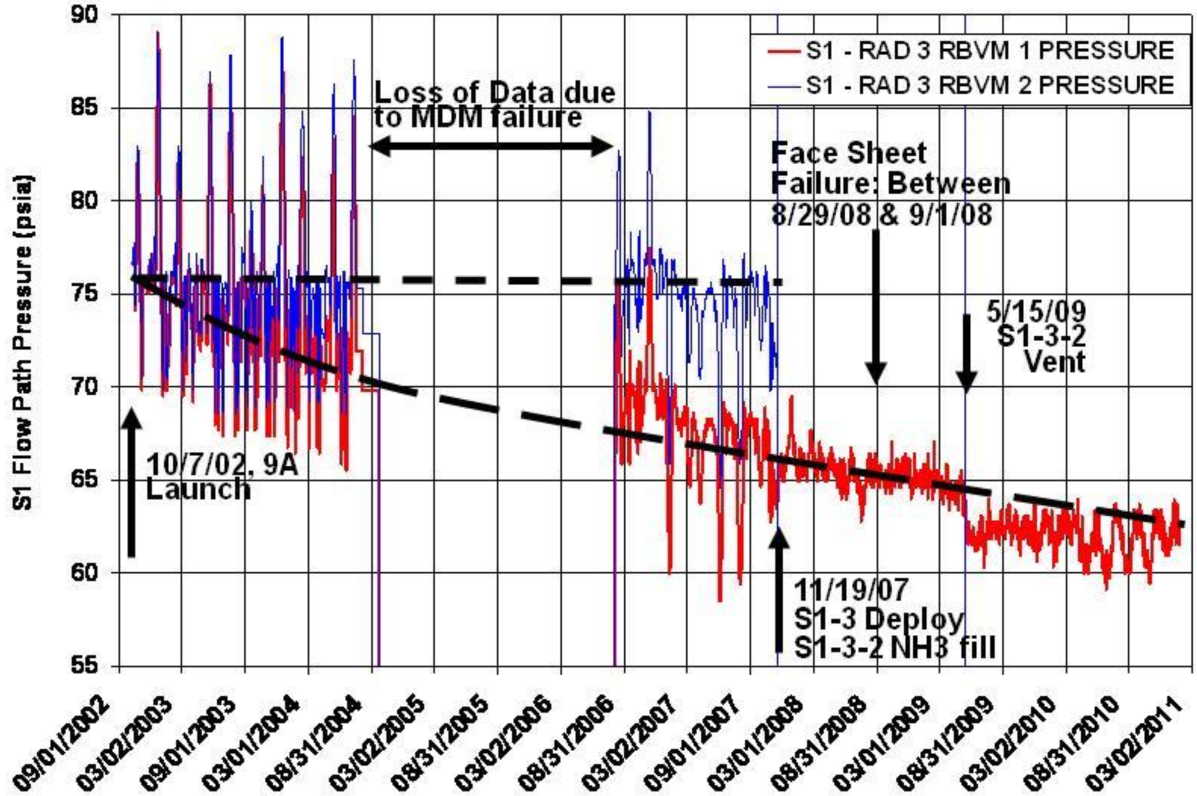


***Figure 5.2-1. S1-3 Array Loop 1 and 2 $N_2$ Pressures***

After $N_2$ venting from S1 array flow path 2, the loop was connected to the ISS loop A, as shown in Figure 5.1-1, and serviced with ammonia. The leak detection capability of loop A is limited and requires a large leak rate to be seen in the flight data. A leak rate as high as $1.5 \times 10^{-2}$ sccs $N_2$ the requirement that can over pressurize the panel cavity over several years would be below the serviced ammonia loop A leak detection capability. Therefore, an internal panel flow tube $N_2$ leak from side 1 or ammonia from side 2 could have existed or occurred and leaked through the extrusion silver-filled epoxy into the panel interior and over pressurized the face sheet.

Camera monitoring of the face sheet during ISS events that can induce loads and vibrations onto the ISS determined that the tip of the peeled up face sheet is deflecting up to 8 inches during these events. Although this displacement was on the face sheet free end the remainder of the panel was not displacing to the same magnitude. A concern was addressed for flexure of the flow tubes that could induce loads on the tubing connection to the headers and could induce a leak at the welded tubing connection, see top half of Figure 5.1-7. Note that delivery, installation, and activation of Node 3 had not occurred when the panel 7 failure was detected. Loss of a large quantity of ammonia from loop A could jeopardize this critical assembly step, induce a motion into the ISS platform, and require loop A ammonia reservicing. As a precaution, the NASA and Boeing EATCS ISS system teams recommended isolating the S1 radiator array from loop 2 and vented the ammonia overboard on May 15, 2009.

The detailed images taken of the radiator panels found that there were witness marks of panel 7 face sheet impacting on panel 8. This verified that the peel-up event was a dynamic event with the panel 7 sheet returning to near vertical to panel 7 after the impact on panel 8.

## 5.3 Review of MMOD Test Coupons and Data

Image review of the ISS S1-3 panel 7 with the face sheet peeled up showed an MMOD impact entering on the panel back side and exiting near the panel top side outer edge, as shown in Figure 5.3-1. The team reviewed three reports [refs. 1, 16 and 17] on MMOD testing and analysis results to determine if an impact could induce the panel 7 damage. The findings in these reports indicated that MMOD particles would induce only localized damage for the size (~0.375-inch-diameter) round exit hole observed in the panel face sheet. None of the test results of larger particles indicated that MMOD could induce the observed face sheet peel. Figure 5.3-2 shows an exit hole through a radiator-like panel that is similar to the hole that was observed on panel 7. However, none of these reports had impacts on a pressurized void. So, no conclusions could be made if the MMOD hit on panel 7 was the initiation impulse or the hit occurred after the face sheet was displaced. MMOD impact testing through pressurized voids by Boeing showed a similar deflection ring around the exit hole, as shown in Figure 5.3-2. This could indicate the MMOD particle impacted a pressurized void in the panel and the impact shock wave initiated the dynamic event of the radiator face sheet peel up.

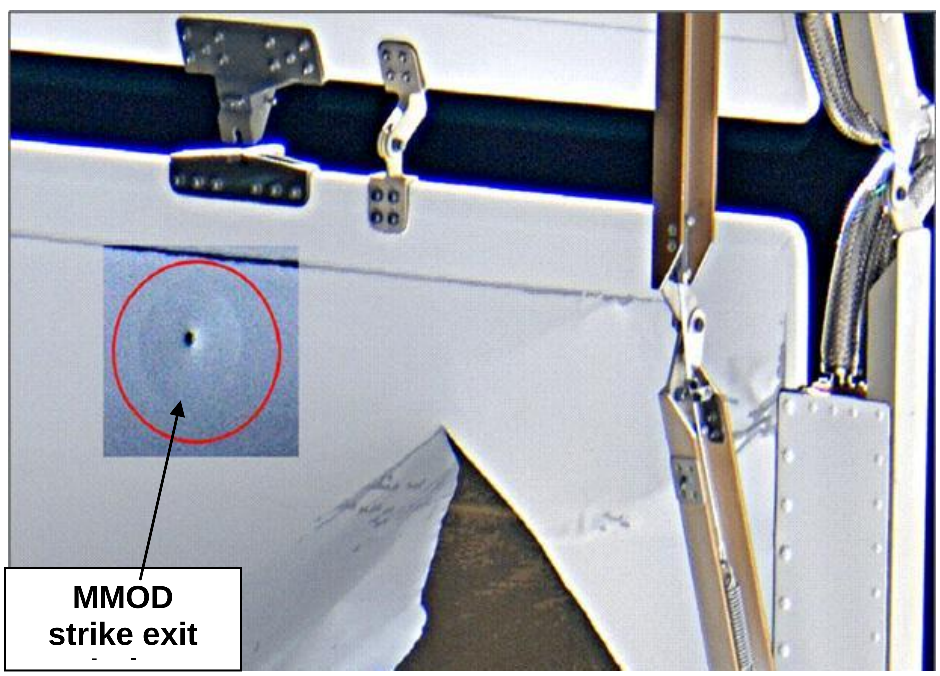


*Figure 5.3-1. Panel 7 MMOD Impact Exit Hole ~ 5/16 Inch (Note ring around hole)*

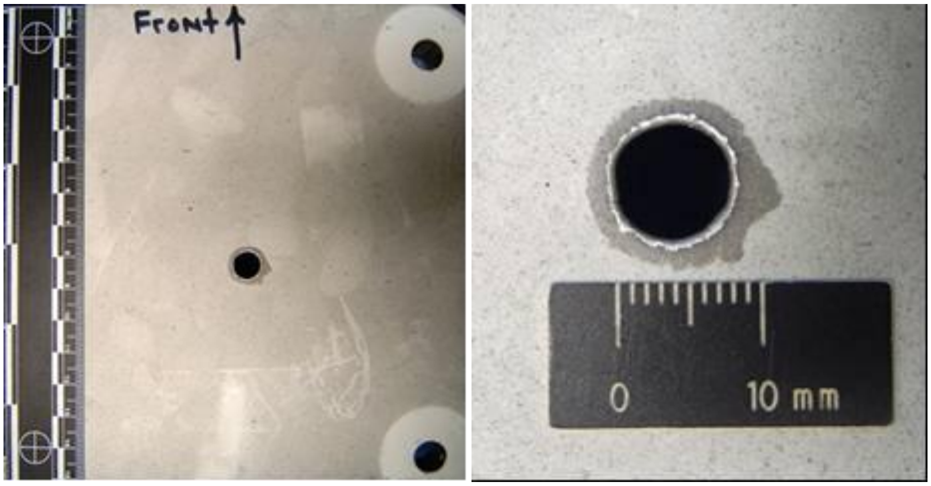


***Figure 5.3-2. Impact Test #9; Exit Side and Exit Hole Size (~0.31-inch-diameter) for a 6.35 mm Projectile [ref. 1]***

## 5.4 IR Thermography

The NASA and Boeing EATCS ISS system teams requested IR video of the radiator arrays during an ISS extravehicular activity (EVA) in March 2009 (before the array was isolated and vented), using the IR camera previously developed by the Space Shuttle Program and qualified for flight on the Space Shuttle Orbiter and ISS. The team made adjustments in the IR analysis software to optimize viewing and interpretation of data in the areas of interest. Figures 5.4-1 through 5.4-3 show the IR images and processed data, which highlight the panel flow paths for a typical HRSR panel. Figure 5.4-1 shows the raw temperature image, the highest temperatures are near the center of each panel where the flow paths are the closest to each other creating a higher local flow and warmer exit temperatures. Figure 5.4-2 shows a temperature gradient as an example of how the IR imagery can be analyzed. Figure 5.4-3 shows a three-dimensional plot of the IR imagery temperature data for a normal panel showing the flow paths for the underlying coolant tubes.

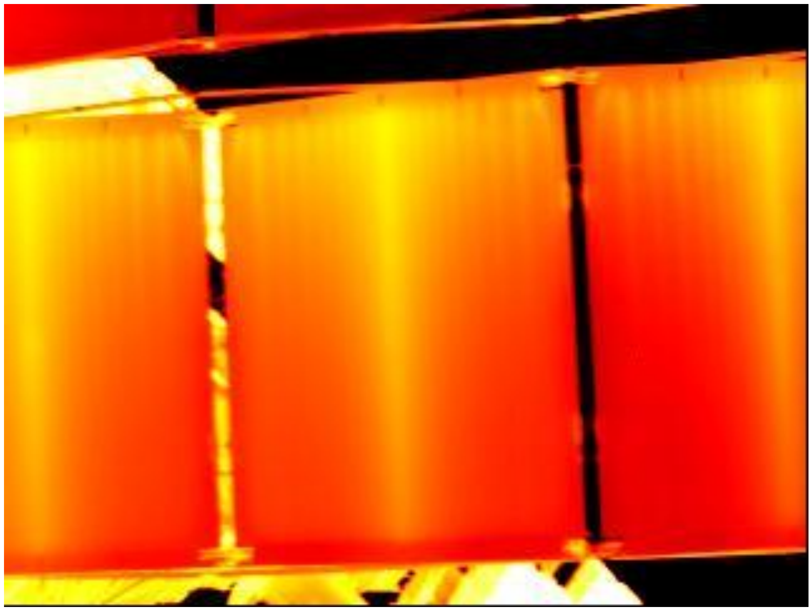

***Figure 5.4-1. Raw Temperature Data Showing Normal Radiator Panel (Center) Temperature Gradients***
*(Note red indicates colder and yellow indicates warmer)*

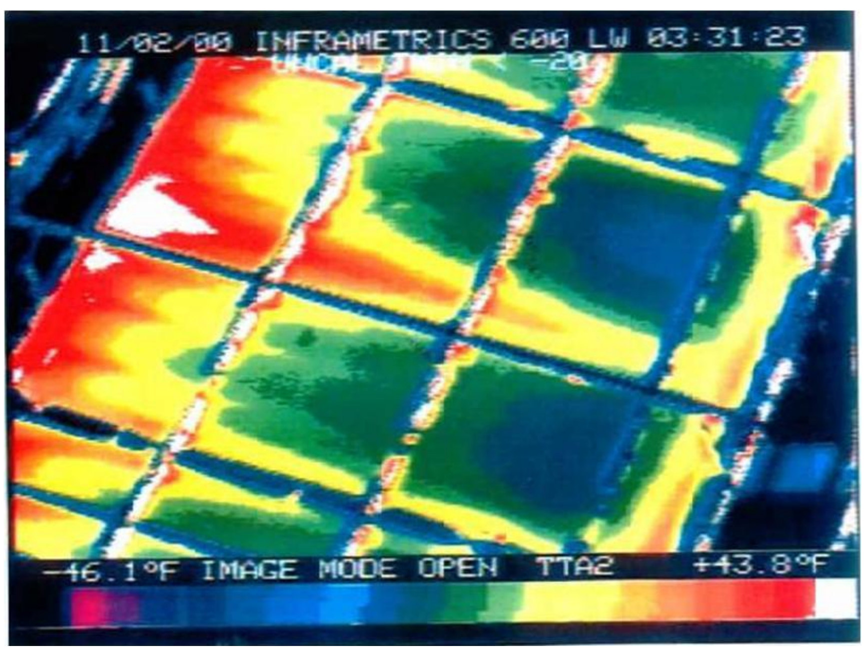


***Figure 5.4-2. Enhanced IR Imagery of a Thermal-Vacuum Ground Test of a Radiator Panel with Temperature Range***

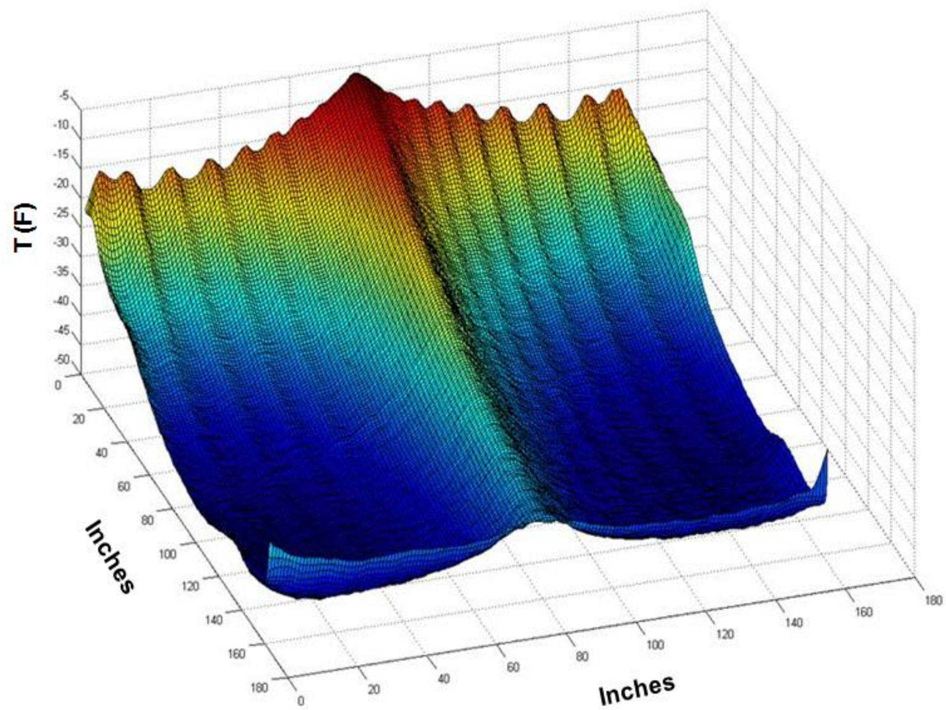


*Figure 5.4-3. Normal Radiator Temperature Contour Plot Showing Flow Paths*
*(Note distance in inches and temperature in °F)*

Figure 5.4-4 depicts the raw temperature data for panel 7 showing a possible nearly frozen outer flow tube under an undamaged face sheet (S1-2). The radiator outlet temperature was approaching -100°F. This is the only other potentially anomalous panel found in the IR imagery review.

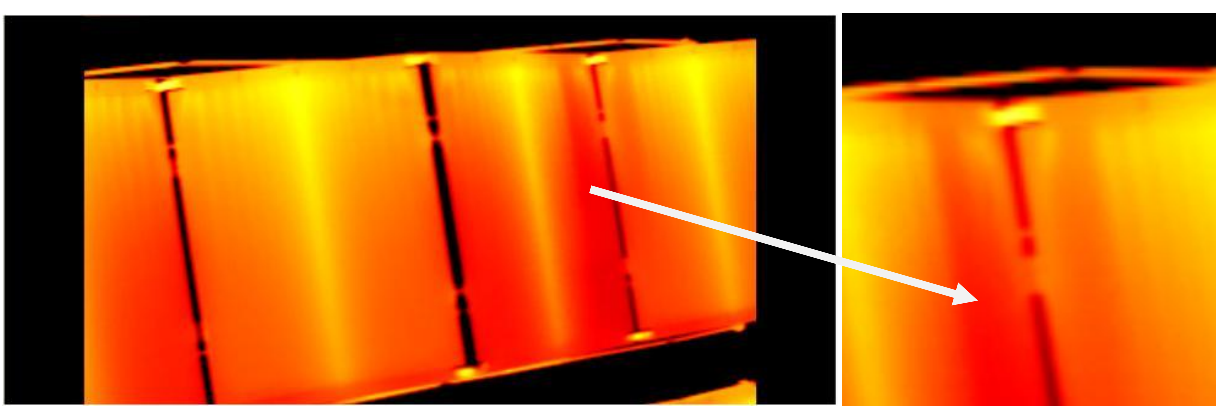

*Figure 5.4-4. Possible Frozen Flow Path on S1-2 Panel 7 (Center Array)*

Review of the IR imagery found usable images for all panels except for some of the P1 panels. The level of detail was greater than expected. Individual flow tubes could be identified in each panel image. The damage to S1-3 panel 7 can be as seen from the back side and the peeled up face sheet side. The IR imagery did not provide any indication of possible cause for the face sheet damage.

Figure 5.4-5 is an example of how the IR imagery temperature data can be analyzed to show that there is heat rejection lost for the area under the peeled up face sheet. However, this reduction has only a small effect on the performance of the total radiator system for Loop A.

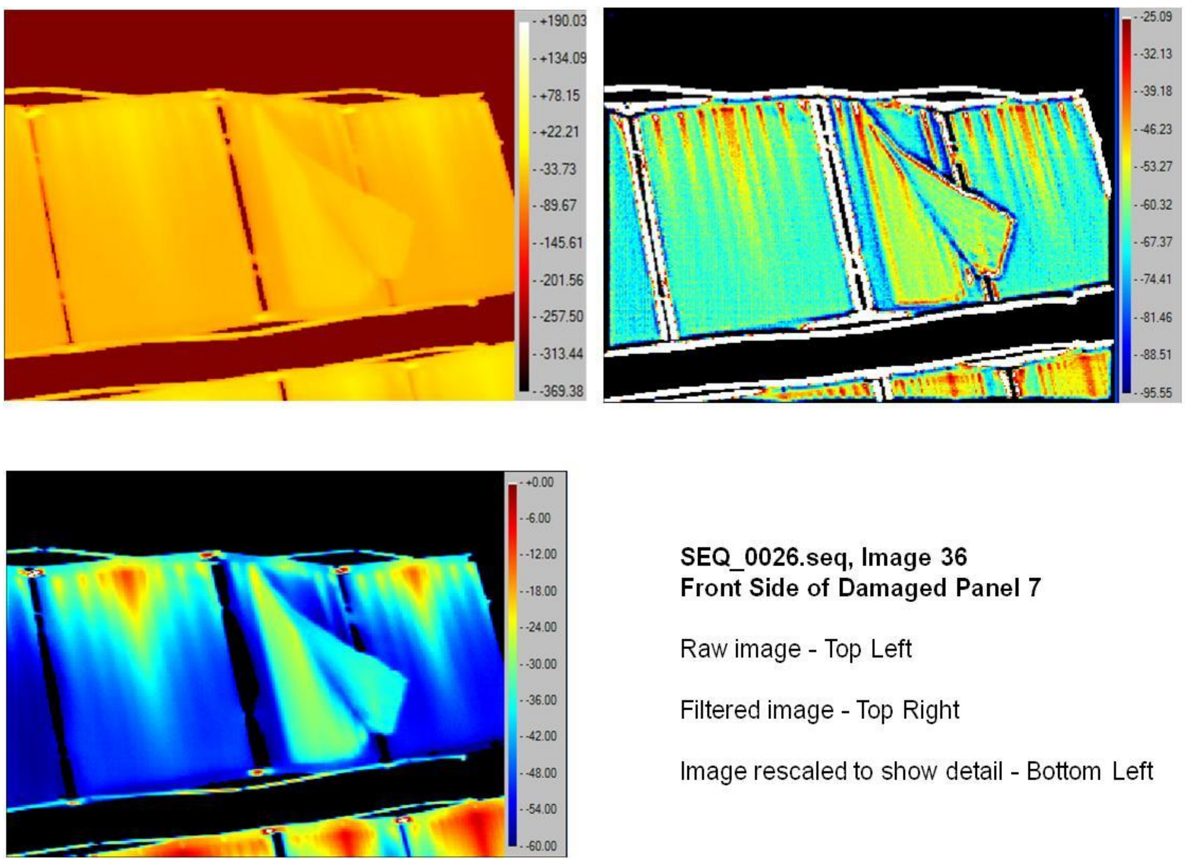


***Figure 5.4-5. IR Imagery Processing Results***

### 5.4.1 NDE Imagery Analysis

To compare adjacent panels quantitatively, a correction is made to the camera viewing angle to each radiator panel. To do this, an affine transform is applied to each panel, which flattens the panel so that the data can be viewed in a planar format. Secondly, a Laplace transform is applied to the temperature data, which can be shown to reduce the steady-state temperature data to the flux through the first layer back surface [refs. 2 and 3], resulting in an improved signal of the flow tubes within the radiator.

The two thermal responses can be considered to be a series of images, $A_i(x, y)$ and $B_i(x, y)$, where $i$ corresponds to time of the image and $x$ and $y$ corresponds to the location of pixels in the image. To register the two thermal data sets, the first unsaturated thermal images (defined as $i = 1$ for each thermal response) are registered to each other. For the cases examined, the baseline data sets are fixed and the data sets from post change are transformed for registration with the initial state. For many cases, a simple rotation and translation is required. However, it is possible that between the data acquisition, the configuration could have sufficiently changed that the specimen plane is in a plane that is rotated relative to initial configuration. For those cases, an affine transform is required.

The affine transform is given by:

$$\begin{bmatrix} a_{1,1} & a_{1,2} & a_{1,3} \\ a_{2,1} & a_{2,2} & a_{2,3} \\ 0 & 0 & a_{3,3} \end{bmatrix} \begin{bmatrix} x \\ y \\ 1 \end{bmatrix} = \begin{bmatrix} x' \\ y' \\ 1 \end{bmatrix} \qquad \text{(Eq. 1)}$$

where $x$ and $y$ are the coordinates of the initial frame of reference, and $x'$ and $y'$ are the transformed reference frame coordinates. The elements of the matrix, ($T_{1,1}$...$T_{3,3}$) are seven independent parameters which represent the affine transform.

When the transformation is a simple rotation by $\theta$, followed by a translation of $x_t$ and $y_t$, and a scaling, then Eq. 1 becomes:

$$\begin{bmatrix} \cos(\theta) & \sin(\theta) & x_t \\ -\sin(\theta) & \cos(\theta) & y_t \\ 0 & 0 & 1/m \end{bmatrix} \begin{bmatrix} x \\ y \\ 1 \end{bmatrix} = \begin{bmatrix} x' \\ y' \\ 1 \end{bmatrix} \qquad \text{(Eq. 2)}$$

where $m$ is the magnification.

Registration of the two thermal responses is performed by selecting a region on interests in A1 $(x,y)$. To determine the proper value for $\psi = [a_{1,1},a_{1,2},a_{1,3},a_{2,1},a_{2,2},a_{2,3},a_{3,3}]$, initial values are chosen for the different elements of $\psi$, and image $B_1(x,y)$ is transformed to $C_1(x,y)$. The pixels of $C_1(x,y)$ that correspond to the pixels of the region of interest in $A_1(x,y)$ are amplitude and offset matched using a least-squares estimation. The sum of the squared differences of the least-squared estimation is used as the cost for a simulated annealing routine that varies $\psi$ to determine $\Psi$, the value of the vector corresponding to the global minimum for the cost. The $\Psi$ is used as the parameters for performing the affine transform of $B_i(x,y)$ for $i = 1$ to $N$ (number of images) to $C_i(x,y)$. $A_i(x,y)$ is then subtracted from $C_i(x,y)$ for $i = 1$ to $N$ to calculate the difference thermography data set.

An example of the results of this process is shown in Figure 5.4-6. A composite specimen with a wedge insert into a delamination was tilted out of the typical measurement plane by approximately 30 degrees and rotated by approximately 16 degrees. This should be considered to be an undesirable initial alignment. However, it is presented as a demonstration of the capability of the registration technique.

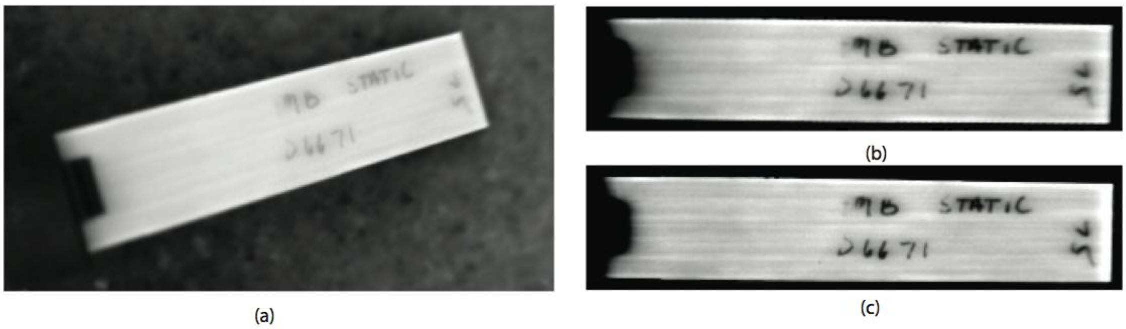


***Figure 5.4-6. Registration of Images Based on Affine Transform***
*(a) Infrared image of specimen tilted out of the normal plane of data acquisition by approximately 30 degrees and rotated by approximately 16 degrees. (b) Results of the affine transform using Ψ. (c) Fixed reference infrared image with tilt ≈ 0 and rotation ≈ 0 that was the target of the optimization routine.*

Applied to the HRSR panels, the images are transformed, as shown in Figure 5.4-7, where the values of the transform matrix are varied to give the optimized mapping of four selected points on the radiator to a fixed size rectangle based on the summed differences of the coordinates of the radiators and the coordinates of the rectangle corners.

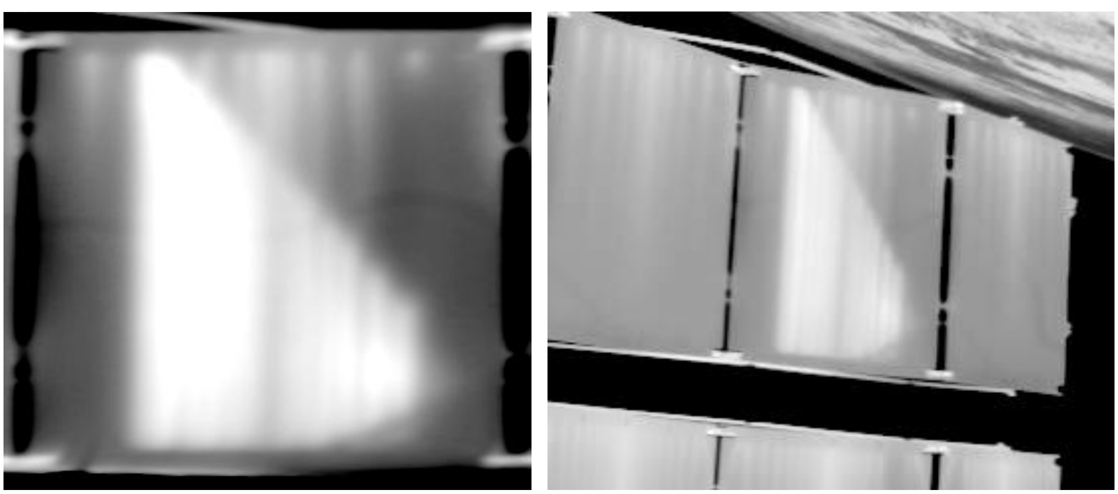

***Figure 5.4-7. Transformation of ISS HRSR Panel from Camera to Normal Views***

After transforming the radiator image from the camera angle to the normal view, a surface laplacian is applied to the thermal data to image the cooling tubes within the radiator, as shown in Figure 5.4-8. It has been shown that for a layered structure in steady state, the laplacian of the surface temperature is proportional to the heat flux out of the first layer.

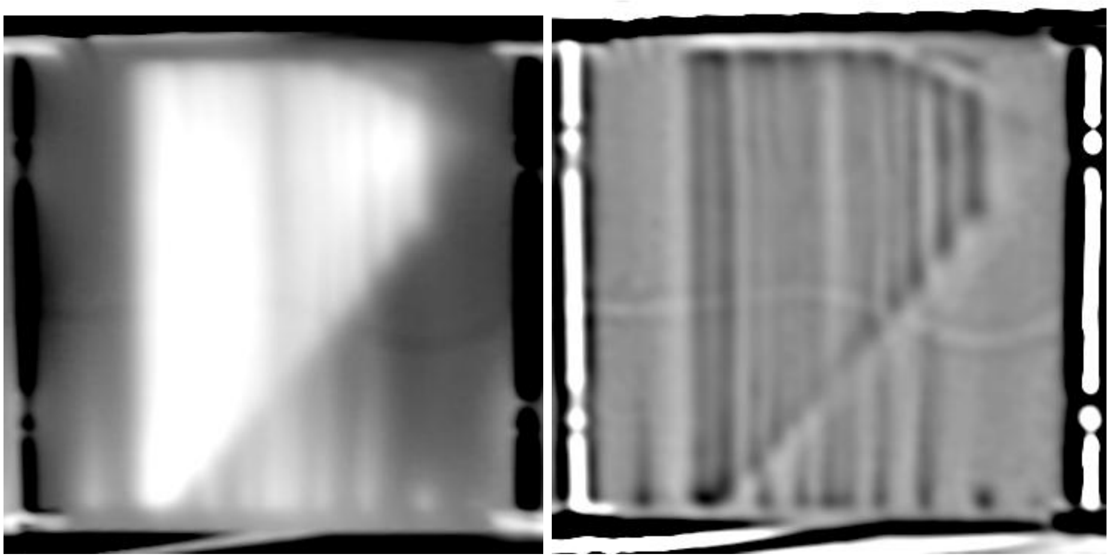

***Figure 5.4-8. (a) Temperature Image of HRSR Panel (b) Laplacian Image***

A comparison of the laplacian images for a damaged panel and an undamaged panel is shown in Figure 5.4-9.

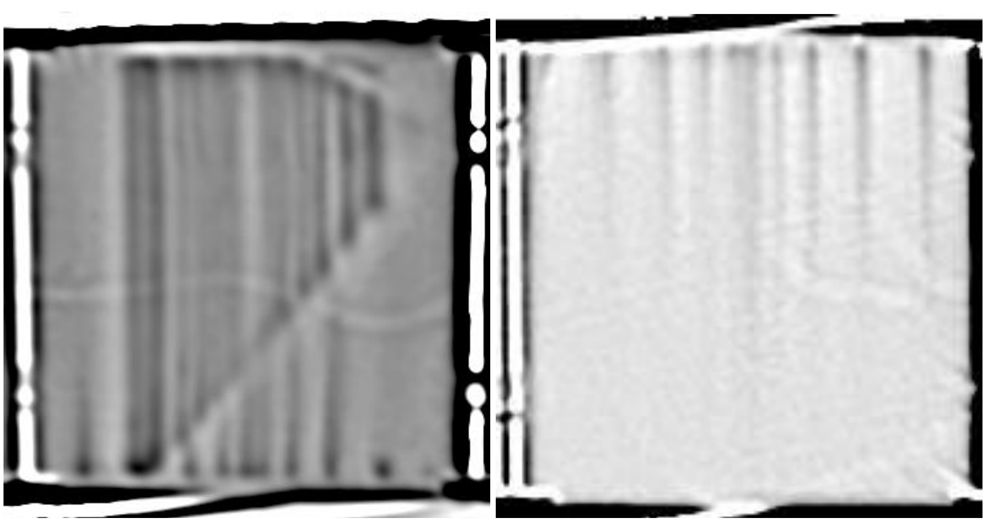

***Figure 5.4-9. (a) Laplacian Image of a Damaged Panel (b) Laplacian Image of an Undamaged Panel***

Each cooling tube was analyzed by plotting its temperature along the length of the tube, and the analogous tube in each panel directly evaluated, see Figure 5.4-10. Temperature profiles for underperforming cooling tubes are readily apparent. The tube entrance is on the right-hand side of the figure.

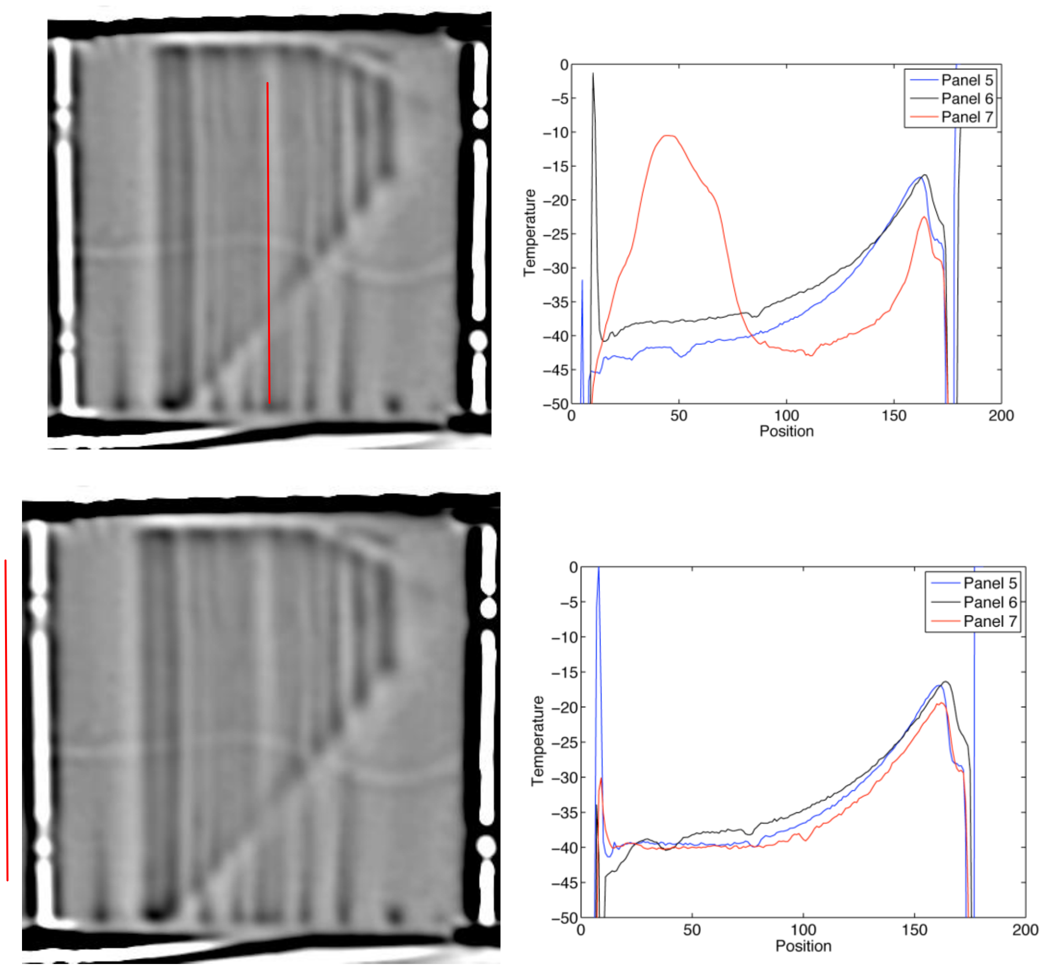


***Figure 5.4-10. Temperature Profiles for Analogous Cooling Tubes Compared for Each Radiator***

In summary, inspection of the performance of the radiators included analyses that converted the raw temperature data, taken at different viewing angles from the astronauts' position to each radiator panel, to a view that is normal to the viewing angle. To compare adjacent panels quantitatively, a correction is made to adjust for the change in the camera viewing angle to each radiator panel using an affine transform applied to each panel, which straightens the panel so that the data can be viewed normal to the screen. A Laplace transform is then applied to the temperature data, which can be shown to reduce the steady-state temperature data to the flux through the back surface of the first layer. Panels with any damage are then easily identifiable. Each cooling tube was analyzed by plotting its temperature along the length of the tube, and the analogous tube in each panel directly evaluated. Performance or non-performance of suspect cooling tubes was then measured.

## 5.5 Form Factor Analysis

In support of the IR imagery review effort, the NESC team performed HRSR form factor analysis to verify the contribution of radiator view-to-space to the overall observed temperature trend. A form factor is a measure of how one object “sees” another. Form factors range from zero (i.e., no direct view from one object to another) to unity (i.e., indicating a perfect, unobstructed view). In this instance, the analysis sought to calculate how each radiator surface could “see” space. A low form factor is indicative of a poor view to space; a high form factor is indicative of a good view. Since radiator heat rejection is due in part to the radiating surfaces’ view to a cold sink environment, understanding the view and the blockage associated with surrounding ISS components was critical to understanding the overall temperature trending. The analysis was complicated by the articulation of the radiators and the solar arrays. A subset of cases studied is presented in Table 5.5-1. Note: thermal radiator rotary joint (TRRJ); solar alpha rotary joint (SARJ); and beta gimbal assembly (BGA).

*Table 5.5-1. Form Factor Analysis Case Summary with Joint Rotation Angles (Degrees)*

| | Case 1 | Case 2 | Case 3 | Case 4 | Case 5 |
|---|---|---|---|---|---|
| | 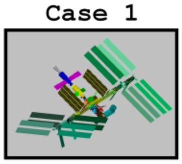 | Deleted | 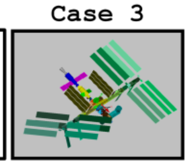 | 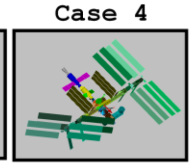 | 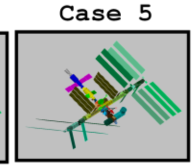 |
| **S1 TRRJ** | 85 | N/A | -95 | -95 | -95 |
| **P1 TRRJ** | 95 | N/A | 95 | 95 | -85 |
| **S SARJ** | 45 | N/A | 45 | 45 | 45 |
| **P SARJ** | 0 | N/A | 0 | 0 | 0 |
| **3B BGA** | 122 | N/A | 142 | -171 | -119 |
| **1B BGA** | -122 | N/A | -142 | 172 | 119 |
| **1A BGA** | 122 | N/A | 142 | -171 | -119 |
| **3A BGA** | -122 | N/A | -142 | 172 | 119 |
| **4A BGA** | -80 | N/A | -80 | -80 | -80 |
| **2A BGA** | 52 | N/A | 61 | 57 | 19 |
| **2B BGA** | -93 | N/A | -93 | -93 | -93 |
| **4B BGA** | 52 | N/A | 61 | 57 | 19 |

A Thermal Desktop® geometric thermal math model of the ISS configuration was obtained and modified to increase the nodalization for the HRSR, as depicted in Figure 5.5-1. Subsequently, joint orientations were set to the values specified in Table 5.5-1 for the various analysis cases.

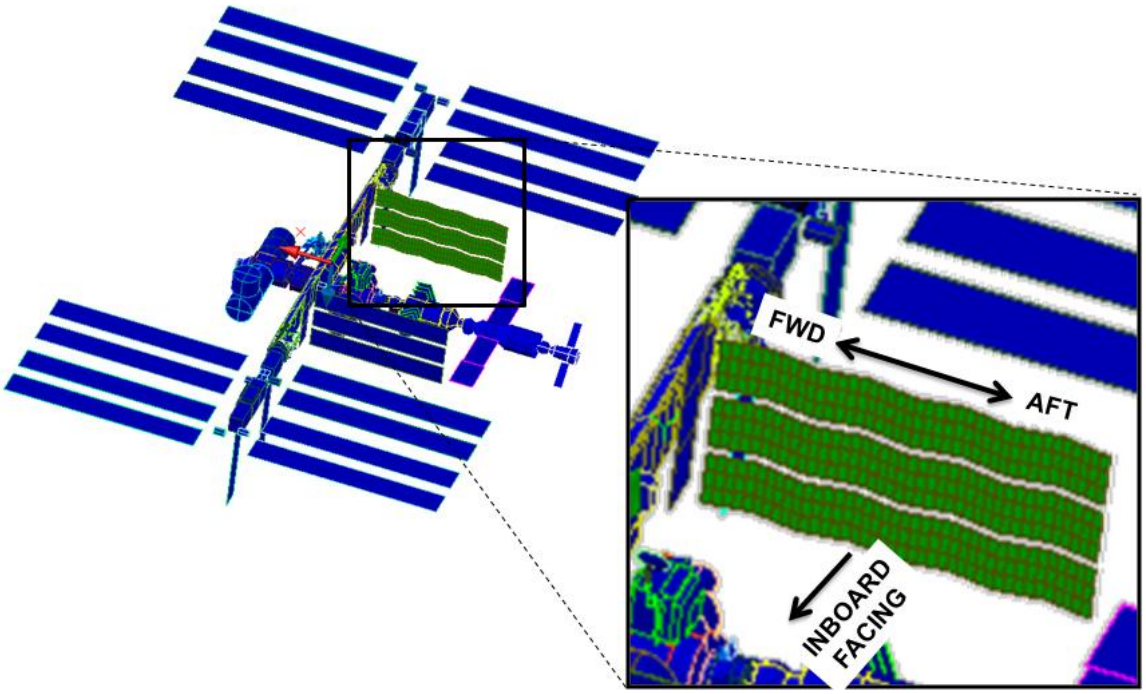


***Figure 5.5-1. Thermal Desktop® Geometric Model of ISS (with Starboard HRSR Nodalization shown)***

Inspection of the geometry suggests that the form factor to space increases as distance from the radiator panel base increases, which leads to the expectation of decreasing temperatures from the forward to the aft direction. Additionally, there is a difference in form factor to space on adjacent panels due to the accordion-fold orientation (i.e., every other panel shows the increasing form factor to space trend whereas the panels in between show a different, but increasing, trend which is explained by their different orientation). This trending provides a qualitative correlation with the observed decreasing temperature trend (i.e., corresponding points on similarly pointed panels, moving from forward to aft) observed in the IR imagery, as shown in Figure 5.5-2.

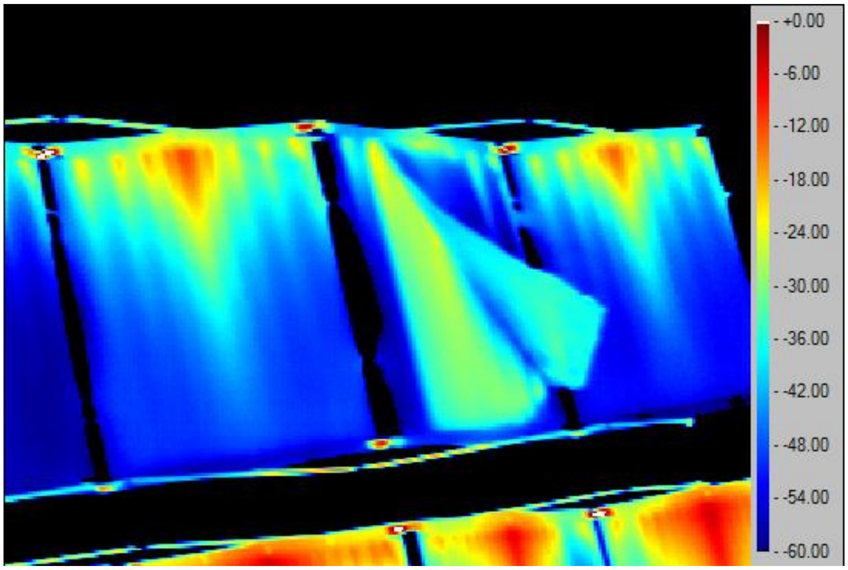


***Figure 5.5-2. IR Imagery Depicting Panel-to-Panel Temperature Trends***

A Monte Carlo ray tracing analysis was performed using the Thermal Desktop® RadCAD® application using 1,000,000 rays per node. Non-HRSR surfaces were considered blockers and the form factor to space for each HRSR node was calculated. A sample output is depicted in Figure 5.5-3. Results for the cases defined in Table 5.5-1 are provided in Appendix A. The Monte Carlo analysis shows a qualitative correlation with the decreasing temperature trends observed in the IR imagery.

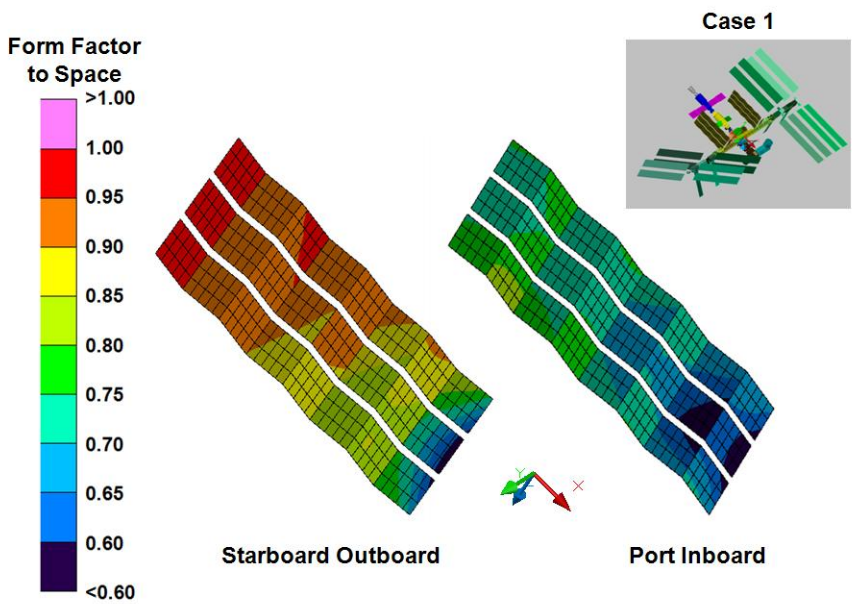


***Figure 5.5-3. Form Factor to Space Results for Case 1***

# 6.0 LS-DYNA® Analysis

## 6.1 Background

To assess the scenario of an internal pressure type root cause for the radiator face sheet failure, a physics-based model was developed. The goal was to derive an analytical model of a radiator panel, which was pressurized to failure. The failure characteristics of the modeled failed radiator panel were compared to those of HRSR panel 7, with the similarities or differences used to determine whether a pressure event leading to rupture was a plausible root cause. Additionally, an estimate of the magnitude of pressure at rupture was desired to further assess the plausibility of such a failure scenario.

Like most engineering assessments that are forensics in nature, the exact state prior to failure was unknown. The model did not attempt to mimic the exact conditions of this failure. Rather, it attempted to model plausible conditions and to study the sensitivity of the features of the modeled failure event to the possible variability of these assumptions.

### 6.1.1 LS-DYNA® Overview

LS-DYNA® is an advanced general purpose, multi-physics software package capable of simulating complex problems. It is based on nonlinear time-consistent, transient dynamic finite element analysis using explicit time integration. Among the features required of the current analysis are time consistency, highly nonlinear material behavior, propagation of failure, and contact. LS-DYNA® was chosen for this analysis because these features fit with the software's core competency.

### 6.1.2 Material Definition

An accurate material model is essential to capture complex non-linear material behavior. The Johnson-Cook model for aluminum was chosen because it includes a nonlinear stress-strain relationship, strain rate effects, and failure criteria. The model parameters were derived from an experimentally verified Federal Aviation Administration (FAA) paper. According to reference 4, "*The model can accurately represent the stress-strain response of the material*." The strain rate effects were obtained from a Hopkinson pressure bar technique, which is used to characterize high strain rates and large strains. Failure properties were derived from destructive coupon testing.

### 6.1.3 Model Evolution

In creating the finite element model, it was important to perform and document the progression of refinement. Model checks and parameter studies were performed to check accuracy, identify and fix errors, and mitigate uncertainty. Additionally, the sensitivity of the results to the refinements must be thoroughly understood. A cursory description of the earlier models is presented to highlight their specifics, purpose, findings, and to provide context for the evolution of the model throughout the study. A discussion of the final model is presented in Section 6.5.

The governing assumption of this model was that pressure increases beneath the face sheet until it ruptures under a quasi-static state. The goal of the first model version was to create a simplified representation of the basic physics of a radiator panel with the face sheet pressurized to failure.

## 6.2 Model 1.0

For this analysis, it was recognized that a number of assumptions were unrealistic, but were modeled to create an initial simulation. The initial version of the model is summarized as:

a. FAA certified nonlinear Johnson-Cook material definition included strain rate dependence and failure,

b. The face sheet and frame are modeled with relatively coarse shell elements,

c. The face sheet material includes strain rate effects and failure,

d. The face sheet is simply constrained, directly to the frame,

e. The radiator acreage is comprised of three lap bonded face sheets. The face sheet shown on Figure 6.2-1 did not delaminate from the honeycomb substrate, so it was left constrained in the model,

f. The face sheet is divided into three unequally pressured regions created with a discontinuous load distribution, and

g. Pressure was ramped linearly to failure initiation, then immediately set to zero for the remainder of the analysis.

The limitations of these assumptions are summarized as:

a. The load distribution is unrealistic,

b. No failure strength was defined between face sheet-to-face sheet lap shear bonds,

c. The simplified face sheet-frame constraint is unrealistic,

d. The load ramp down at burst was not included, and

e. The analysis mesh was too coarse to capture the observed face sheet wrinkling.

In the simulation, the face sheet is lifted in the direction of pressure (Figure 6.2-1, top). The failure initiated at the edge on the side of the largest load and propagated in both directions along the edge, turned the corners and continued along the edge (Figure 6.2-1, bottom). The face sheet lifted and folded over while tearing from the edge as shown in Figures 6.2-2 and 6.2-3.

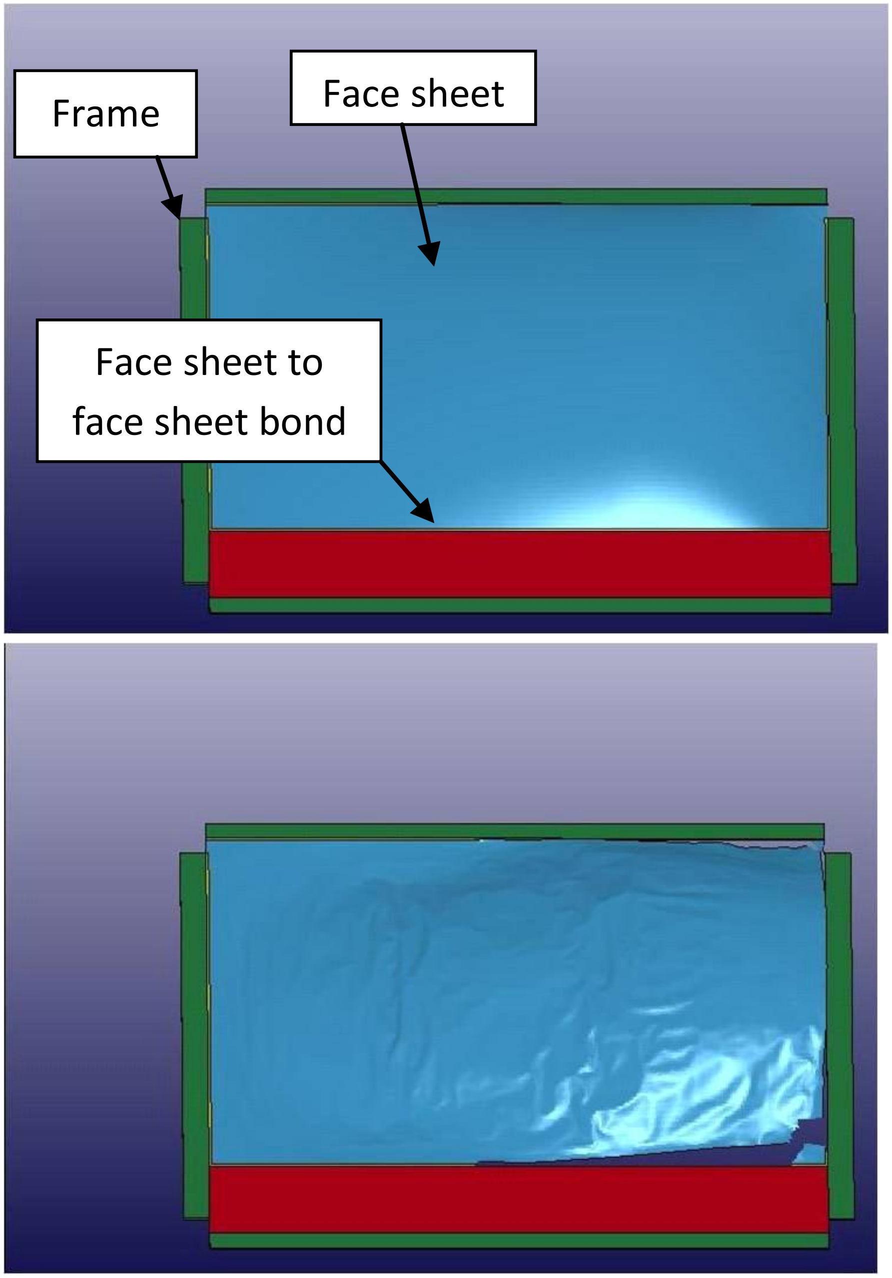


*Figure 6.2-1. (Top) State of Face Sheet Prior to Failure Initiation, (Bottom) Face Sheet Failure Propagation*

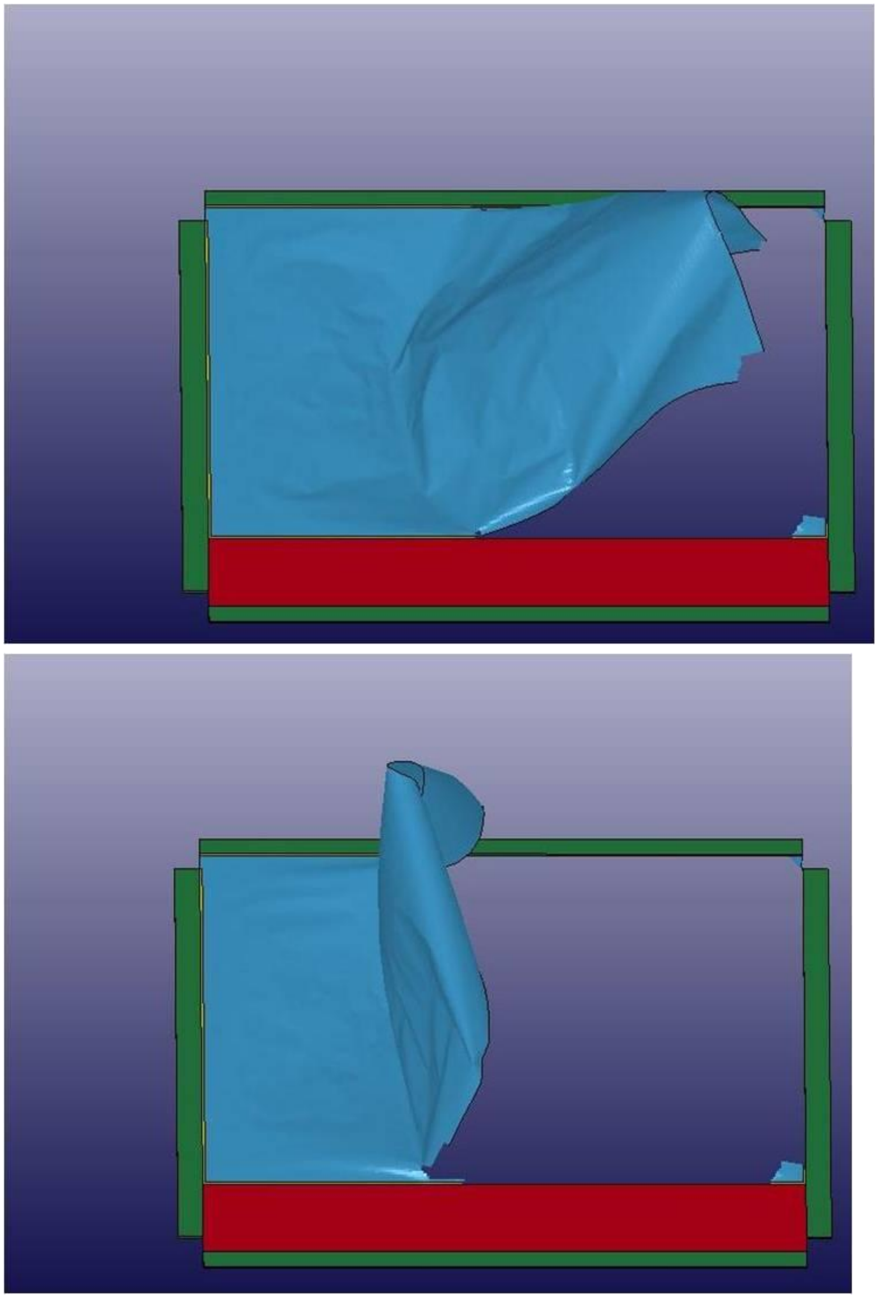

*Figure 6.2-2. Face Sheet Lifting*

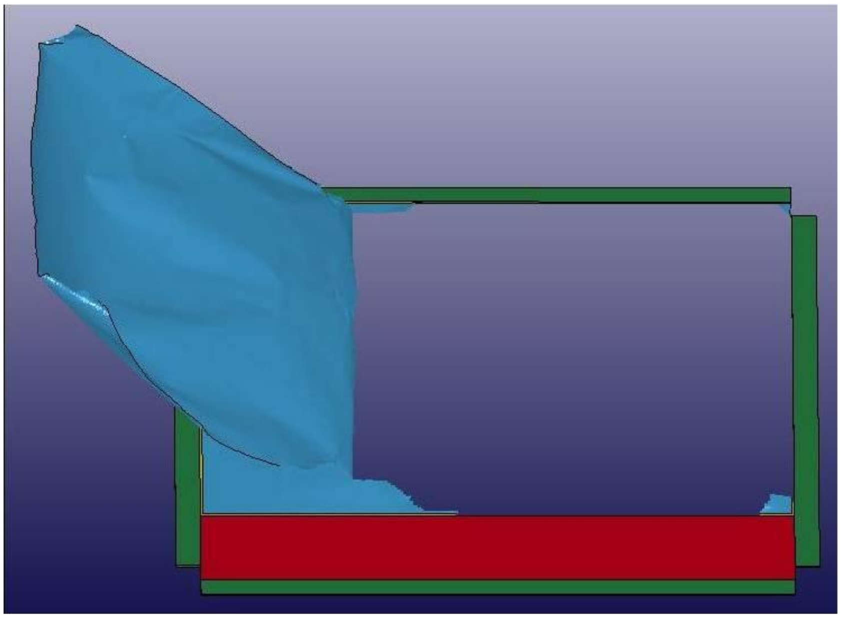

*Figure 6.2-3. Face Sheet Fold Over*

### 6.2.1 Model 1.0 Results Discussion

The energy that allowed the face sheet to fold was a combination of the potential energy from the face sheet stress state at the time of failure and the residual kinetic energy in the face sheet from the applied load ramp-up. The kinetic energy is an artifact of the load modeling technique and is not desired as the model is attempting to represent a quasi-static state at failure. The assumed instantaneous zeroing of pressure at initiation of failure was not realistic. A rupturing pressurized container will equalize pressure based on the initial pressure, time-dependent size of the opening, and the escaping gas viscosity. This was difficult to calculate without testing, but two estimation methods were implemented in subsequent versions of the model. Although the definition of this pressure ramp down may affect the energy in the face sheet when it folds (i.e., resulting in an extra force), it is not critical since it will not affect the rupture pressure as overload occurs prior to its implementation. The effect of this pressure ramp down on the final damaged state is discussed in Section 6.3.

As previously stated, the honeycomb substrate was not included in the model as it was not expected to add to the face sheet loading during rupture. However, the lack of a honeycomb boundary in the model resulted in an analytical artifact in which the face sheet penetrated into the volume in which the honeycomb would have been (Figure 6.2-4). In reality, contact with the honeycomb would constrain the face sheet from entering this volume. An analytical contact surface representing the honeycomb boundary was added to Model 2.0.

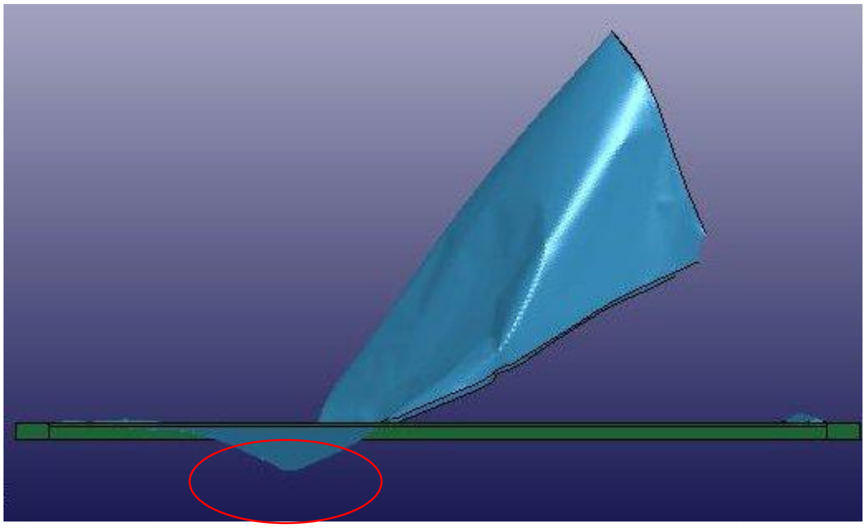

*Figure 6.2-4. Side View of Figure 6.2-2 Depicting Incorrect Penetration of the Face Sheet into the Honeycomb Volume*

A mesh density study was performed in this version, with the finer mesh showing wrinkling (Figure 6.2-1), but resulting in less permanent deformation than expected. A third, finer mesh was added to Model 2.0 to capture the permanent deformation due to wrinkling.

## 6.3 Models 2.0 and 3.0

While Model 1.0 successfully reproduced several of the features observed in the HRSR panel 7 failure imagery, considerable refinement was necessary. Model 2.0 was developed with the aim of more accurately representing the rupture event physics. Updates and features of this model are summarized as:

a. A contact surface representing the honeycomb boundary was included to constrain the face sheet from penetrating into the honeycomb volume and neighboring radiator panels,

b. Analytical contact was added among face sheet shell elements to keep them from penetrating themselves and the frame,

c. A friction coefficient of 0.2 was included in the contact definition as a typical value of smooth metal contact. The friction coefficient is used for face sheet honeycomb contact, and the contact with the neighboring panel friction does not play in the overlapping face sheet until the bond fails and is pulled apart,

d. Face sheet bolt holes were added and the associated constraint updated to represent the flight configuration (Figure 6.3-1),

e. The lap shear epoxy bond between face sheets was modeled,

f. The load distribution was modified to a radial definition. This was chosen as a possible "bubble" size and location. The peak loading area was approximately 14 inches in diameter with a center of 16.7 inches to the left of the bolt hole constraint, and 19.2 inches up from the face sheet-to-face sheet bond line,

g. The load up curve was modified to represent a quasi-static state at rupture,

h. The load ramp down post rupture was added and its sensitivity studied,

i. The face sheet density was increased to account for the paint mass, and

j. The mesh density was increased to capture the wrinkling permanent deformation.

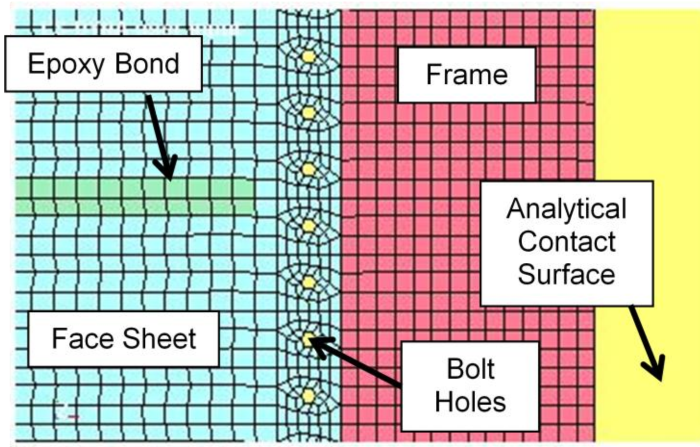


***Figure 6.3-1. Radiator Features (Models 2.0 and 3.0)***

The limitations and assumptions for Model 2.0 and 3.0 are listed as:

a. The strength of the epoxy lap shear bond was estimated,

b. The pressure time history after rupture initiates was unknown and required a sensitivity study, and

c. The radial load distribution location and size was arbitrarily chosen.

### 6.3.1 Models 2.0 and 3.0 Results Discussion

The pressure ramp down rate was difficult to estimate because the gas mass flow is a function of time since the rupture area is growing during failure propagation.

A first order approximation was needed to study the sensitivity of the final state to this pressure ramp down. This estimate was based on anecdotal data of pressure release durations of tank ruptures. The rupture data were for higher pressure, thicker walls, a different gas, and not chocked flow. Nonetheless, a best estimate was established by scaling to represent the lower pressures and the different gas in the radiator rupture. Mitigation of this uncertainty by utilizing a completely different method of calculating this ramp down is discussed in Section 6.5, which utilizes choked flow equations to calculate the pressure drop time history.

A comparison between Figures 6.3-3 and 6.3-4 shows the sensitivity of the pressure ramp down to the final state of the face sheet. The uncertainty in the load ramp down after rupture was studied by analyzing two different definitions for the pressure decay during the rupture event (Figure 6.3-2). The two definitions are the only difference between Models 2.0 and 3.0. Model 4.0 implemented the original linear version of the load ramp down. The final model version (i.e., 5.0) used a different curve based on an updated calculation.

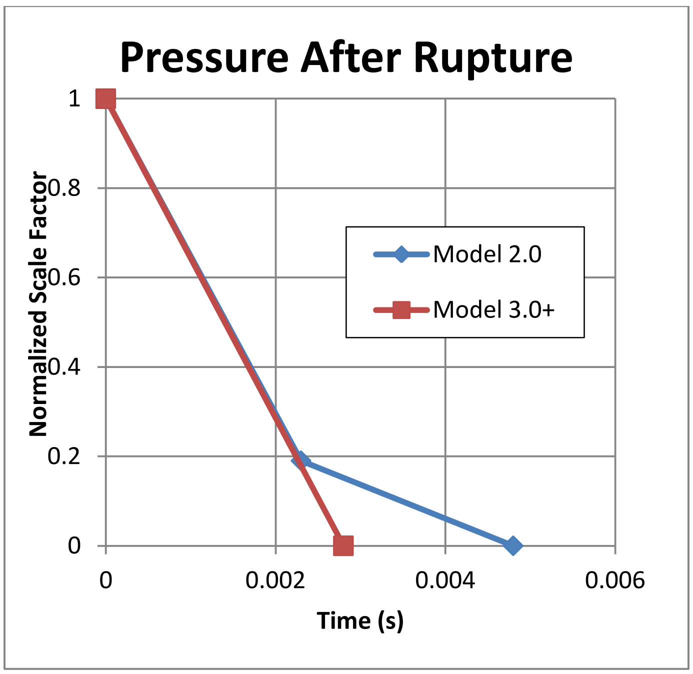


*Figure 6.3-2. Pressure Ramp Down Study for Models 2.0 and 3.0*

In the simulation, the failure was initiated at the face sheet-to-face sheet lap shear bond. The failure propagated around the right corner, and then continued tearing along bolt holes. The face sheet lifted and began to fold. In both models, with greater face sheet-to-radiator angle, the face sheet begins to tear from the bolted constraint (see Figures 6.3-3 and 6.3-4). Key events in the time sequence begin with: first element failure at 0 seconds, followed by full bolt pullout and face sheet-to-face sheet bond failure at 0.05 seconds, maximum face sheet height above panel at 0.15 seconds, face sheet initial contact with itself at 0.21 seconds, and then impacts the neighboring panel at 0.25 seconds. The tearing was much greater in Model 3.0. The face sheet made a high-energy contact with itself (i.e., a whipping motion), and extensive permanent face sheet wrinkling occurred.

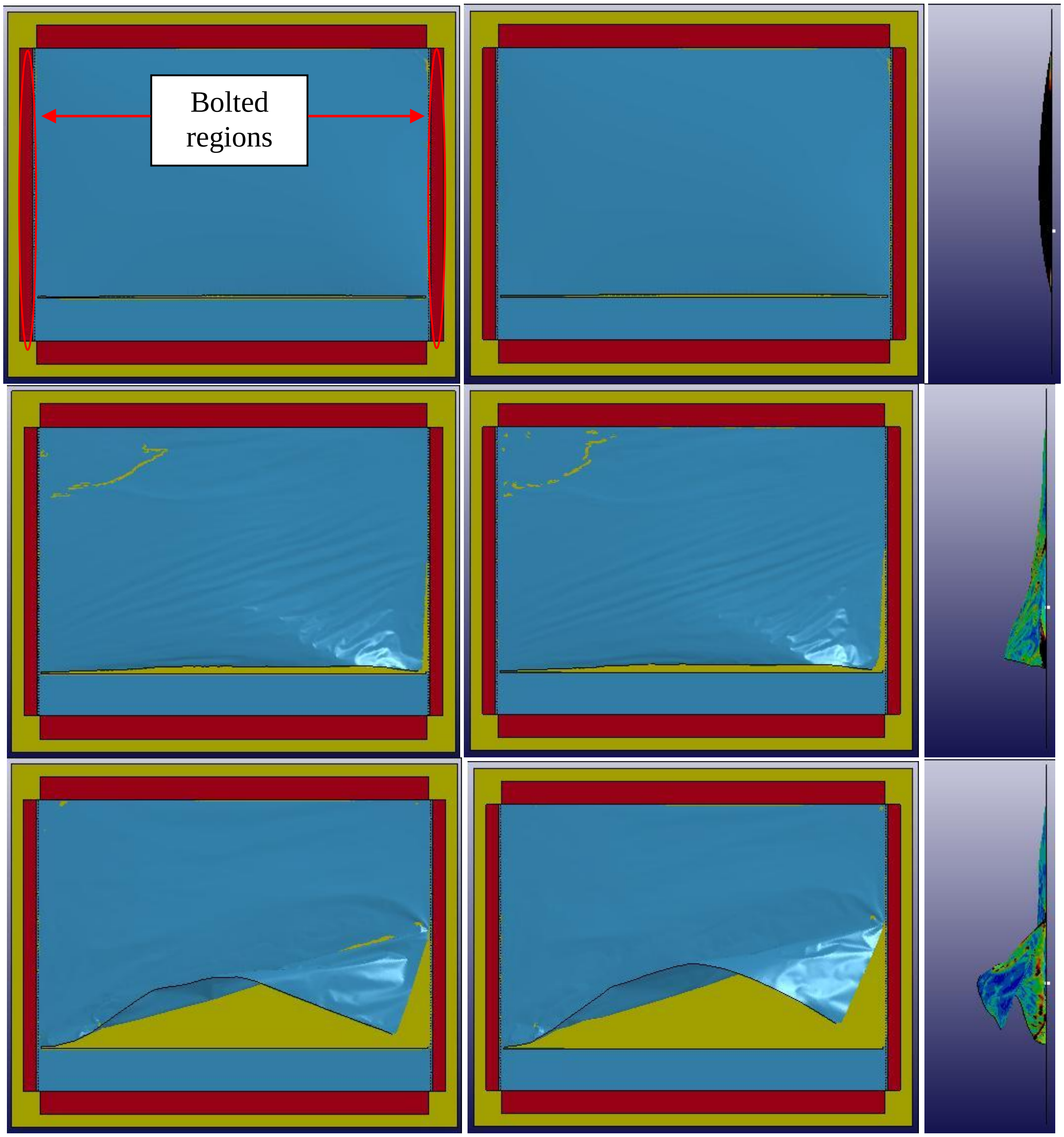


*Figure 6.3-3. Failure Propagation in Model 2.0, Front and Side Views*

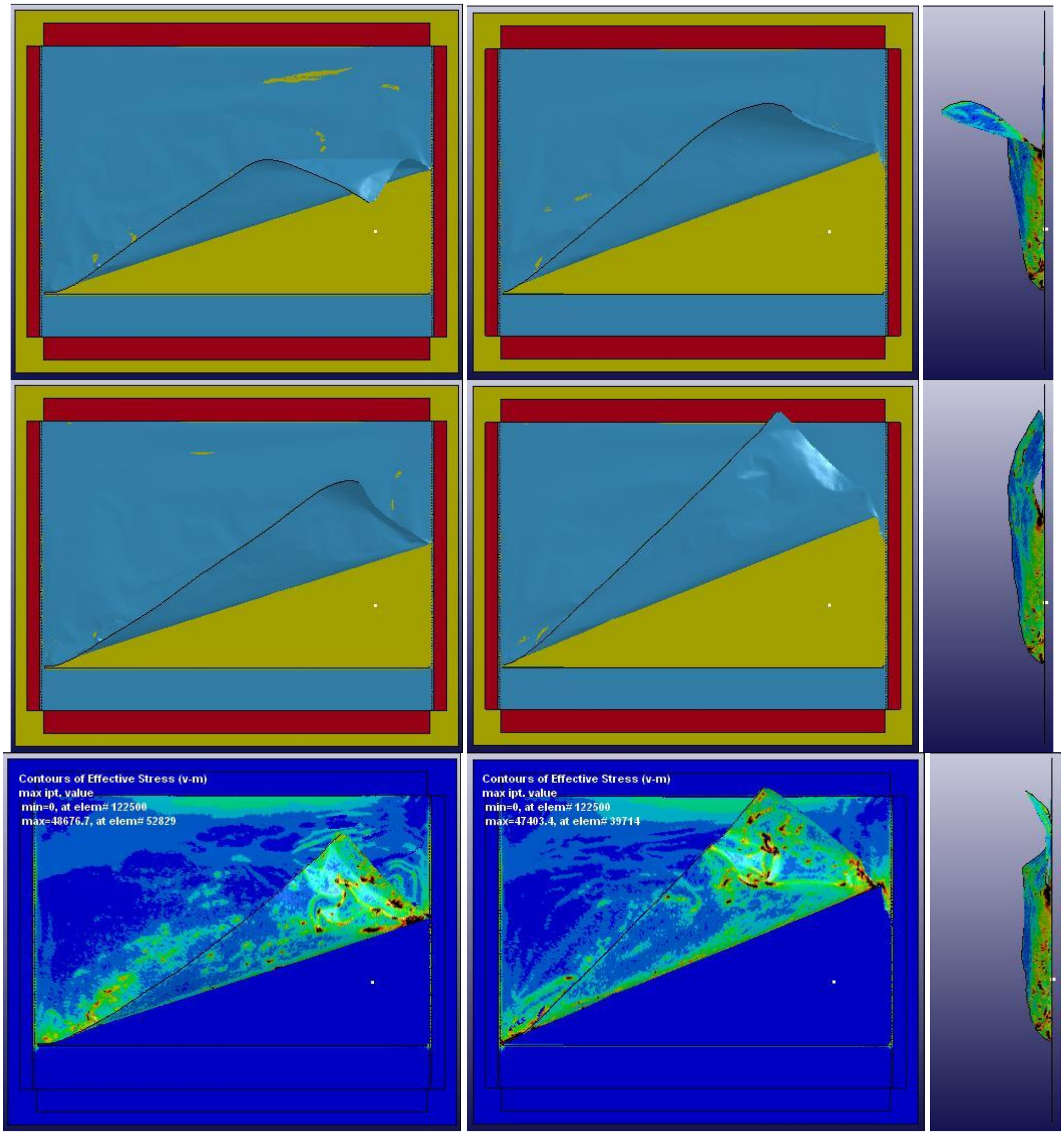


***Figure 6.3-4. Failure Propagation in Model 3.0, Front and Side Views***

Figure 6.3-4 includes a side view of the stress state (note the stresses in the folded region). The model shows permanent deformation in this folded region. Due to computational constraints, the model was not run long enough to show the face sheet final resting form. However, this permanent deformation implies curvature will remain in the face sheet during its resting state. On-orbit images of the damaged panel 7 show this phenomenon, as seen in Figure 6.3-5.

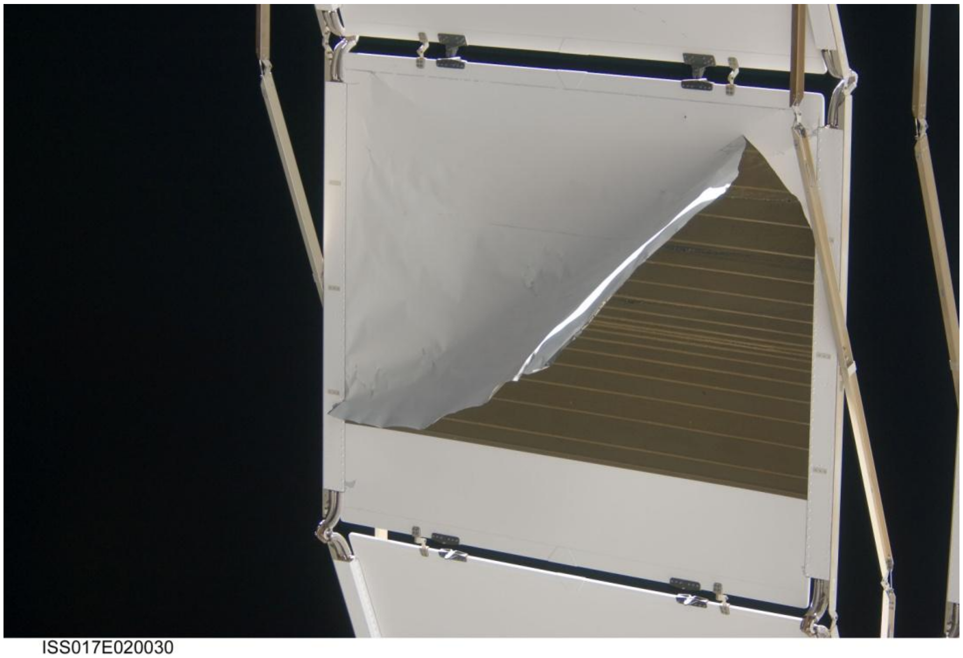


*Figure 6.3-5. On-orbit Image of Radiator Panel showing Face Sheet Displacement*

Figure 6.3-6 presents another similarity of the model to the on-orbit photos in the tearing away of the face sheet from the bolted constraint region.

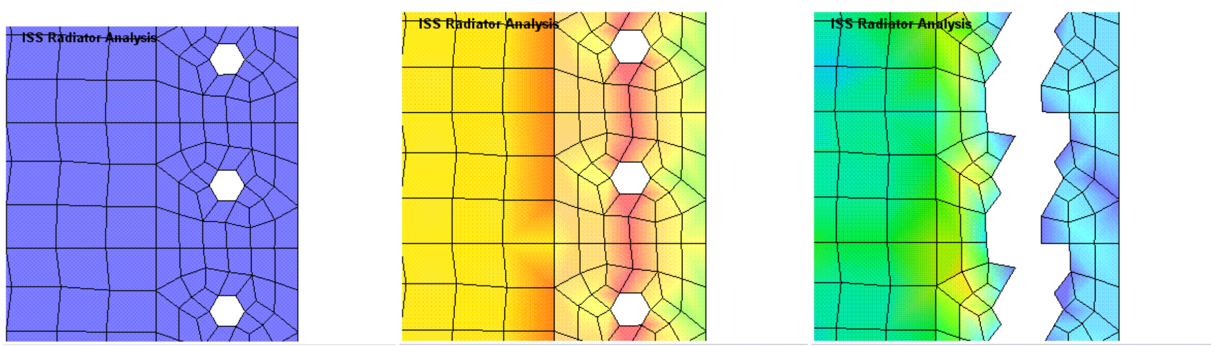


*Figure 6.3-6. Face Sheet Tearing Along the Bolt Holes*

Figure 6.3-7 shows a comparison of modeling wrinkling features to similar features from on-orbit images. Note that the face sheet in the model snapshot is in a folded position only because it was not run long enough to equalize to the lifted resting position.

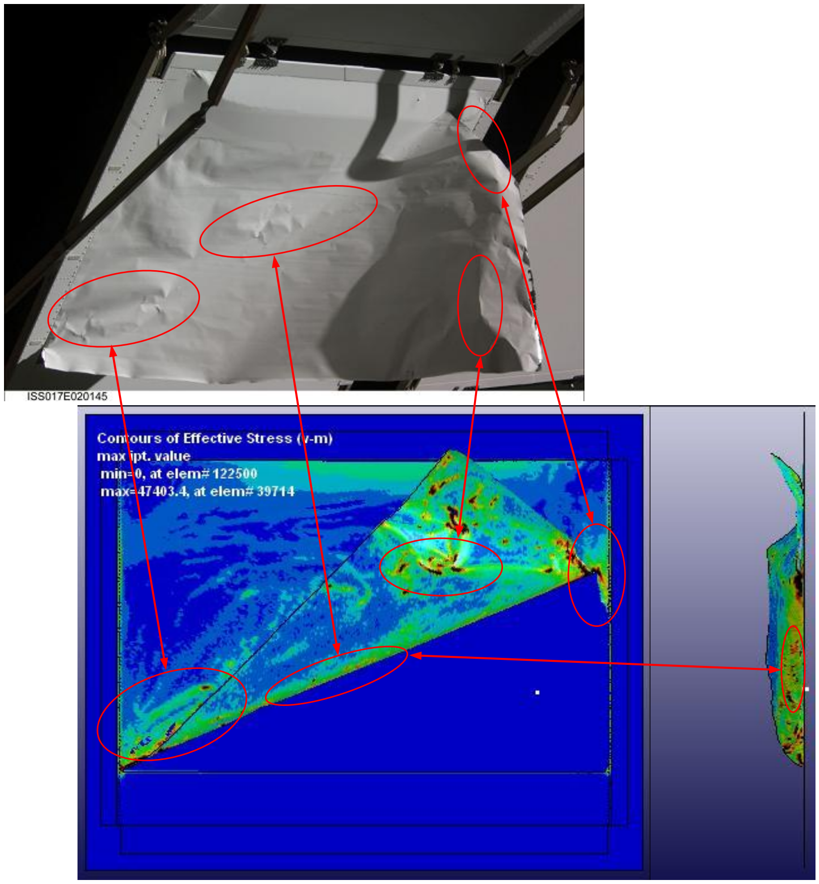


*Figure 6.3-7. Comparison of Wrinkling Features to On-orbit Images*

## 6.4 Model 4.0

While significant fidelity was added in Models 2.0 and 3.0, a prominent conclusion from the model was the importance of strength properties of the face sheet constraints. Updated strength properties for the face sheet-to-face sheet bond were implemented in Model 4.0.

Updates and features of Model 4.0 are summarized as:

a. The face sheet-to-face sheet bond failure properties were updated based on coupon testing, and

b. Failure was observed to initiate at bolt holes.

The limitations for Model 4.0 are:

a. Pressure time history after rupture initiated was unknown resulting in a sensitivity study, and

b. The radial load distribution location and size was arbitrarily chosen.

### 6.4.1 Model 4.0 Results Discussion

In previous models, the face sheet-to-face sheet bond strength was not available, and was roughly estimated. Model 4.0 was an update to the bond strength properties in lap shear and peel. Lap shear properties were derived from a lap shear pull test to failure of two bonded coupons representing face sheets. Once failure at the bond initiates, it is expected to go into peel. Face sheet peeling is an "unzipping" as the face sheet is peeled from the bond, traveling down the bond length. Face sheet peel strength is significantly lower than the lap shear strength. Peel strength was derived by peel test; see setup in Figure 6.4-1.

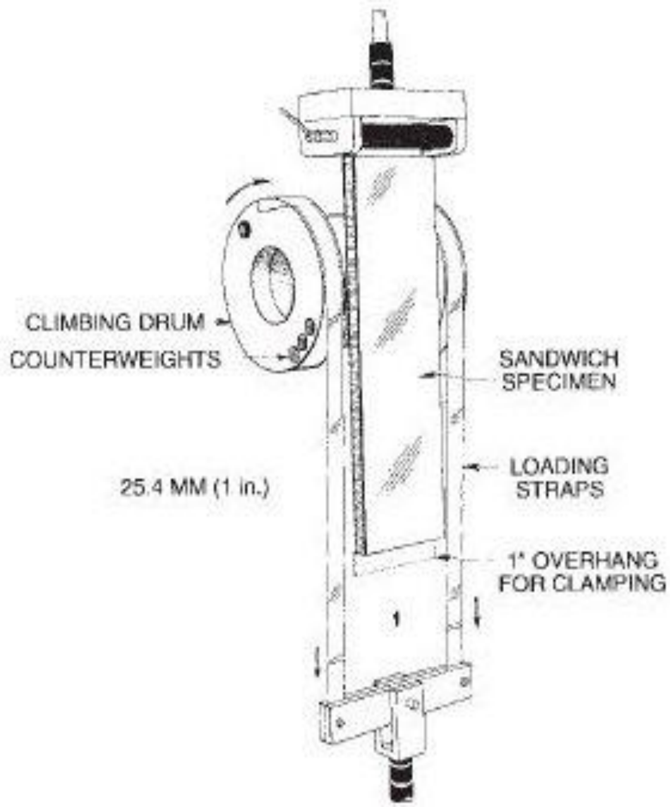


***Figure 6.4-1. Peel Test Configuration***
*(Reprinted, with permission, from ASTM D1781-98(2004) Standard Test Method for Climbing Drum Peel for Adhesives, copyright ASTM International, 100 Barr Harbor Drive, West Conshohocken, PA 19428)*

The updated lap shear strength was higher than that estimated for previous models, which caused the failure to occur at a higher pressure. Consequently, the failure in Model 4.0 initiated at the bolt holes as opposed to the bond as in the previous models. The failure propagated in both directions along the bolt holes. In the model, when the failure front reached the bond, the face sheet-to-face sheet bond strength was modified to the bond peel strength. As previously stated, this was done because when failure at the bond initiated, it was expected to go into peel. The bond failed as the face sheet lifted from the panel. Additionally, the on-orbit images (Figure 6.3-5) showed that this bond had separated rather than ruptured.

Similar to previous models, the face sheet lifted and folded on itself, and tore from the bolted region, as shown in Figure 6.4-2. Previous models showed the impact of the face sheet top edge in a whipping motion. In Model 4.0, the pressure at rupture was higher. This added rupture energy allowed the face sheet to tear further along the bolted region, which caused the impact to occur off the panel.

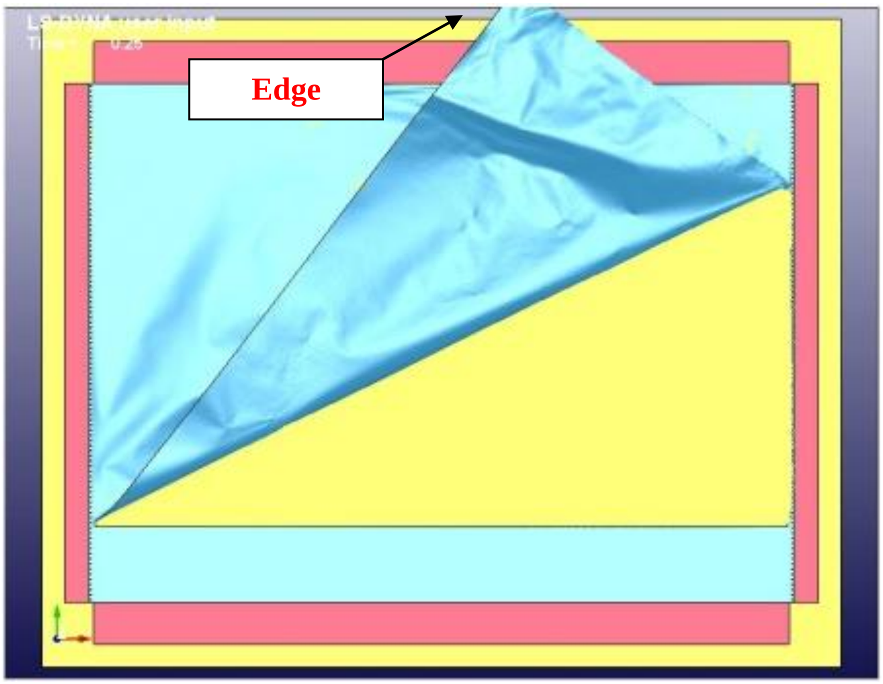


***Figure 6.4-2. Model 4.0 at Impact State***

On-orbit images showing marking (Figure 6.4-3) on the neighboring panel confirm face sheet impact on the neighboring panel. A simple paper model of the panel was used to show that the markings line up with a folded face sheet and is shown in Figure 6.4-4.

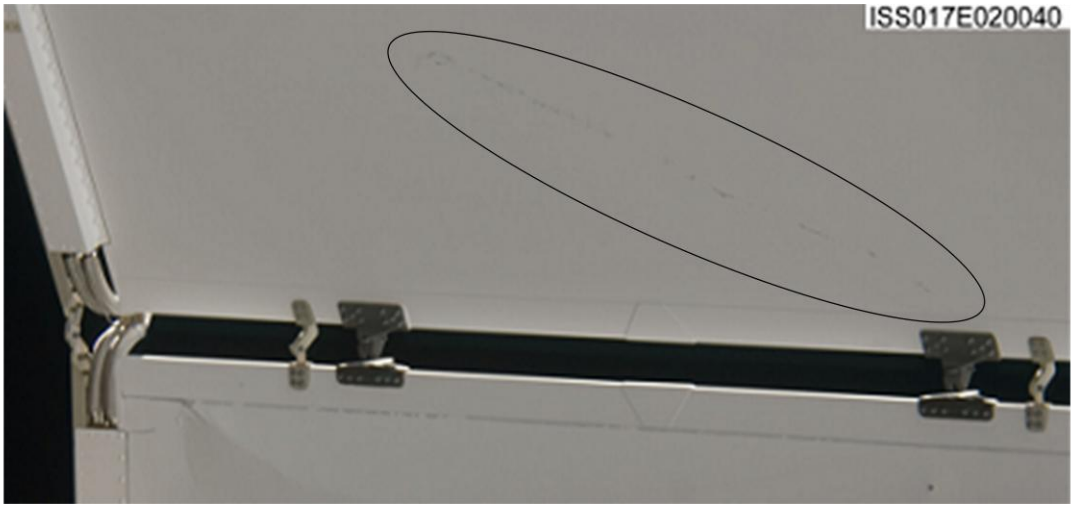


*Figure 6.4-3. Marking on Panel 7 Neighboring Panel*

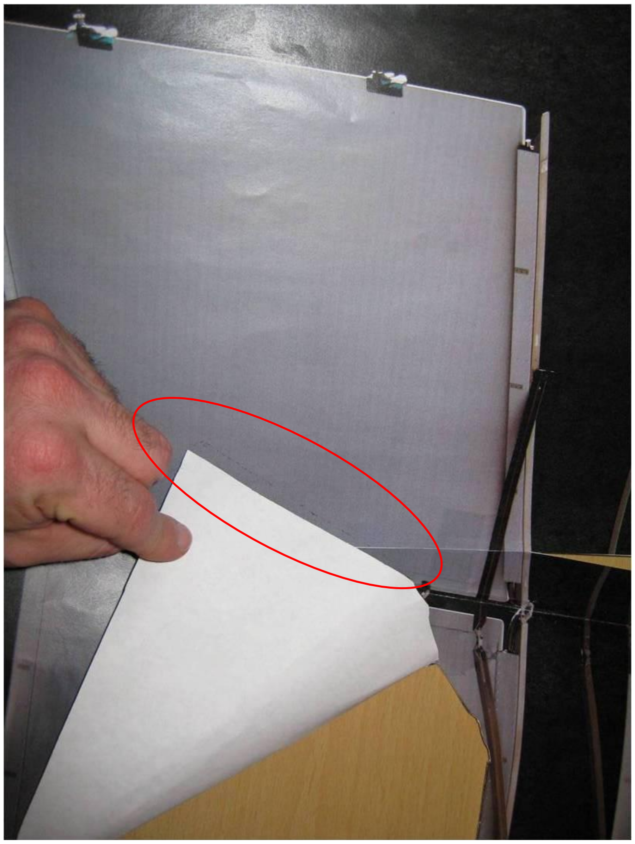

*Figure 6.4-4. Simple Paper Model shows the Folded Face Sheet Lines up with the Marking on the Neighboring Panel*

Because the initial failure occurs at the face sheet constraints, Model 4.0 highlighted the importance of fidelity and accuracy of these constraints. The face sheet failure was driven by the strength of the bolted region, and accuracy of this constraint was scrutinized in Model 5.0.

### 6.4.2 Peer Review

A peer review was conducted by the Boeing LS-DYNA® team. The team performed error checks and conducted studies to confirm the results.

As previously stated, a model assumption was that the face sheet state at rupture would be considered quasi-static. To show the ability of the model to replicate a quasi-static state, the sensitivity of the results to the load ramp was studied by the peer review team. It was shown that the rupture pressure and the failure propagation were not sensitive to load ramp rates.

There was concern that there was no frame over the bolted region. Potentially, a frame could alter the stress at the constraint by causing a concentration where the lifted face sheet is in contact with the frame edge. Consequently, it was shown the rupture pressure and the failure propagation was not sensitive to the frame surface as the failure was driven by the bolt hole strength. Nevertheless, the frame surface was retained in the model as added fidelity.

A model assumption was the face sheet delamination area was relatively large at rupture. The area of the loading profile was chosen to envelope the higher end of the pressure, although it was arbitrarily chosen. The peer review team studied the sensitivity of the pressure at rupture to the loading profile. This study showed that the pressure at rupture was inversely proportional to the loading profile area.

As a result of the peer review, the NESC analysis used an updated frame mesh provided by the peer review team for subsequent analyses. This change resulted in a change in failure pressure of less than 3 percent. Additionally, sensitivity analysis performed by the peer review team showed the analysis was not sensitive to the load-up rate. Finally, the peer reviewers cautioned that the pressure at rupture showed sensitivity to the size of the delaminated “bubble” area.

## 6.5 Model 5.0

Discussions from the peer review and assessment of the previous models led to additional scrutiny of the pressure loading profile, the pressure unloading time history, and the bolt constraint modeling.

The loading profile was updated in Model 5.0 to a uniform face sheet pressure. Because the loading was symmetric, the elemental differences in stress at rupture in the bolted regions on either side of the radiator were within 1 percent. When failure initiated, it relieved stress in the face sheet, and subsequently relieved the mirrored bolted region. Failure occurred on the same side as previous models, but that occurrence was arbitrary (i.e., each side had an equal chance of being the location of failure initiation due to model symmetry).

The pressure unloading time history profile did not affect the rupture pressure because it was implemented after rupture had already been initiated. However, Models 2.0 and 3.0 showed that the failed face sheet final state was sensitive to this pressure drop time history as the face sheet ruptures. The previous definition of this pressure unloading was a rough estimate based on arbitrary data. The model versions failed at different pressures, so the engineering judgment based estimate was not deterministic. Hence, in Model 5.0, a new definition of the pressure unloading time history was calculated utilizing a choked flow equation with ammonia gas properties [refs. 5 and 6]. The results of the calculation are shown in Figure 6.5-1, with additional detail in Appendix B.

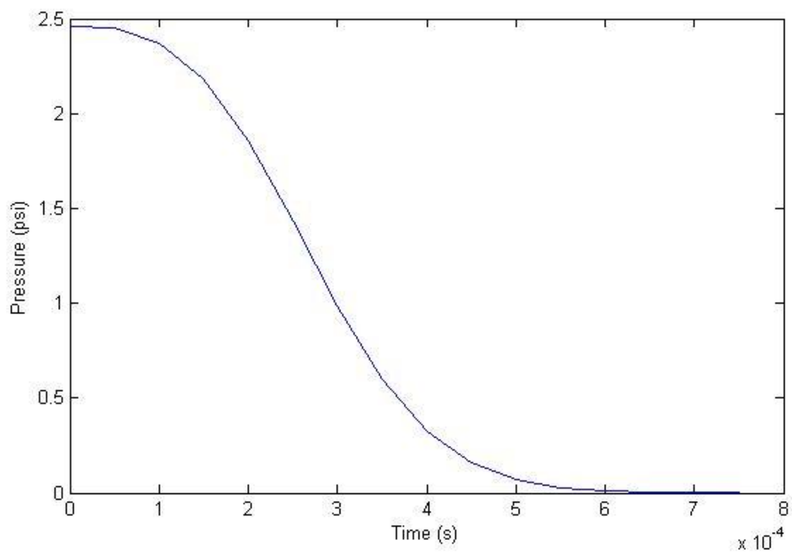


***Figure 6.5-1. Calculated Pressure Unloading Time History***

Per the peer review team, frame fidelity was added by including the panel used to sandwich the bolted region. The bolted constraint was modified to represent bolts as separate parts in contact with the face sheet bolt holes as shown in Figure 6.5-2.

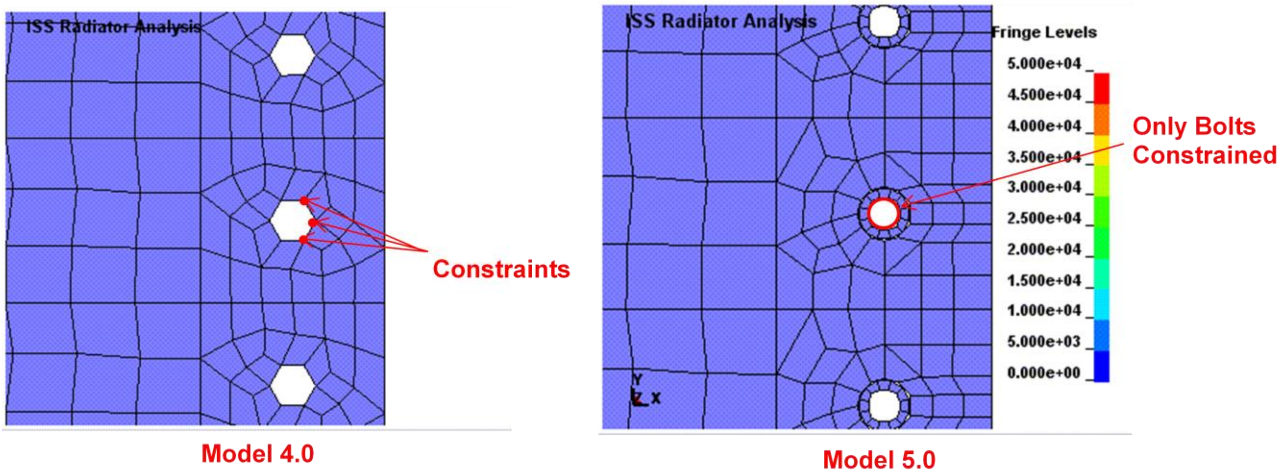


*Figure 6.5-2. A Comparison of Bolted Constraint Definitions*

### 6.5.1 Model 5.0 Features

Updates and features of Model 5.0 are summarized as:

a. A pressure-fed bubble formed on the face sheet and grew until rupture,

b. FAA certified nonlinear Johnson-Cook material definition includes strain rate dependence and failure,

c. A uniform pressure was applied to the entire face sheet,

d. A contact surface with a friction coefficient of 0.2 prevented interference of the face sheet into the honeycomb volume and the neighboring face sheet,

e. Modeling techniques were used to represent a quasi-static state prior to rupture. It was desired to reduce the face sheet kinetic energy at rupture. This kinetic energy was accumulated during pressurization;

   i. Load ramp up rate was reduced as face sheet stresses approached the failure criteria to mitigate residual velocity and dynamic contribution to the face sheet rupture event,

   ii. Mass damping was used to slow the face sheet elements prior to rupture. Prior to failure initiation, this damping was inhibited to preserve the rupture event physics,

   iii. Physics of the rupture event were insensitive to the load rate at failure,

f. The definition of pressure unloading was updated by utilizing ammonia gaseous choked flow equations,

g. The epoxy bond between overlapped face sheets was represented by a row of elements with double thickness and unique failure criteria. Initially, failure was based on lap shear strength. When failed elements reach the bond, the joint was allowed to go into peel by reducing the failure criteria of these elements to the bond's peel strength. The lap shear and peel test strengths were based on coupon testing,

h. Mesh density studies were performed to capture face sheet wrinkling,

i. The frame surface that sandwiches the bolted region was modeled, and

j. Face sheet bolt holes and corresponding bolts were modeled as separate components with contact.

### 6.5.2 Model 5.0 Results Discussion

In the Model 5.0 simulation, the face sheet was lifted in the direction of pressure. The failure initiated at the bolt holes as they began to pull from the bolts (Figure 6.5-3). The red regions in this figure indicate locations where stresses were approaching the material failure criterion. When this criterion is exceeded, the element was deleted, allowing for the bolt to pullout. The bolt pullout phenomenon propagated in both directions from the initiation location as the face sheet began to lift locally. Further from the failure initiation location, the failure phenomenon transitioned from bolt pullout to tearing along the bolt holes. As the failure reached the face sheet-to-face sheet bond, the bond failed in peel. The face sheet proceeded to lift and to fold. As the angle of the face sheet to the radiator increased, the face sheet began to tear from the bolted region. The face sheet then made contact with the analytical contact surface representing the neighboring face sheet in a high-energy whipping motion.

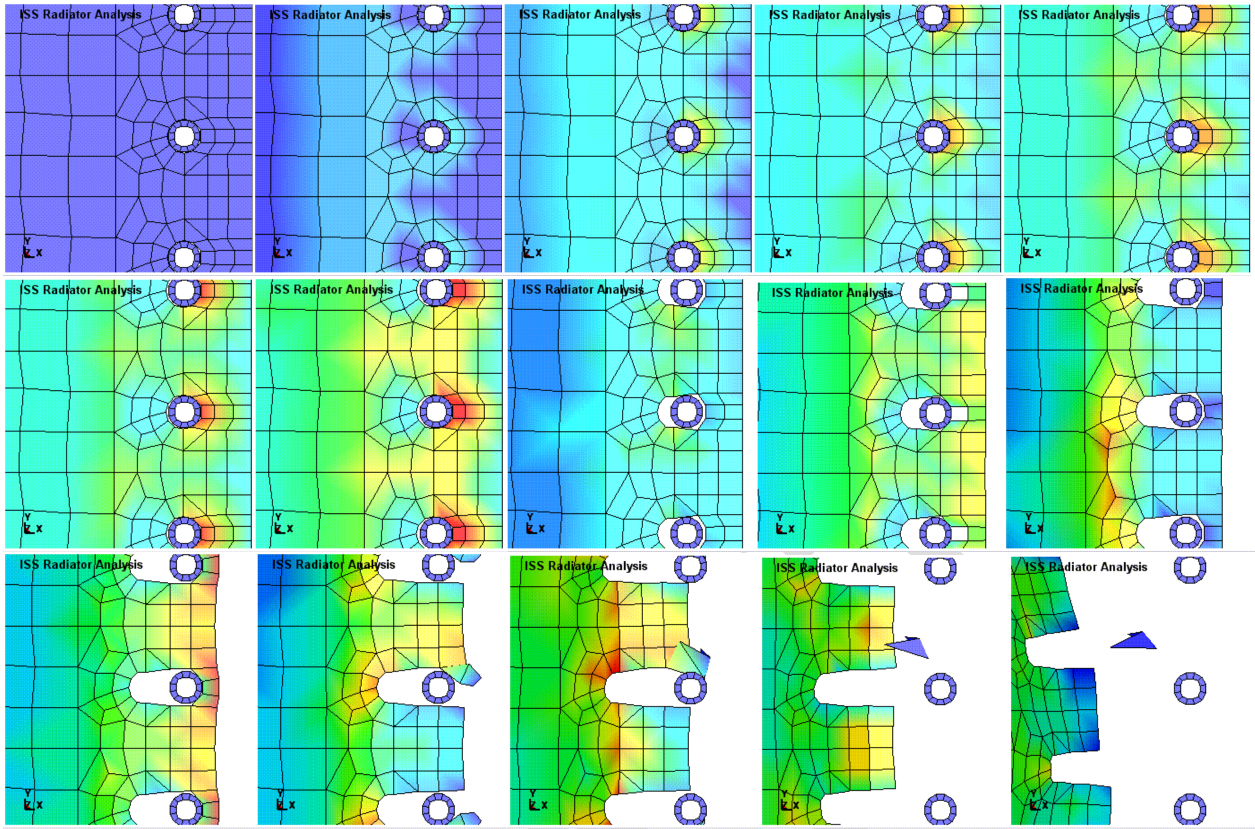


*Figure 6.5-3. Zoomed View of the Failure Progression as the Face Sheet Pulls from the Bolts*

The model and the on-orbit images show a distinct bolt pullout region. Figure 6.5-4 shows the bolt pullout region to be the location of failure initiation. It may be theorized that the on-orbit face sheet rupture initiated where the bolt pullout features initiated in the region where bolt pullout features have been discovered. In another similarity to the model, the on-orbit images show a permanent transition from bolt pullout to tearing across the bolt holes.

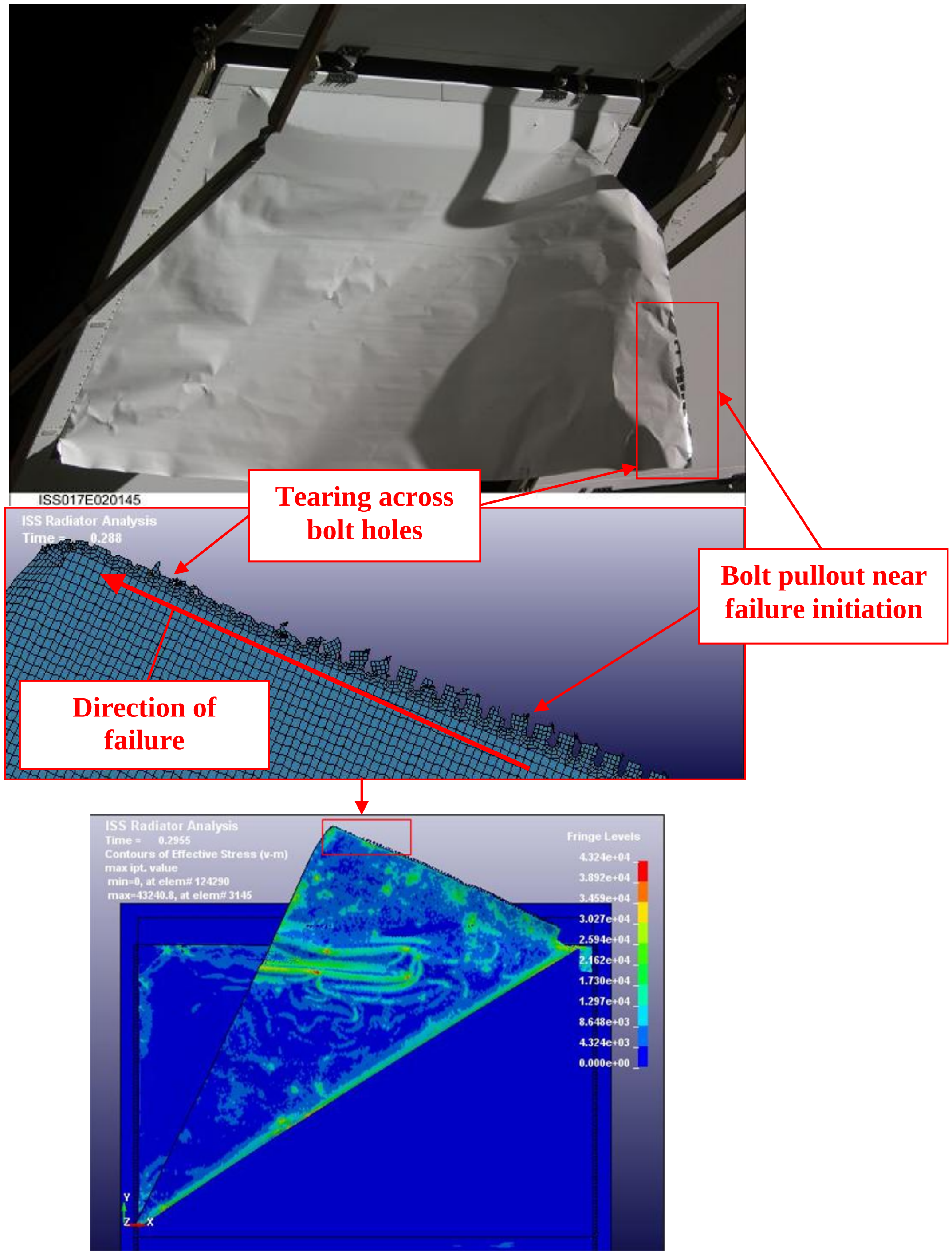


***Figure 6.5-4. Comparison of Bolt Pullout Near Failure Initiation and Tearing Along Bolt Holes***

In Model 5.0, the failure propagated further than in previous models. This allowed the location of the high-energy impact of the face sheet edge to correspond more closely with the on-orbit markings on the neighboring panel as shown in Figure 6.5-5.

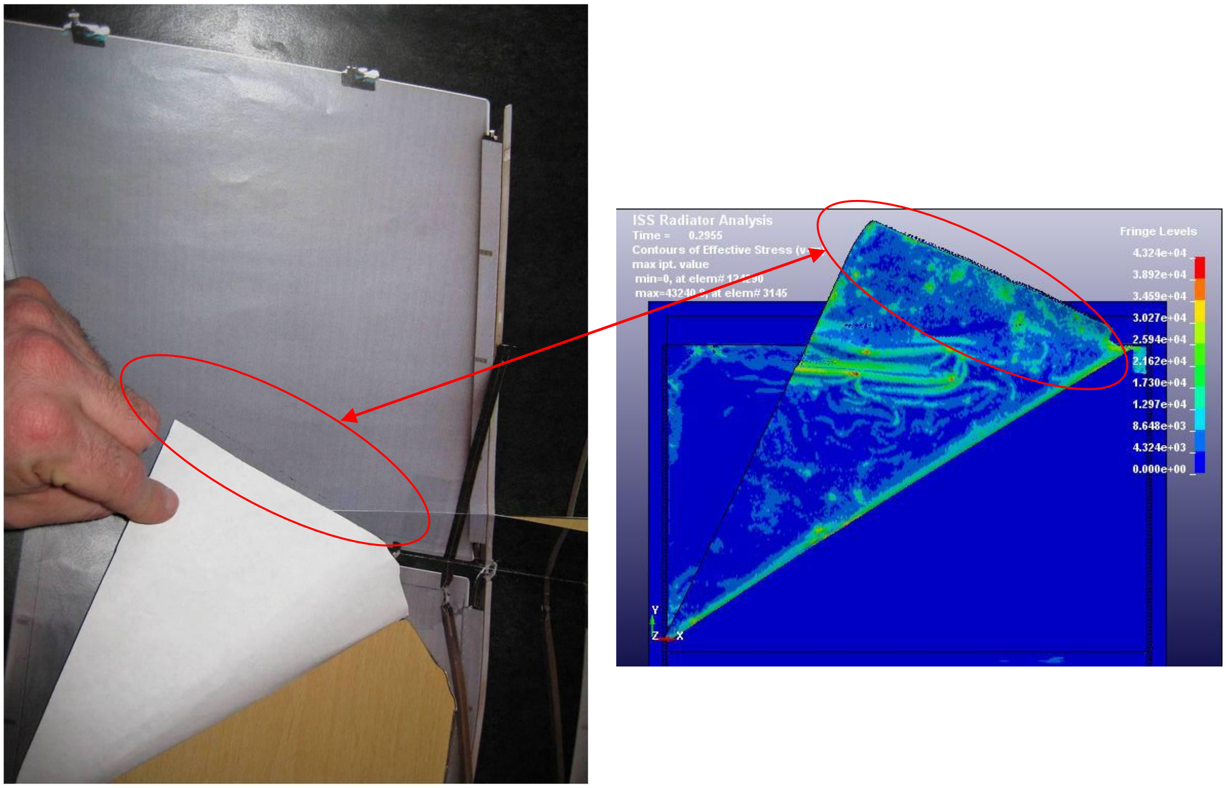


***Figure 6.5-5. Comparison of the Location of the Contact Edge in the LS-DYNA® Model to the Paper Model***

Table 6.5-1 is a summary of the similarities between the LS-DYNA® model and the on-orbit radiator images.

*Table 6.5-1. Feature Comparison Between Model Predictions and On-orbit Images*

| LS-DYNA® Model | On-Orbit Radiator Images |
|---|---|
| **Failure initiates at the bolt holes by pullout.** | **Show bolt pullout.** |
| **As failure propagates from initiation point, face sheet lift up causes the failure to change from bolt pullout to tearing between holes.** | **Show tearing across bolt holes from pullout region.** |
| **Residual pressure and potential energy from stress state cause the face sheet to violently fold.** | **Permanent deformation of face sheet in lifted up position and wrinkling features indicate a fold.** |
| **The face sheet shows widespread permanent wrinkling. The wrinkling is prominent along the crease of the fold.** | **Show widespread wrinkling. A line of creasing similar to the fold crease in the model is visible. Other similar wrinkling features are visible.** |
| **In all model versions, when the face sheet is lifted to higher angles, it starts to tear from the bolted region.** | **Show that the face sheet tore from bolted region.** |
| **The corner and edge of the face sheet make high-energy contact with the contact surface representing the neighboring radiator panel.** | **Show markings where the edge of the face sheet is theorized to have impacted neighboring panel.** |

## 6.6 LS-DYNA® Analysis Conclusions

The primary analysis goal was to use a physical model as a tool to assess the plausibility of the radiator failure being caused by a pressure event. The earliest model version, which attempted to show only the basic physics of a face sheet rupture event, was able to replicate some features observed in the on-orbit failure imagery. As the model development progressed, an increased understanding of the possible failure propagation developed. Even with refined fidelity, the final model does not attempt to mimic the exact conditions of the failure event. However, the final model version shows that with similar conditions based on the assumptions stated, similar failure characteristics arise.

The secondary analysis goal was to estimate the pressure magnitude that would cause this type of failure. It was shown that the failure pressure was highly dependent on the loading area. Based on the on-orbit images, the delaminated region prior to failure was expected to be large. However, because the face sheet delaminated area was unknown, it was difficult to derive this pressure. Nonetheless, in the analyses performed, the rupture pressure remained on the order of less than 10 psia. This pressure magnitude was within the plausibility of the gas pressure that could have fed the area under the face sheet to cause a pressure rupture. Although bond and material testing were included in the model verification, it must be noted that this model is not expected to undergo test validation. Caution must be used when attempting to extract estimated rupture pressure as there is unknown uncertainty in complex multi-physics models with a lack of correlating test data. Engineering judgment must be used to weigh the risk of this uncertainty.

# 7.0 NESC Supported Radiator Testing

## 7.1 Radiator Tests

During the July 2009, Technical Interchange Meeting (TIM), tests were identified that could potentially determine the viability of a subset of fault tree legs and lend credibility to the most likely failure scenario. As a result of this meeting, LMMFC engineers formulated a test plan for the proposed tests [ref. 7].

The list of proposed tests was presented to the ISS Multi-lateral Vehicle Control Board (MVCB) on October 1, 2010, and to the Space Station Program Control Board (SSPCB) on October 20, 2010 [ref. 8], but testing was not approved. The NESC recognized the value of the proposed testing and engaged the radiator team to establish partial funding to sponsor a subset of the overall test plan and prioritized the test sequence. Figure 7.1-1 depicts the subset of testing presented to the MVCB and SSPCB.

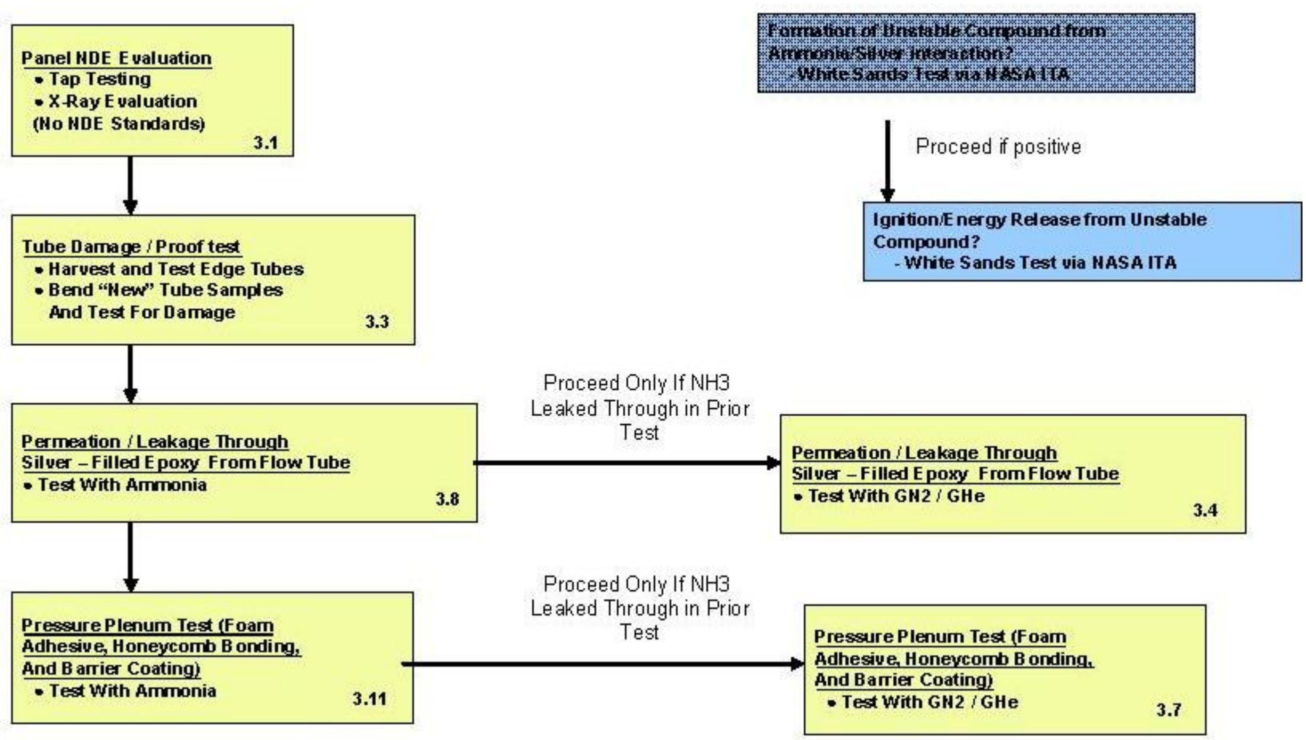


*Figure 7.1-1. Subset of Overall Test Plan Presented to MVCB and SSPCB*

Tests sponsored by NESC are discussed in the following sections and are summarized from information presented in references 9 through 14. The test numbering preserves the originally proposed nomenclature and is maintained for continuity.

### 7.1.1 Test 3.1 -- Panel NDE

This test attempted to understand whether exposure to the basic operating environments over time led to an unexpected level of mechanical deterioration within the radiator panels. The testing performed on the HRSR qualification ORU during the qualification phase was more severe than flight environments. Specifically, the qualification unit was exposed to the environments as shown in Table 7.1-1 [ref. 14].

***Table 7.1-1. Comparison of Test Article Environments to HRSR Environment [ref. 14]***

| Specific Tests/Activities Performed | Comparison to HRS Environment |
|---|---|
| Acceptance Acoustic Test (138 dB-OA, 60 sec.) | Represents flight acoustic environment. |
| Qualification Acoustic Test (144 dB-OA, 188 sec.) | 6 dB (or 100%) greater than flight vibration and 3x duration. |
| Stowed Static Limit Loads Test | Represents highest ORU structural loads during flight. |
| Stowed Static Ultimate Loads Test | 40% higher than flight loads, no yielding or damaged detected; Successful deploy and retract following test. |
| Deployed Static Limit Loads Test | Represented highest ORU deployed structural loads. |
| Deployed Static Ultimate Loads Test | 50% higher than flight loads, no yielding or damage detected; Successful deploy and retract following test. |
| Transportation Environment - Mileage | Qual ORU travelled 5150 miles, or 1300 miles more than S1-3 and 4000 miles more than each of the other flight HRS ORUs. |
| Transportation Environment - Shock Exceedances | Qual ORU & S1-3 experienced highest transportation events. |

The team concluded that the eight qualification radiator panels would be ideal sources of additional test data and subscale test articles to support this investigation. Flash thermography tests were conducted and the data were reviewed for each panel. These data were used to identify specific panels and locations within the panels where hardware elements could be harvested to support subsequent tests. Additionally, tap tests were conducted by qualified inspectors on the radiator panels in accordance with an established procedure. These results were compared with findings from the flash thermography tests.

Each radiator panel was X-rayed with attention given to the flow tubes, extrusions, manifolds, and the honeycomb from edge to edge. The X-rays were reviewed for any abnormalities. Special attention was given to separations at the foam adhesive bond lines and at flow tube bends in tube positions 1 and 22.

As a result of the testing, it was concluded that the radiator panels and flow tubes currently on-orbit have not been damaged from exposure to design environments as demonstrated by the absence of damage to the similar components from the severely tested qualification ORU panels. Furthermore, tap testing on 0.25-inch centers found no voids or face sheet debonding.

### 7.1.2 Test 3.3 -- Tube Damage/Proof Test

This test was designed to understand whether design and manufacturing introduced weaknesses into the panel by tube bending operations performed after the proof tests. The focus of this test was to evaluate the affect that four bends in panel edge flow tube would have on grain deformation, crack formation, and overall structural integrity. Each tube was leak-tested using helium at 1050 +/- 50 psig for a minimum of 2 hours. The tubes were leak-tested after bending with no detectable pressure decay. Bent tubing samples were subjected to X-ray and dye penetrant inspection. Bent regions underwent metallographic examination for grain distortion, surface cracks, or other defects that might affect tube integrity.

For tubes removed from the qualification panel stack, the flow tube in each extrusion was pressurized with helium to 1050 +/- 50 psig for a minimum of 4 hours with no detectable pressure decay. From this suite of tubes, two were selected for hydrostatic proof testing at a pressure of 39,000 +/- 1000 psig for 5 minutes using deionized water after a thermal stabilization period. After the test, the tubes were drained and purged with $N_2$.

Subsequently, the four flow tube/extrusion assemblies were dissected to remove the approximately 8-foot straight section, leaving the tube bend regions. The four bent tube assemblies were dried in a 200°F oven for 24 hours with an internal 125 to 175°F $N_2$ purge to dry potential leak paths through the tube walls. The silver-filled epoxy and corner fittings were removed from the eight harvested tubing sections.

Finally, the tubes were sliced in the bend plane and mounted for metallographic inspection with particular attention given in the bend plane near the centerline where elongation and compression are maximized. These areas were examined for grain distortion, surface cracks, or other defects that could affect the tube integrity.

Only one defect was discovered during inspection and measured at 0.158 × 0.0017 inches with 0.0006-inch-depth (Figure 7.1-2). This defect is believed to be due to a tube extrusion or straightening and not the bending operation.

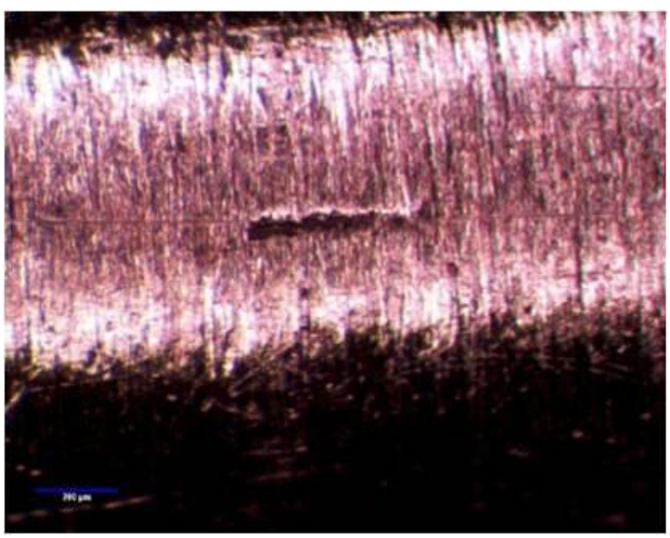

***Figure 7.1-2. Parent Material Defect Detected During Inspection***

Testing on limited samples did not reveal the presence of leaks in factory-supplied tubes. Further, bending of flow tubes did not introduce flaws, and flow tubes in panels were not damaged when exposed to flight environments. However, testing was performed on a limited numbers of samples, and does not guarantee that the 2.4 miles of on-orbit flow tubes were leak free. The pressure bubble that formed in panel 7 is likely due to a panel flow tube that leaked, either $N_2$ or ammonia (i.e., the only pressurized component in the panel), to create and feed a pressure bubble that led to panel 7 face sheet failure.

### 7.1.3 Test 3.8 -- Permeation/Leakage Through Silver-Filled Epoxy From Flow Tube

The objective of this test was to determine whether a silver-filled epoxy layer could seal a tube leak internal to a flow tube extrusion, and to determine if the silver-filled epoxy used to bond flow tubes into the aluminum extrusions was permeable to ammonia vapor pressure or liquid. While the proposed testing procedure is described here, it should be noted that testing was suspended due to completing the test.

This test was performed using five flow tube extrusions approximately 30 inches in length excised from five separate flow tube assemblies on non-flight panels representative of flight panel construction.

The flow tube assemblies were modified to allow for the installation of Swagelok®-type pressure fittings. The tube extrusion assemblies were modified to allow ammonia pressure inside the tube to be in direct contact with the silver-filled epoxy bond material. Holes drilled through the aluminum extrusions to permit this contact were less than or equal to a 0.067-inch-diameter (shown in Figure 7.1-3).

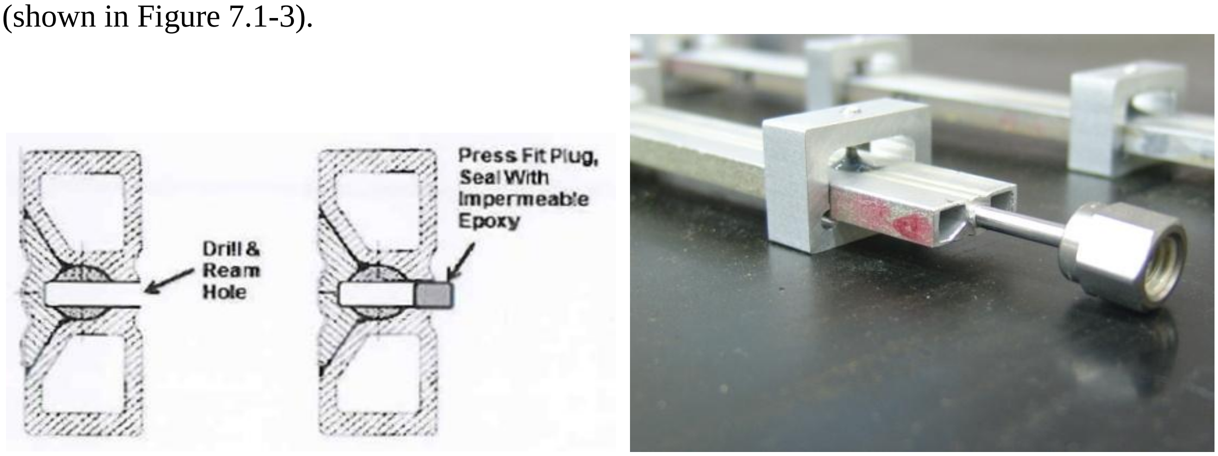


***Figure 7.1-3. Silver-Filled Epoxy Testing with Ammonia***

As originally planned, the tubes were to be pressurized using ammonia vapor for a minimum of 24 hours at pressures of 50 +/-10 and 100 +/-10, 20 +- 20, 300 +/- 30, 400 +/- 40, and 500 +/- 50 psig. Ammonia leakage through the silver-filled epoxy was to be performed using a litmus type indicator or ammonia gas detector.

Due to exhaustion of test funds, testing was suspended after approximately 312 hours of ammonia exposure and before destructive inspection of the ammonia/epoxy interface. At that point, leakage or permeability was not detected on sticks 6-4 and 8-4, with pressures ranging from approximately 20 to 175 psig. Reactions of the ammonia and silver in the epoxy were not observed. However, separate materials testing [ref. 15] showed some indication of a chemical reaction between ammonia and the epoxy tested in ammonia-filled test tubes.

#### 7.1.4 Test 3.11 --Panel Segment Pressure Tests

This test was designed to answer:

1) Does an internal ammonia, helium, or $N_2$ migrate into the panel interior, or does it migrate to the panel edge and exhaust to space?

2) Does ammonia, helium, or $N_2$ permeate or attack the bonded honeycomb structure that ultimately led to the face sheet rupture as observed on HRSR panel 7?

In answering these questions, this test was to determine the failure mode(s) and failure pressure(s) when a radiator panel segment is exposed to pressurized ammonia vapor and/or liquid. The test was to evaluate the integrity of the film sheet adhesive bond between the face sheets and honeycomb core; evaluate the integrity of the expanding foam adhesive between the flow tube extrusion and honeycomb core; evaluate the permeability/sealing capabilities of the barrier coating (Epon™ 828) region under the panel manifold cover; and the ammonia pressure(s), at which the internal construction and/or barrier coating regions fail.

The proposed testing procedure is presented for documentation purposes. However, due to events that transpired during test configuration proof testing, this test procedure was not completed as originally planned.

Four test segments were harvested from a flight radiator ground test panel:

1. 1st segment, 6-7 (small with narrow flow tube spacing, Figure 7.1-4),
2. 2nd segment, 8-8 (large with wide flow tube spacing, Figure 7.1-5),
3. 3rd segment, 6-3 (small with narrow flow tube spacing near the center regions, Figure 7.1-6), and
4. 4th segment, 6-2 (large with wide flow tube spacing, Figure 7.1-7).

Only panel segments 6-7 and 8-8 were pressure-tested prior to the test termination. Each test article was comprised of a portion of four or more flow tubes adjacent to a manifold cover. The edge of the radiator panel segments (i.e., perpendicular to the flow tubes) was sealed with Epon™ 828 barrier coating around an attached pressure plenum.

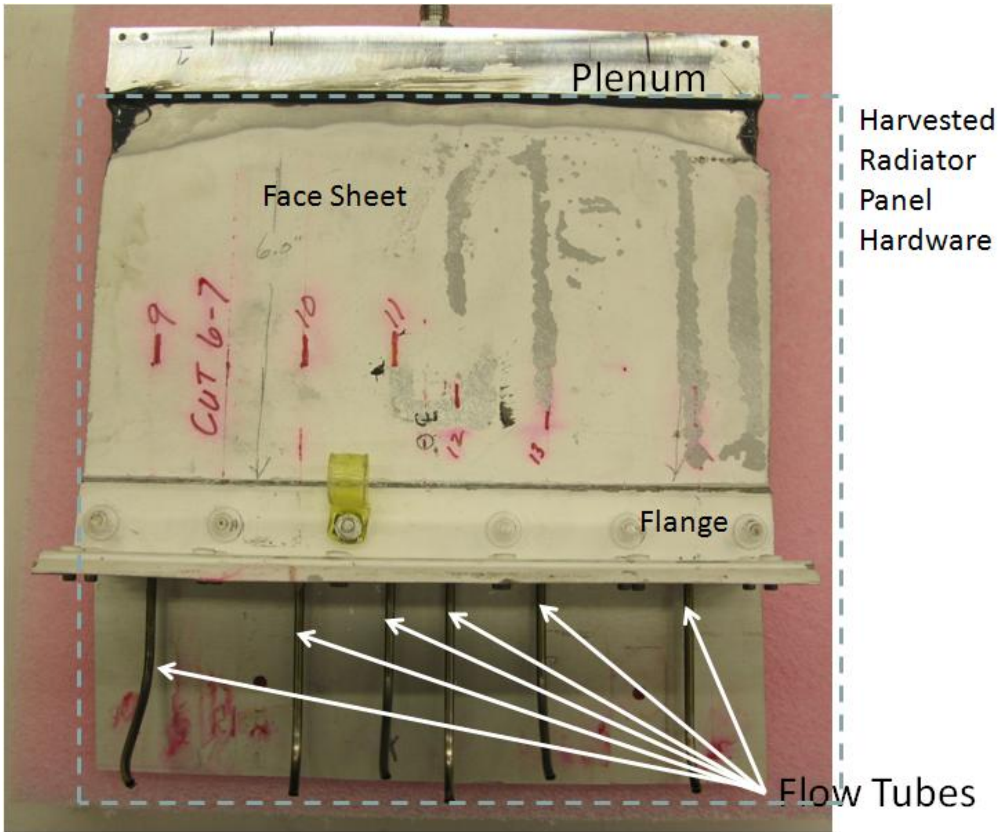


*Figure 7.1-4. Panel Test Segment 6-7*

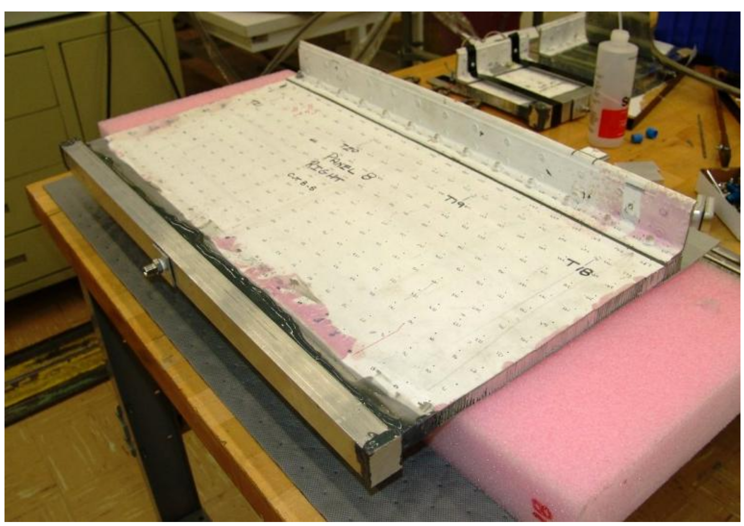

*Figure 7.1-5. Panel Test Segment 8-8*


*Figure 7.1-6. Panel Test Segment 6-3*

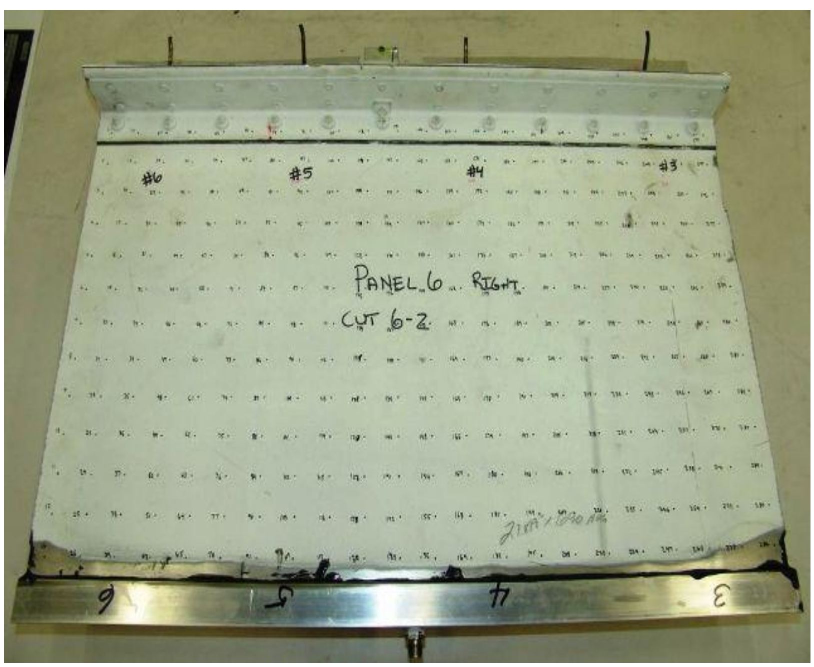


*Figure 7.1-7. Panel Test Segment 6-2*

If panel segment 6-7 passed the leak test, then ammonia would be introduced into the pressure port to 5 psig and held for 24 hours. Ammonia leakage would be monitored at the test article exit face, including eight foam adhesive locations. If no leakage was found, then the test would be repeated using 15, 30, 50, 75, 100, and 150 psig. Testing above and beyond this pressure was to be determined by test personnel and held for 24 hours prior to terminating the test.

Panel segment 6-7 failed during test between 20-30 psig with an audible noise, and pressure testing was terminated when an external leak occurred from the face sheet edge. The helium did not vent through the barrier coating to the plenum. The face sheet held pressure until it "jumped" over an extrusion bond and the face sheet separated from the core (as shown in Figures 7.1-8 through 7.1-10). This appears to be similar to the on-orbit panel 7 failure on a limited scale.

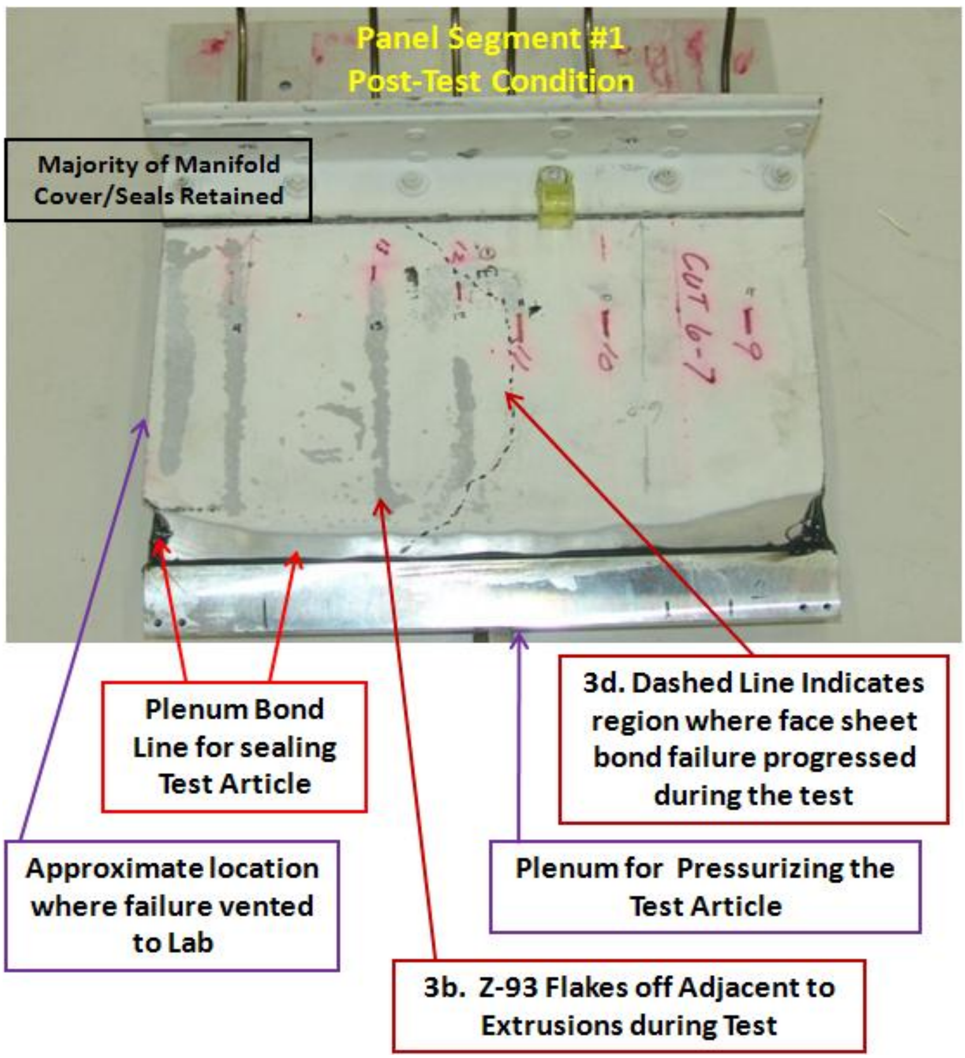


*Figure 7.1-8. Panel Segment 6-7, Post Leak Test Condition*

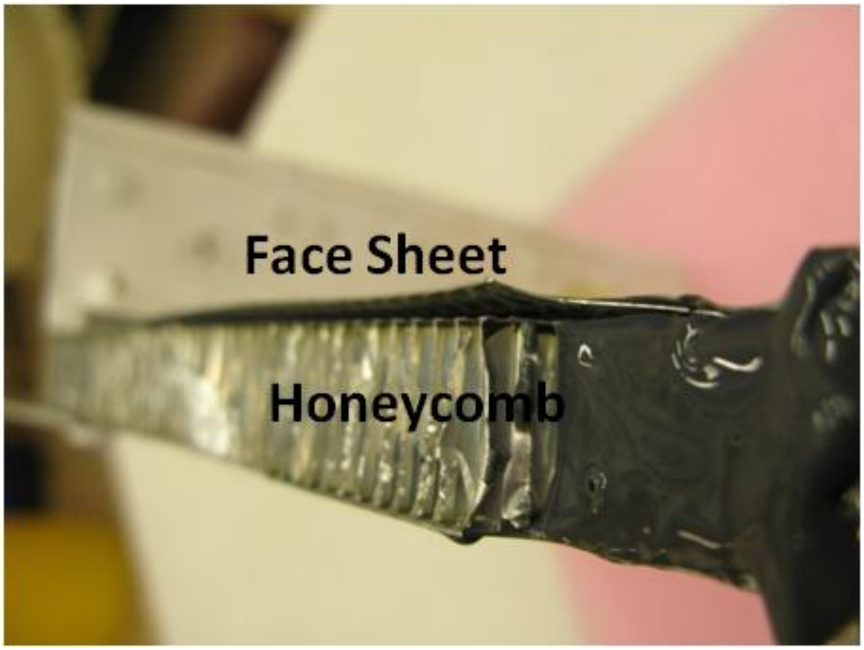


*Figure 7.1-9. Delaminated Face Sheet*

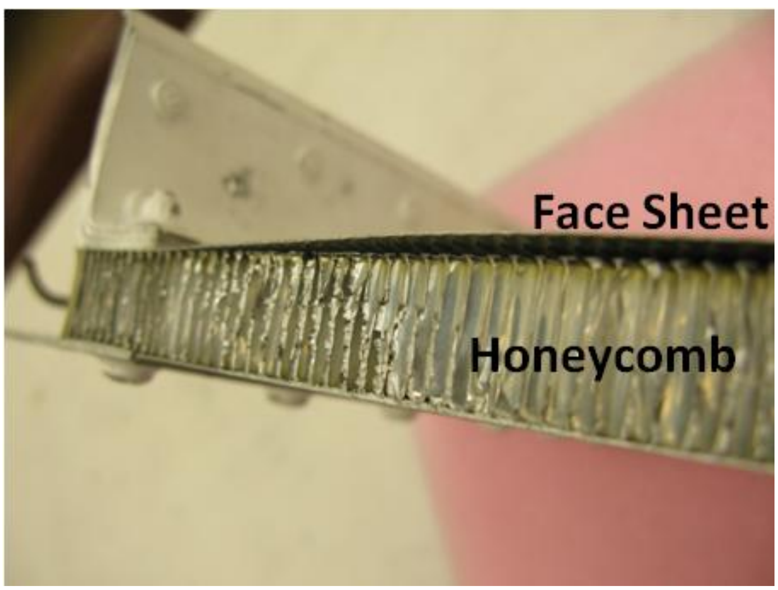


*Figure 7.1-10. Delaminated Face Sheet*

The failure mode resulted in Z-93 face sheet paint flaking parallel to the extrusions, which is not consistent with the on-orbit failure (Figure 7.1-8). This may be due to specimen size and the narrow flow tube spacing in the test segment. The failure mode initiation was not a face sheet delamination, but a series of football-shaped "lagoons" in the core peeling the core from the face sheet that progressed into a sequential series of HOneycomb Before Expansion (HOBE) joint bond failures (see Appendix C for HOBE bond description). This evolved into self-feeding with separation of the face sheet between HOBE joints and over flow tube extrusion paths. The lagoons were evident in the X-ray examination (see Figure 7.1-11) and teardown imagery (see Figures 7.1-12 and 7.1-13). Also evident in Figure 7.1-11 are three "infant" lagoons that were forming between flow tubes 10 and 11. These lagoons were located at various locations along the flow tube length. They had not grown to a size where gross face sheet debonding failure would have occurred. This suggests when the panel interior is pressurized, a number of failure points (lagoons) may form simultaneously. The spacing of the "infant" lagoons suggests that their formation is not necessarily sequential. Instead, the high pressure can migrate and attack areas where the HOBE bonds are the weakest. These insights strengthen the comparison between the failed test article and the magnitude of the damage pattern observed on the back side of panel 7. Figure 7.1-13 shows the face sheet delamination paths that occurred during the leak test.

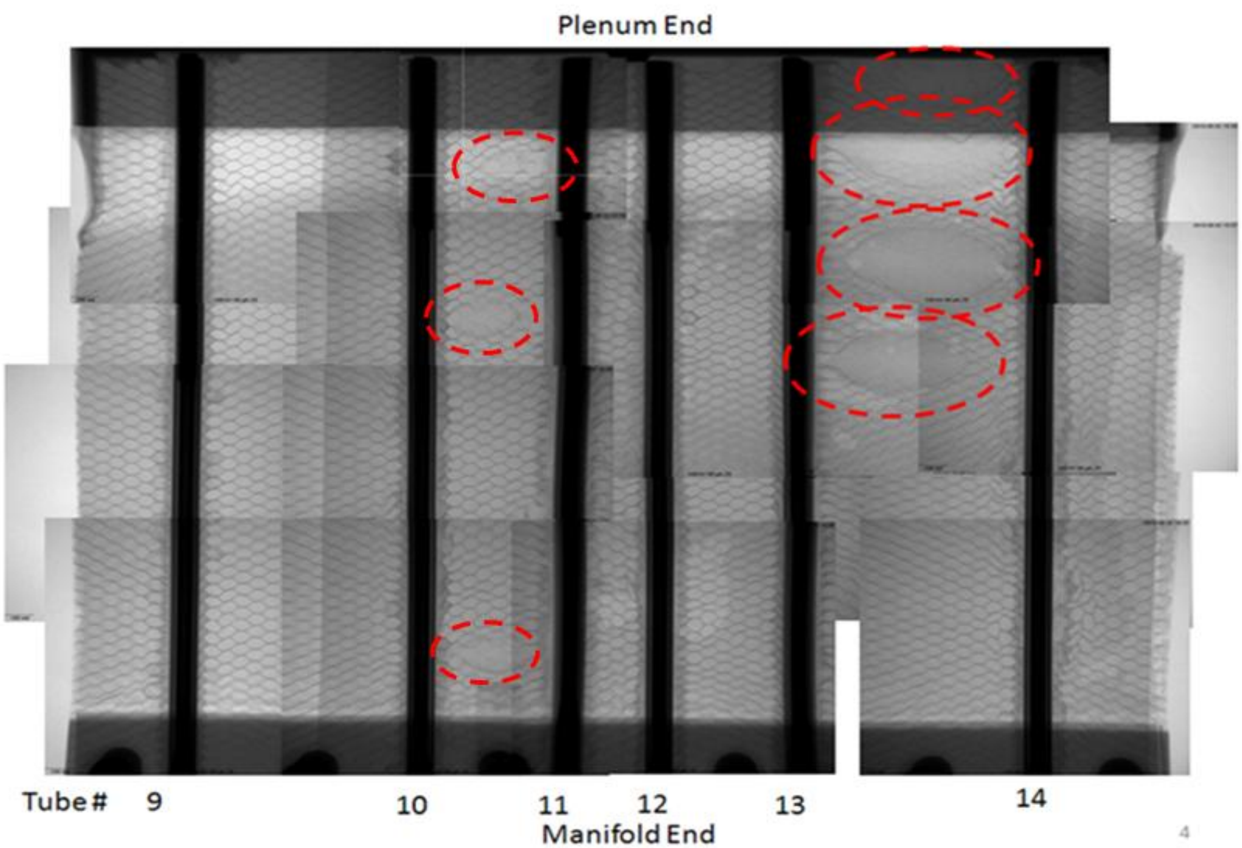


*Figure 7.1-11. X-Ray View Depicting Lagoons*

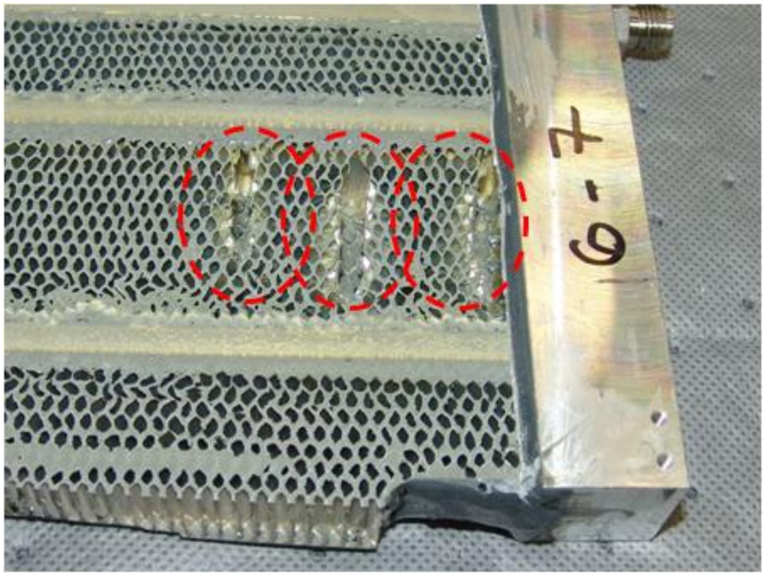


*Figure 7.1-12. HOBE Lagoons Revealed After Removal of Face Sheet*

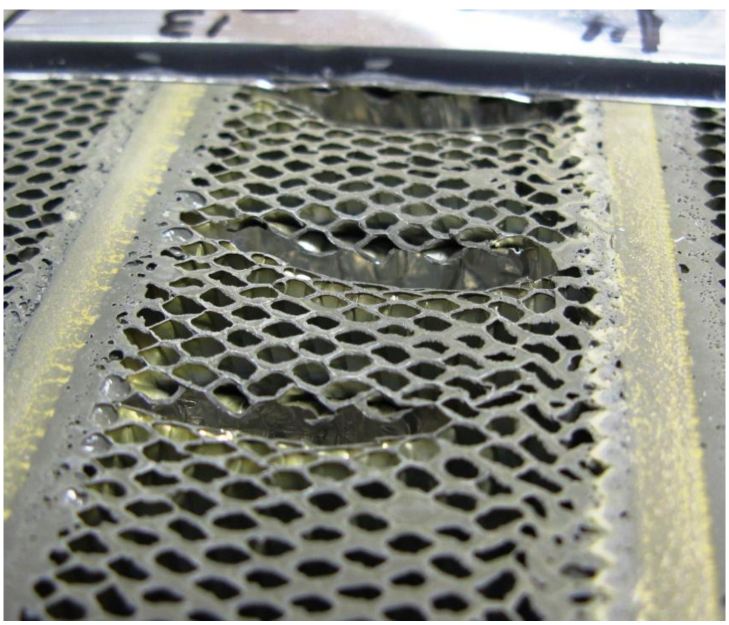

*Figure 7.1-13. HOBE Bond Failures from the Face Sheet*

Testing was started with ammonia at 40 psig for panel segment 8-8 (large). The panel internal structure began failing at low pressures (i.e., approximately 20 to 40 psig), as demonstrated by an audible noise, measured pressure reductions, and with accumulators unable to feed the increasing volume. Failure was not detected by X-ray or tap testing, thus this incipient failure was still in its infancy. Work stoppage prevented any further evaluation of this panel.

The findings from this test were serendipitous given that the failure in the HOBE bond and the resulting delamination occurred during proof testing. It was believed what was demonstrated during this test was indicative of the mechanism that caused propagation of the face sheet failure. When a HOBE bond fails, the characteristic orientation of the football-shaped lagoons will be perpendicular to the panel flow tubes. This is observed to be the orientation of the ripples on the back side of panel 7, as shown in Figure 7.1-14. This failure orientation characteristic further strengthens the comparison of what was observed in the failed test article with what was seen on-orbit.

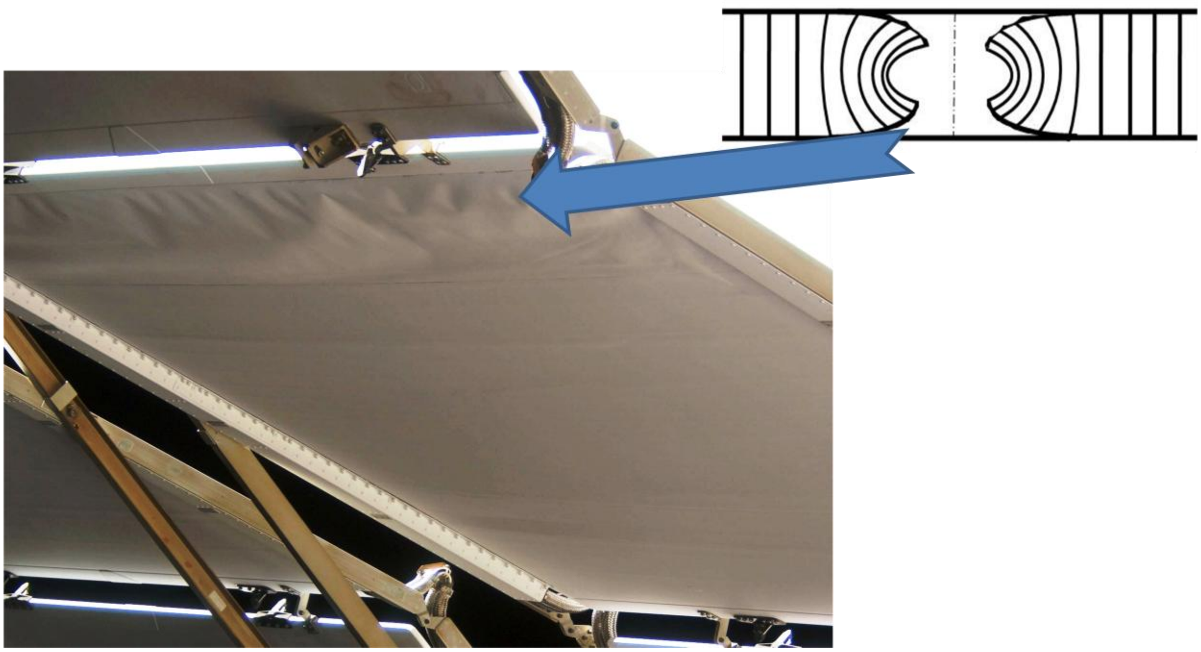

*Figure 7.1-14. Comparison Between Test Failure and Panel 7 Images Showing Ripples Perpendicular to the Flow Tube Orientation*

## 7.2 General Discussion of Test Results

The testing demonstrated what the team believes to be how face sheet delamination propagated. It demonstrated that the bolted interface can seal the face sheet in such a way that a pressure bubble can form.

Of interest is whether there exists a systemic issue that could be present in the on-orbit 47 HRSR and 42 PVR panels. The testing suggests that this is not likely and would be difficult to quantify. While $N_2$ leaks were seen from the on-orbit data, the screening of the test tubes and tubing history suggests that this type of failure is not common. There are other panels that had indicated $N_2$ leak rates prior to ammonia servicing (e.g., panels loops P1-2-1, P1-2-2, and P1-3-2). These leaks were smaller than observed in the panel 7. Since these were less than the flow paths' QD allowable leak rate, it is believed that the observed leaks are due to multiple QDs and fittings within each flow path rather than tube leak. A high-resolution video survey was conducted of three fourths of the radiator surfaces and no face sheet wrinkles were detected that would indicate a panel leak.

The testing was designed to look for tube weakness, failure due to exposure to the design and qualification environments, and potential for tube leaks to breach adhesive. Of the mechanisms studied, test 3.11 serendipitously showed a mechanism for which a tube with a leak could pressurize the region beneath the face sheet. This lends credibility to the failure scenario and may be representative of events that took place in the causal chain.

### 7.3 Concluding Remarks

The on-orbit imagery, LS-DYNA® simulations, ground panel segment testing, MMOD impact testing, and similar Space Shuttle Orbiter coldplate rupture testing with face sheet peel up indicate that the observed damage was likely an over pressure failure event of the radiator S1-3 panel 7 face sheet. An internal leak of either $N_2$ or ammonia occurred over the 4 years or less time that initiated HOBE failures in the honeycomb beneath the -105 bottom -103 face sheet (Figure 5.1-6) as evident by the HOBE wrinkle in the face sheet. The ground panel segment pressure testing showed that a small leak into a honeycomb section will initiate a HOBE void that will separate from either the top or bottom face sheet to start new HOBE voids in the same honeycomb section. It is also possible for the leak to traverse an extrusion flow tube to initiate HOBE voids in the adjacent honeycomb section. The HOBE voids start in 20-40 psig pressure range and will grow at the leak rate that will maintain this pressure range as the total pressurized volume continues to increase.

There is a critical pressure level and cross section area beneath the face sheet that will cause a run-away face sheet separation. The two panel 7 end face sheets over the HOBE voids did not separate at the strong attachment radiator end edge. More than 75 percent of these two face sheets separated from one side of the honeycomb sections. Nearly 100 percent of the top center -103 face sheet separated either from the honeycomb or with the honeycomb from the bottom face sheet. The center face sheet sheared the bond to the face sheet -101 section and sheared or tore away from one panel outer edge in the run-away event.

It is unknown whether the run-away event was initiated by the shock wave resulting from an MMOD impact into the pressurized void or internal pressure.

## 8.0 Findings, Observations, and NESC Recommendations

### 8.1 Findings

The following findings were identified:

**F-1**. Testing on a limited number of Inconel® tubing samples did not reveal the presence of detectable leaks.

**F-2.** Examination of a small sample of flow tube bends found the bending of flow tubes did not introduce flaws into the tubes that could leak $N_2$ or ammonia into the radiator panel interior. The flow tube bend radius is within the ductility limits of the Inconel® 718 material by analysis.

**F-3.** After 312 hours of ammonia exposure, leakage or permeability through silver-filled epoxy bonds was not detected on panel test sticks (6-4 and 8-4), with pressures ranging roughly from 20 to 175 psig.

**F-4**. The failure mode initiation in the lab tested panel segment was not a face sheet delamination. Rather, it was a leak that created a series of football-shaped "lagoons" in the core peeling the core away from the face sheet that progressed into a sequential series of HOBE joint bond failures.

**F-5.** Over time, a leak below the specified allowable leak rate or an undetected ammonia leak into the radiator interior will overpressurize the panel face sheet. Ground testing determined that pressures less than 40 psig within a honeycomb cell will initiate HOBE failure and separate the HOBE void from one of the face sheets.

**F-6.** The panel 7 MMOD impact appears to have occurred prior to the face sheet failure.

**F-7.** The long-term exposure compatibility of the silver-filled epoxy to ammonia was not tested as part of qualification and is unknown.

**F-8.** Tap testing of the qualification and spare flight panels would not detect a 0.5-inch × 2-inch void or smaller over the flow tube extrusions, or 0.5-inch × 0.5-inch or smaller void over the honeycomb core.

**F-9.** NDE of radiator panels used in the environmental qualification test program found the flow tubes in the panels were not damaged when exposed to "flight" panel environments.

**F-10.** The actual panel and array assembly leak rates were not recorded, but were verified to meet the 15-year requirement of $1.7 \times 10^{-3}$ sccs $N_2$.

**F-11.** LS-DYNA® analysis predicted the observed HRSR panel 7 face sheet impact on panel 8.

**F-12.** LS-DYNA® analysis suggests that low pressure behind the face sheet in more than a 50-percent debonded area (on the order of 10-20 psig) could cause a dynamic face sheet peel.

## 8.2 Observation

The following observation was identified:

**O-1.** The radiator panel interior sealed volume was not tested or evaluated as part of design qualification as a possible pressure vessel as a parent metal tubing leak was considered “improbable.”

## 8.3 NESC Recommendations

The following NESC recommendations were identified and directed towards the ISS Program:

**R-1.** Monitor HRSR and PVR panels with high-resolution videos and imagery to detect deformations in the panel face sheets for a pending face sheet peel up. ***(F-1, F-4, F-5, F-6, F-7, F-8, F-9, F-10, F-11, F-12)***

**R-2.** Obtain high-resolution imagery to verify there are no detectable face sheet deformations prior to an ammonia fill of any radiator panel flow path. ***(F-2, F-3, F-7)***

**R-3.** Perform long-term (i.e., 20 years) compatibility studies of ammonia and silver-filled epoxy. ***(F-7)***

# 9.0 Alternate Viewpoints

There were no alternate viewpoints identified during the course of this assessment by the NESC team or the NRB quorum.

# 10.0 Other Deliverables

No unique hardware, software, or data packages, outside those contained in this report, were disseminated to other parties outside this assessment.

# 11.0 Lessons Learned

The following lessons learned apply to future projects developing radiator panels or systems.

**L-1.** Sealed volumes that have internal pressurized components should be considered and tested as pressure vessels and tested for rupture pressure for design margin versus maximum operating internal pressures or internal volumes should be vented to ensure no over pressure event can occur.

**L-2.** Leak rates of flight-pressurized systems (panel tubing) should be measured and recorded during testing at the assembly level.

# 12.0 Definition of Terms

| | |
|---|---|
| Corrective Actions | Changes to design processes, work instructions, workmanship practices, training, inspections, tests, procedures, specifications, drawings, tools, |

| | |
|---|---|
| | equipment, facilities, resources, or material that result in preventing, minimizing, or limiting the potential for recurrence of a problem. |
| Finding | A conclusion based on facts established by the investigating authority. |
| Lessons Learned | Knowledge or understanding gained by experience. The experience may be positive, as in a successful test or mission, or negative, as in a mishap or failure. A lesson must be significant in that it has real or assumed impact on operations; valid in that it is factually and technically correct; and applicable in that it identifies a specific design, process, or decision that reduces or limits the potential for failures and mishaps, or reinforces a positive result. |
| Observation | A factor, event, or circumstance identified during the assessment that did not contribute to the problem, but if left uncorrected has the potential to cause a mishap, injury, or increase the severity should a mishap occur. Alternatively, an observation could be a positive acknowledgement of a Center/Program/Project/Organization's operational structure, tools, and/or support provided. |
| Problem | The subject of the independent technical assessment/inspection. |
| Proximate Cause | The event(s) that occurred, including any condition(s) that existed immediately before the undesired outcome, directly resulted in its occurrence and, if eliminated or modified, would have prevented the undesired outcome. |
| Recommendation | An action identified by the assessment team to correct a root cause or deficiency identified during the investigation. The recommendations may be used by the responsible Center/Program/Project/Organization in the preparation of a corrective action plan. |
| Root Cause | One of multiple factors (events, conditions, or organizational factors) that contributed to or created the proximate cause and subsequent undesired outcome and, if eliminated or modified, would have prevented the undesired outcome. Typically, multiple root causes contribute to an undesired outcome. |

# 13.0 Acronyms List

| | |
|---|---|
| BGA | Beta Gimbal Assembly |
| DC | Direct Current |
| DDCU | DC to DC Converter Unit |
| EATCS | External Active Thermal Control System |
| EPS | Electrical Power System |
| EVA | Extravehicular Activity |

| | |
|---|---|
| FAA | Federal Aviation Administration |
| FCV | Flow Control Valve |
| HOBE | Honeycomb-Before Expansion |
| HRS | Heat Rejection Subsystem |
| HRSR | Heat Rejection Subsystem Radiator |
| HX | Heat Exchanger |
| IR | Infrared |
| ISS | International Space Station |
| JSC | Johnson Space Center |
| LaRC | Langley Research Center |
| LMMFC | Lockheed Martin Missiles and Fire Control |
| MMOD | Micro Meteoroid Orbital Debris |
| MVCB | Multi-lateral Vehicle Control Board |
| $N_2$ | Nitrogen |
| NDE | Nondestructive Evaluation |
| NESC | NASA Engineering and Safety Center |
| NRB | NESC Review Board |
| ORU | Orbital Replaceable Unit |
| PM | Pump Module |
| psia | Pounds Per Square Inch Absolute |
| psig | Pounds Per Square Inch Gauge |
| PVR | Photovoltaic Radiator |
| QD | Quick Disconnect |
| RBVM | Radiator Beam Valve Module |
| SARJ | Solar Alpha Rotary Joint |
| sccs | Standard Cubic Centimeter Per Second |
| SSPCB | Space Station Program Control Board |
| TIM | Technical Interchange Meetings |
| TRRJ | Thermal Radiator Rotary Joint |

# 14.0 References

1. Hypervelocity Impact Test Plan for ISS P6 Photovoltaic Radiator (PVR) Panel Test Series (February 23, 2009).
2. Howell, Patricia A., Cramer, K. Elliott, and Winfree, William P., “Thermal method for Depth of Damage Determination in Insulating Materials,” Review of Progress in Quantitative Nondestructive Evaluation. Edited by D.O. Thompson and D.E. Chimenti, Plenum Press, New York, 1993.
3. Cramer, K. Elliott, Howell, Patricia A., and Winfree, William P., “Quantitative Thermal Depth Imaging of Subsurface Damage in Insulating Materials,” Proc. SPIE Vol. 1993, pp. 188-196, Thermosense XV.

4. Office of Aviation Research. (2000, September). *Experimental Investigations of Material Models for Ti-6Al-4V Titanium and 2024-T3 Aluminum* (Publication No. DOT/FAA/AR-00/25). Washington, DC: National Technical Information Service.
5. Rasouli, F., and Williams, T. (1995, March). Application of Dispersion Modeling to Indoor Gas Release Scenarios. *Journal of Air Waste Management Association, 43*(3), 191-5.
6. National Institute of Standards and Technology (2011). *Thermophysical Properties of Fluid Systems*. (2011). Retrieved from http://webbook.nist.gov/chemistry/fluid.
7. Statement of Work for HRS Radiator Panel Element Tests Supporting Failure Investigation of ISS Radiator S1-3, Panel #7, Document No: 3-56200 HRS/S.O.W.
8. Raetz, J., and Morton, R., Heat Rejection Subsystem (HRS) S1-3 Damaged Radiator Panel #7, Test Planning, (SSPCB Presentation), October 20, 2009.
9. Space Station Heat Rejection Subsystem (HRS) S1-3 Damaged Radiator Panel #7, Test Familiarity Package (Abbreviated Test Program).
10. E-mail communication from Boeing/John Raetz on January 6, 2010.
11. E-mail communication from Boeing/Siamak Ghofranian on January 6, 2010 and January 12, 2010.
12. E-mail communication from Boeing/John Raetz on January 12, 2010.
13. Heat Rejection System (HRS) Radiator, HRS On-Orbit Panel 7 Face Sheet Investigation, September 3, 2010.
14. S1-3 Heat Rejection Subsystem Radiator Panel #7 Face Sheet Separation Anomaly, Priority Testing, Results Overview & Major Conclusions, Morton, R., Harkness, B., and Wright, D., January 6, 2011.
15. Harper, S., White Sands Test Facility (WSTF) 09-43528 (report transmittal memorandum), August 12, 2009.
16. Journal of Solar Energy Engineering, *On Protection of Freedom's Solar Dynamic Radiator From the Orbital Debris Environment: Part 1 -- Preliminary Analysis and Testing,* Vol. 114. August 1992.
17. NASA Technical Memorandum 104514. *On Protection of Freedom's Solar Dynamic Radiator From the Orbital Debris Environment: Part 2: Further Testing and Analyses, April 1992.*

# 15.0 Appendices

# Appendix A. Radiator Panel Form Factor to Space Results

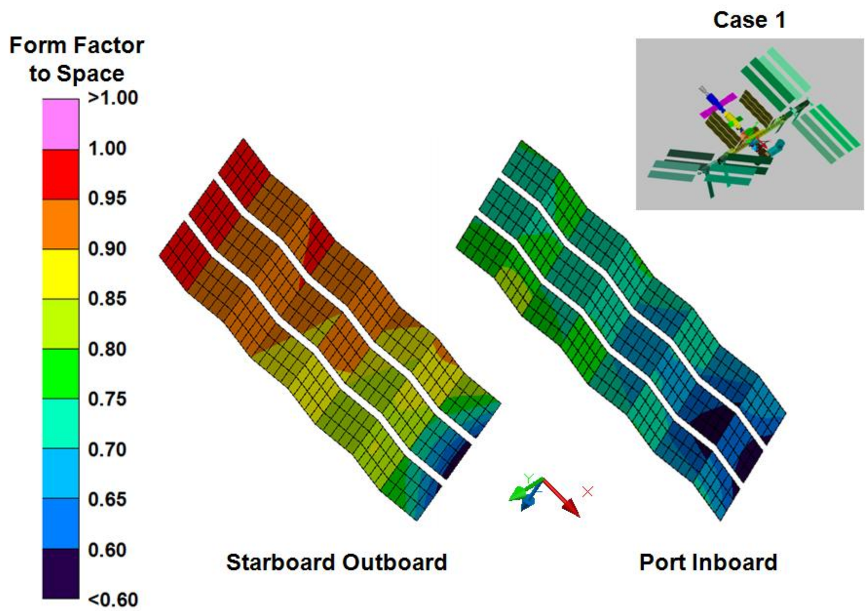


**Figure A-1 – Case 1 Results for the Starboard Outboard and Port Inboard Surfaces**

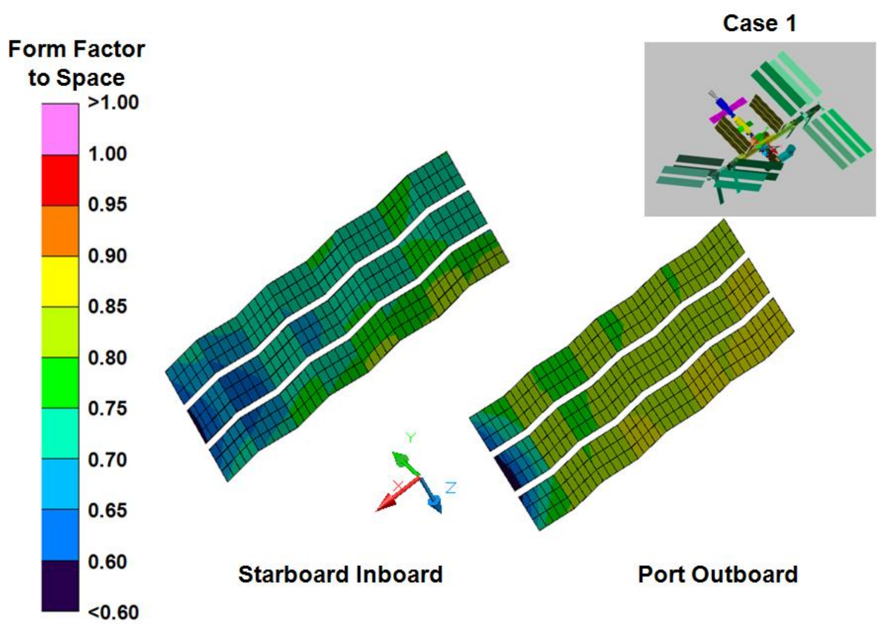


**Figure A-2 – Case 1 Results for the Starboard Inboard and Port Outboard Surfaces**

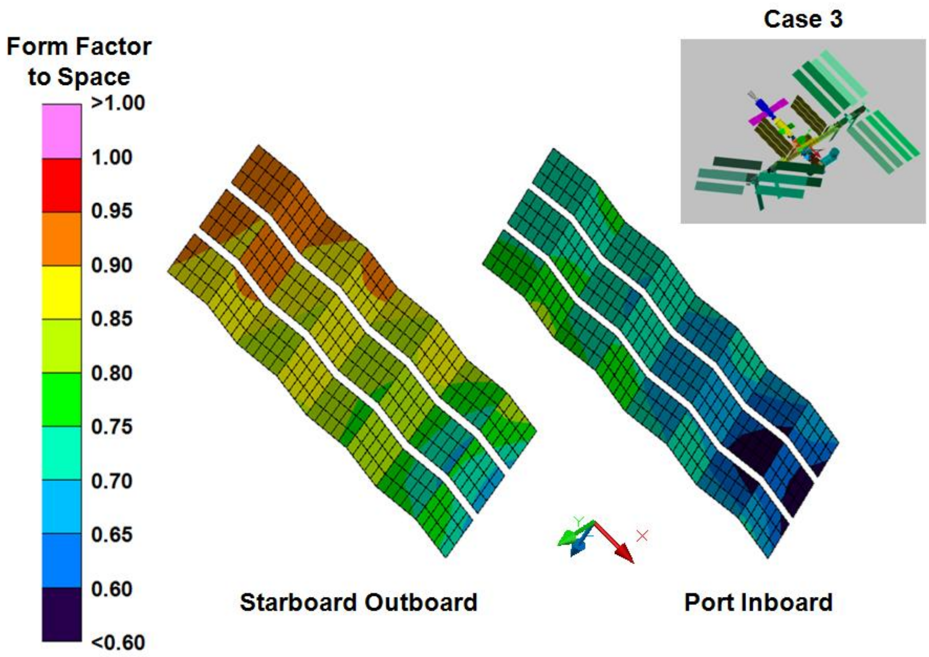


**Figure A-3 – Case 3 Results for the Starboard Outboard and Port Inboard Surfaces**

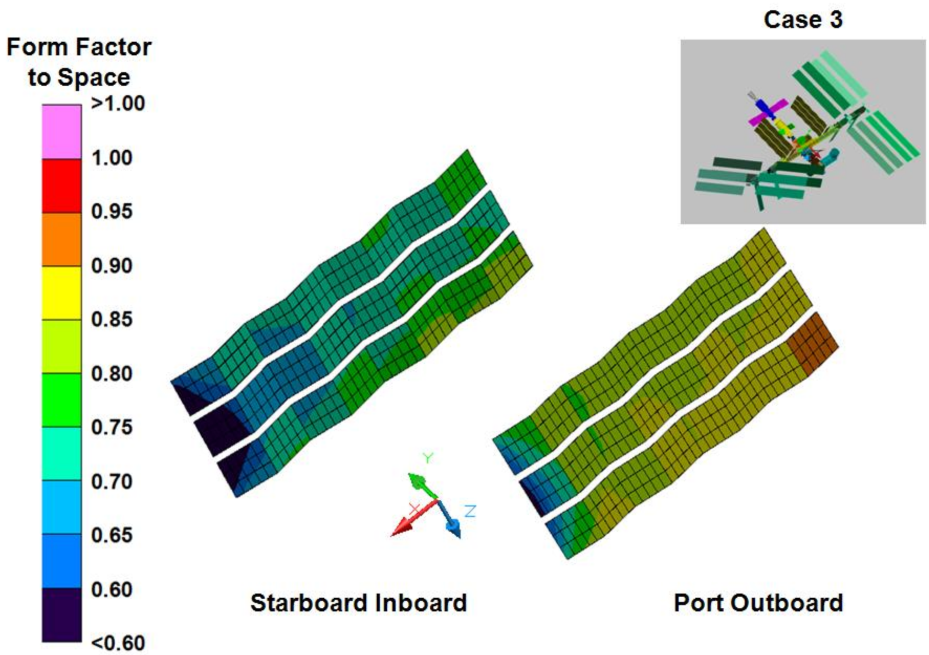


**Figure A-4 – Case 3 Results for the Starboard Inboard and Port Outboard Surfaces**

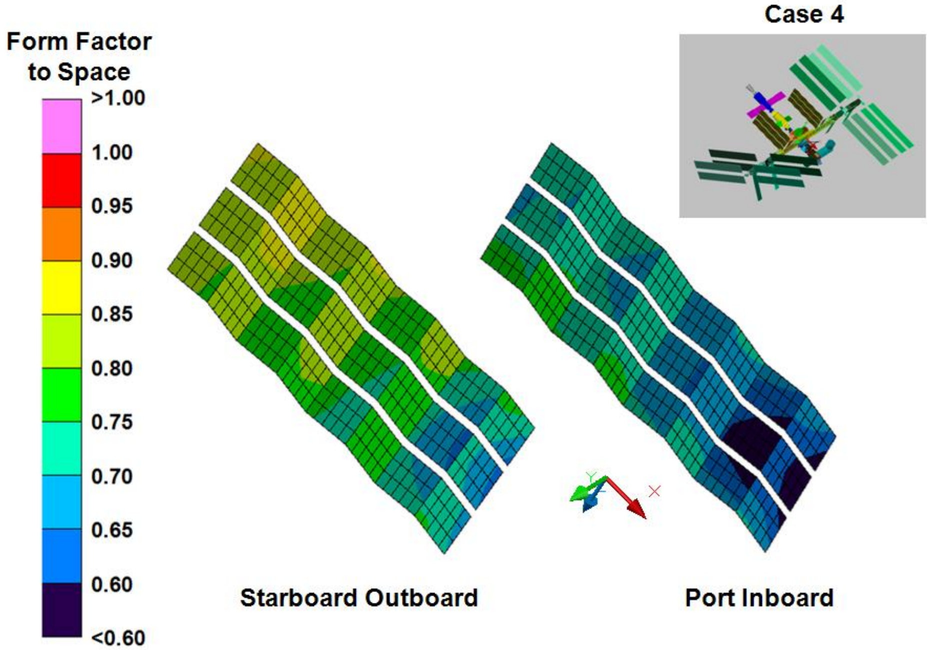


**Figure A-5 – Case 4 Results for the Starboard Outboard and Port Inboard Surfaces**

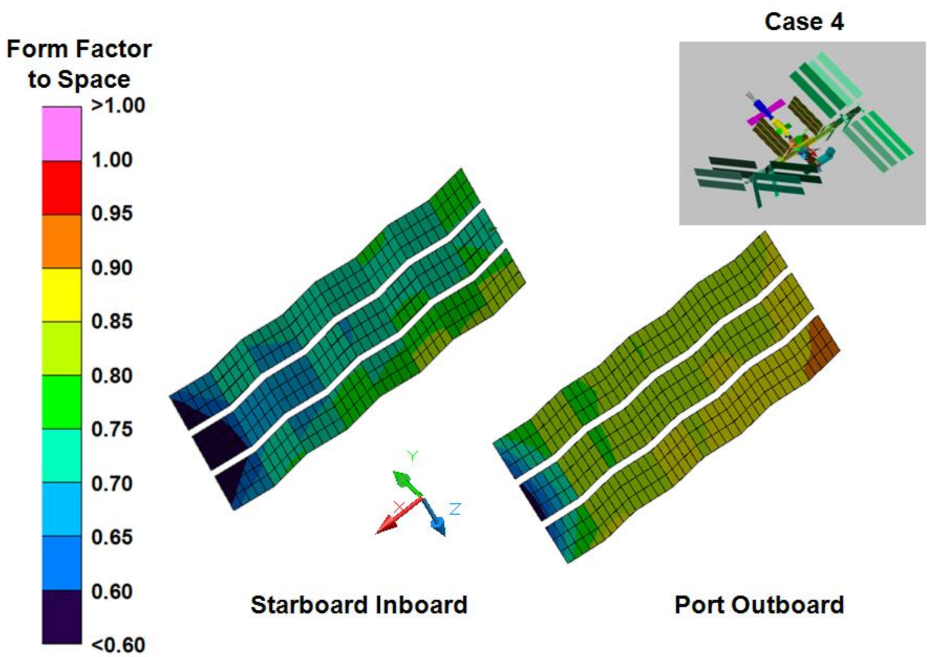


**Figure A-6 – Case 4 Results for the Starboard Inboard and Port Outboard Surfaces**

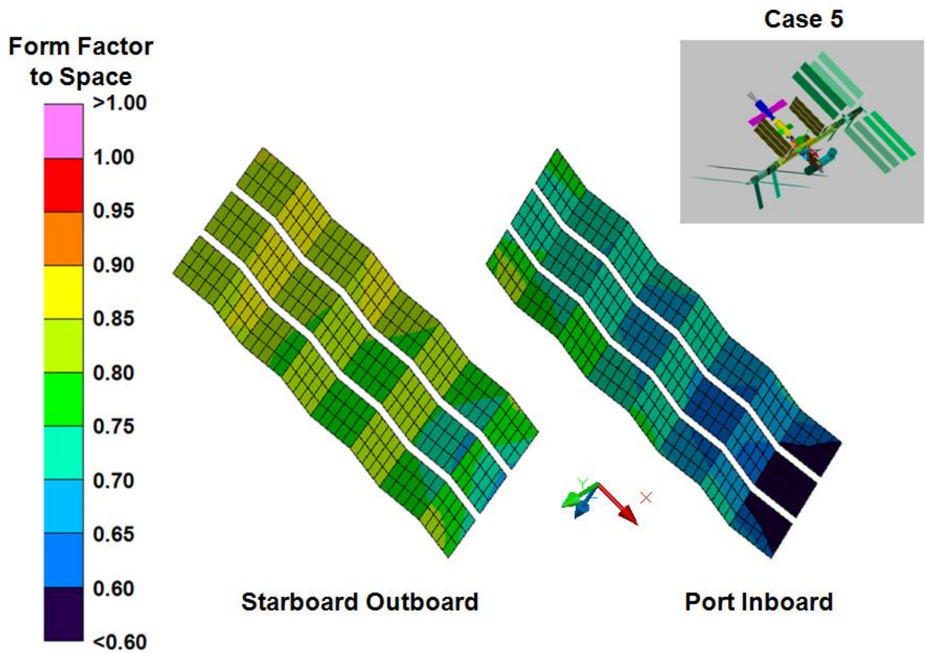


**Figure A-7 – Case 5 Results for the Starboard Outboard and Port Inboard Surfaces**

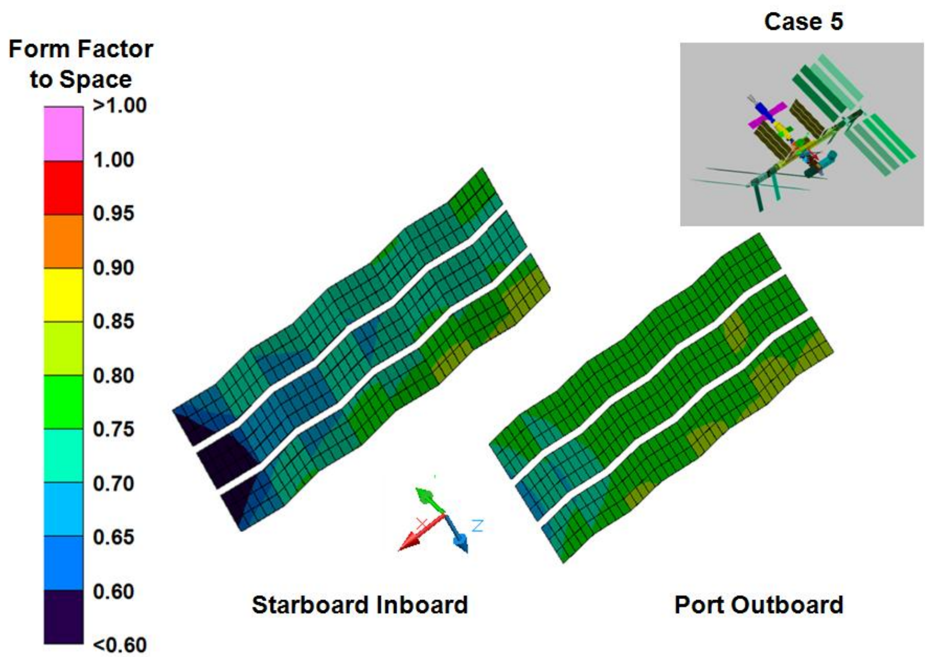


**Figure A-8 – Case 5 Results for the Starboard Inboard and Port Outboard Surfaces**

# Appendix B. Calculation of the Pressure Unloading Time History

From Rasouli and Williams (1995) [ref. 5]:

$$P_2 = \left[ P_0^{(1-k)/2k} + \frac{t \cdot C \cdot A(t) \cdot (k-1)}{2 \cdot V \cdot k} \cdot \frac{k-1}{2k} \sqrt{\frac{g_c \cdot R \cdot k^3 \cdot T_0}{M \cdot P_0^{(k-1)/k}} \cdot \left[\frac{2}{k+1}\right]^{(k+1)/(k-1)}} \right]^{2k/(1-k)}$$

$P_0$ = initial pressure

$P_2$ = pressure at time $t$

$t$ = time

$k = c_p/c_v$ (Values obtained from the US National Institute of Standards and Technology. The Institute serves a website with a $c_p$ and $c_v$ calculator [ref. 4]. Inputs are the gas type, initial pressure, and temperature.)

$C$ = coefficient of discharge

$A(t)$ = area of the leak hole. (The area of the source leak is the time dependent rupture area. In this model, the rupture hole is a function of time. This rupture area was measured in the model at time intervals, and fit to an exponential equation.)

$V$ = volume of the source vessel

$g_c$ = gravitational conversion factor

$R$ = universal gas constant

$M$ = Molecular weight

$T_0$ = Initial gas temperature

# Appendix C. Honeycomb Core (HOneycomb Before Expansion (HOBE)) Bond

Honeycomb core honeycomb before expansion (HOBE) bonds (Figure C-1) are alternating strips of adhesive applied to thin sheets of aluminum foil, 0.0007 inches thick. The sheets are stacked together with the adhesive in an alternating pattern. The stack is bonded together and is now called the HOBE. The HOBE is sliced into the required thickness, then expanded producing the core in a honeycomb shape.

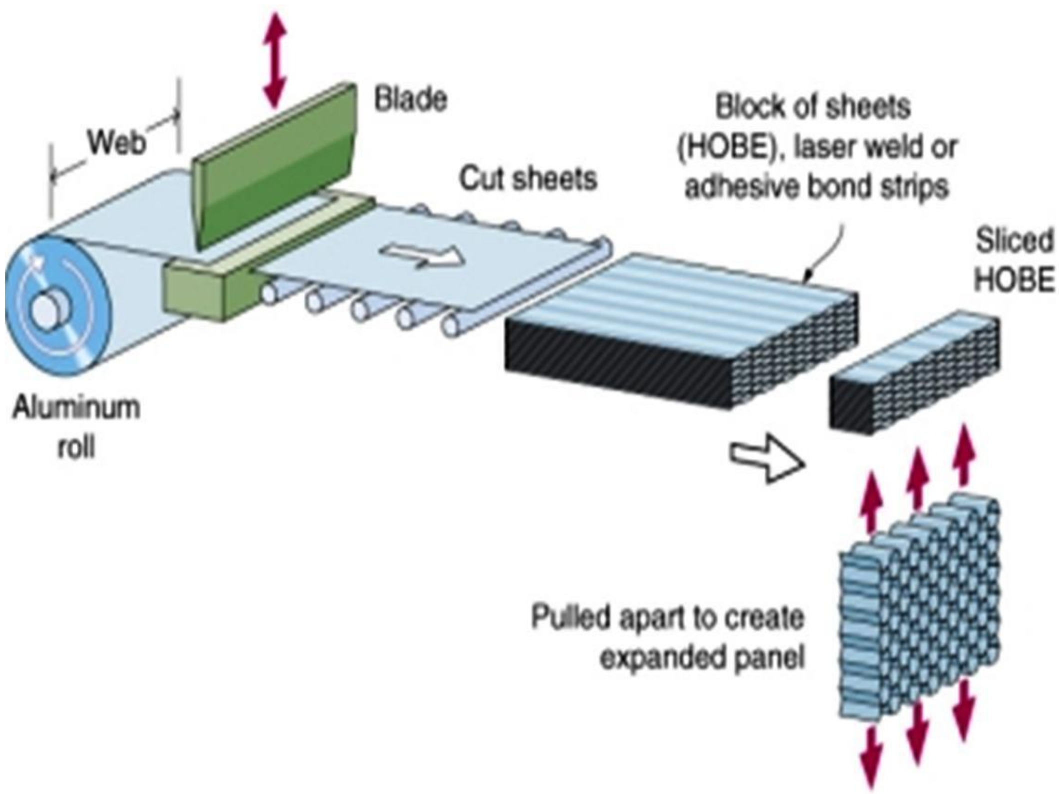


***Figure C-1. Honeycomb Core HOBE Bond Process***

How the HOBE bond occurs and creates the football-shaped lagoons is shown in Figure C-2. This causes additional face sheet delamination and path to form new lagoons.

- Gas enters into a cell from a flow tube extrusion and pressurizes it
- The Weak Link is the HOBE Bonds, perpendicular to the flow tube extrusions
- As the HOBE bond fails, it 'peels' the core away from the facesheet, producing the football shaped lagoon
- This initiating additional core peel from the facesheet
- Provides pressure paths to new core HOBE bonds, producing more core lagoons and sequentially the bond failure grows larger

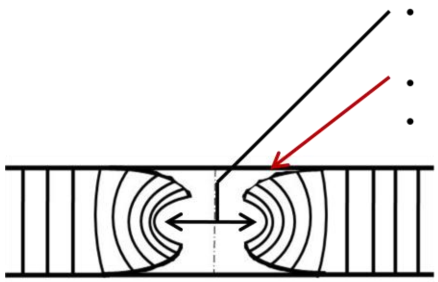

*Figure C-2. HOBE Bond Failure Drives Panel Delamination*

## REPORT DOCUMENTATION PAGE

*Form Approved*
*OMB No. 0704-0188*



**1. REPORT DATE** *(DD-MM-YYYY)*
01- 03 - 2012

**2. REPORT TYPE**
Technical Memorandum

**3. DATES COVERED** *(From - To)*
March 2009 - February 2012

**4. TITLE AND SUBTITLE**
International Space Station (ISS) Heat Rejection Subsystem (HRS) Radiator Face Sheet Damage

**5a. CONTRACT NUMBER**

**5b. GRANT NUMBER**

**5c. PROGRAM ELEMENT NUMBER**

**6. AUTHOR(S)**
Rotter, Henry A.

**5d. PROJECT NUMBER**

**5e. TASK NUMBER**

**5f. WORK UNIT NUMBER**
869021.07.07.03.01

**7. PERFORMING ORGANIZATION NAME(S) AND ADDRESS(ES)**
NASA Langley Research Center
Hampton, VA 23681-2199

**8. PERFORMING ORGANIZATION REPORT NUMBER**
L-20131 NESC-RP-09-00529

**9. SPONSORING/MONITORING AGENCY NAME(S) AND ADDRESS(ES)**
National Aeronautics and Space Administration
Washington, DC 20546-0001

**10. SPONSOR/MONITOR'S ACRONYM(S)**
NASA

**11. SPONSOR/MONITOR'S REPORT NUMBER(S)**
NASA/TM-2012-217348

**12. DISTRIBUTION/AVAILABILITY STATEMENT**
Unclassified - Distribution limited to NASA Contractors and U.S. Government Only.
Subject Category 16 - Space Transportation and Safety
Availability: NASA CASI (443) 757-5802

**13. SUPPLEMENTARY NOTES**

**14. ABSTRACT**
The starboard side International Space Station heat rejection subsystem radiator (HRSR) was launched on October 2002, and deployed and serviced in November 2007. A survey of previous International Space Station images and videos verified this radiator was in the normal configuration on August 29, 2008. However, on September 1, 2008, a video survey of International Space Station indicated a face sheet had debonded and peeled up on HRSR S1-3 panel 7 with no apparent source for the damage. On February 18, 2009, the International Space Station Program Manager requested the NASA Engineering and Safety Center to support the NASA and Boeing External Active Thermal Control System International Space Station system teams to determine the possible causes of the HRSR face sheet damage. This document contains the outcome of the NASA Engineering and Safety Center assessment.

**15. SUBJECT TERMS**
Heat rejection subsystem radiator; Face sheet; NASA Engineering and Safety Center; Nondestructive evaluation; External Active Thermal Control System

| 16. SECURITY CLASSIFICATION OF: a. REPORT | b. ABSTRACT | c. THIS PAGE | 17. LIMITATION OF ABSTRACT | 18. NUMBER OF PAGES | 19a. NAME OF RESPONSIBLE PERSON |
|---|---|---|---|---|---|
| | | | | | STI Help Desk (email: help@sti.nasa.gov) |
| | | | | | **19b. TELEPHONE NUMBER** *(Include area code)* |
| U | U | U | UU | 88 | (443) 757-5802 |